

# Hybrid Quantum-Classical Methods for Noisy Intermediate Scaling Quantum Machines

by

Diksha Dhawan

A dissertation submitted in partial fulfillment  
of the requirements for the degree of  
Doctor of Philosophy  
(Chemistry)  
in The University of Michigan  
2022

Doctoral Committee:

Professor Dominika Zgid, Chair  
Professor Eitan Geva  
Professor Emanuel Gull  
Professor Nicolai Lehnert

Diksha Dhawan

ddhawan@umich.edu

ORCID iD: 0000-0002-1129-3166

© Diksha Dhawan 2022

Dedicated to my Grandmother, Smt.Sita Devi

## ACKNOWLEDGEMENTS

I am deeply grateful to many people without whom this thesis would not have been possible. Foremost, I would like to convey my sincere gratitude towards my advisor Professor Dominika Zgid for guiding me through my Ph.D. I am fortunate to have her as my advisor. She has been extremely patient with me, from sitting with me for hours debugging a code in my first year to giving feedback on my writing, she has shaped me as a scientist. She is an incredible mentor who has encouraged me and believed in me even when I did not. Her knowledge of the field, positivity towards the research, and her advice both professional and personal have guided me throughout my journey.

I would like to thank Professor Eitan Geva for being on my committee and for his constant support throughout the program. I am also grateful to Professor Emanuel Gull and Professor Nicolai Lehnert for agreeing to be on my committee and their guidance during my Ph.D.

I am also indebted to my previous advisor Dr. Debashree Ghosh for introducing me to the field of electronic structure theory. While working for her I developed the skill set that helped me during my research. I also must thank my peers in her group, Samik who taught me the basics of research, Rahul for helping me sharpen my coding skills and Paulami for teaching me patience, and to all of them for being amazing friends and co-workers.

I would also like to extend my thanks to my group members. Alicia, Blair and Yanbing were there for me when I joined the group, our weekly meetings helped me

gain confidence in my understanding of the field. Blair has always been there for me and provided me with valuable advice at every step of the way. Avijit and Alex for helping me with my work even when they had a lot to do themselves. Thanks to Yuting, Pavel, Vibin, Gaurav and Ming for the scientific and non-scientific discussions and for maintaining a friendly and fun environment in the group.

I am extremely thankful to my family and friends. My parents, who taught me how to dream and follow those dreams with passion. They have always encouraged me to do what I loved doing, no matter the circumstances. My brother, who has taught me how to persevere through tough times. Arup, for believing in me and encouraging me. Thanks to Ariba for always providing a listening ear, she has always been there for me when I needed a friend. Our evening coffee and cooking experiments have always been the much needed distraction. To Nirmal, my 3am friend who knows how to put sense into me when needed. Kristina, who has been an amazing friend and classmate. Ankit, Sweta and Achu for being the home away from home. To all my friends old and new, Apoorva, Aastha, Ritu, Hitesh, Yogita, Aman, Sumedh, Shobhit and Shamalee for being there for me.

Last but not the least, to Chiku, my non-hooman companian, for just being cute and silly.

# TABLE OF CONTENTS

DEDICATION . . . . .	ii
ACKNOWLEDGEMENTS . . . . .	iii
Table of Contents . . . . .	iv
LIST OF FIGURES . . . . .	viii
LIST OF TABLES . . . . .	x
LIST OF ABBREVIATIONS . . . . .	xii
ABSTRACT . . . . .	xiv
CHAPTER	
<b>I. Introduction</b> . . . . .	1
1.1 Electron Correlation . . . . .	3
1.2 Electronic Structure Theory Formalisms . . . . .	5
1.2.1 Wavefunction Theories . . . . .	5
1.2.2 Density Based Theories . . . . .	6
1.2.3 Green's Function Theories . . . . .	7
1.3 Quantum Chemistry on Quantum Computers . . . . .	8
<b>II. Quantum Computing</b> . . . . .	10
2.1 Experimental Realization . . . . .	11
2.2 Qubit States and Operations . . . . .	12
2.3 Early Quantum Algorithms For Quantum Chemistry . . . . .	15
2.3.1 Fermionic Hamiltonian to Qubit Hamiltonian . . . . .	16
2.3.2 Quantum Phase Estimation(QPE) . . . . .	19
2.3.3 Adiabatic State Preparation . . . . .	21
2.4 Quantum Noise . . . . .	22
2.5 Algorithms For Noisy Intermediate Scaling Quantum(NISQ) Machines . . . . .	23

2.5.1	Variational Quantum Eigensolver(VQE) . . . . .	23
<b>III.</b>	<b>Green’s Function on Quantum Computers . . . . .</b>	<b>27</b>
3.1	Quantum Algorithms For Green’s Function . . . . .	31
3.1.1	Quantum Phase Estimation Based Algorithms . . . . .	31
3.1.2	Variational Quantum Eigensolver Based Algorithms . . . . .	32
3.1.3	Quantum Subspace Expansion Based Algorithms . . . . .	33
<b>IV.</b>	<b>Dynamical Self-energy Mapping (DSEM) for creation of sparse Hamiltonians suitable for quantum computing . . . . .</b>	<b>35</b>
Diksha Dhawan, Mekena Metcalf, Dominika Zgid		
4.1	Abstract . . . . .	35
4.2	Introduction . . . . .	37
4.3	Method . . . . .	39
4.3.1	Approximating self-energy . . . . .	44
4.3.2	Fictitious Hamiltonian . . . . .	46
4.4	Results . . . . .	46
4.4.1	Hamiltonians with parameterized on-site integrals from high frequency expansion . . . . .	47
4.4.2	Modified Hamiltonian parameterization using GF2 self-energy . . . . .	49
4.4.3	Number of gates for different Hamiltonian parameterizations . . . . .	53
4.5	Conclusions . . . . .	54
4.6	Acknowledgements . . . . .	57
<b>V.</b>	<b>Sparse-Hamiltonian approach to the time evolution of molecules on quantum computers . . . . .</b>	<b>58</b>
Christina Daniel, Diksha Dhawan, Dominika Zgid, James Freericks		
5.1	Abstract . . . . .	58
5.2	Introduction . . . . .	59
5.3	Formalism . . . . .	61
5.4	Results . . . . .	62
5.5	Discussion . . . . .	66
5.6	Conclusions . . . . .	67
5.7	Acknowledgement . . . . .	68
<b>VI.</b>	<b>Quantum Subspace Expansion Based Approach for Calculating Green’s Functions . . . . .</b>	<b>69</b>
Diksha Dhawan, Mario Motta, Dominika Zgid		
6.1	Introduction . . . . .	69

6.2	Method . . . . .	71
6.2.1	Green's Function Formulation . . . . .	71
6.2.2	Quantum Subspace Expansion . . . . .	73
6.2.3	Green's Function Calculation Using QSE . . . . .	74
6.2.4	Statistical Analysis . . . . .	75
6.3	Results . . . . .	76
6.3.1	Green's Function from QSE and FCI . . . . .	76
6.4	Conclusions . . . . .	80
<b>VII. Conclusions . . . . .</b>		<b>86</b>
<b>VIII. Future Directions . . . . .</b>		<b>88</b>
<b>Bibliography . . . . .</b>		<b>90</b>



# LIST OF FIGURES

## Figure

2.1	Bloch Sphere representing the state of a single qubit geometrically .	12
2.2	Quantum circuit for creation and measurement of bell state. Here the initial states of two qubits are $ 0\rangle$ and $ 1\rangle$ , entanglement is being produced by the application of the Hadamard gate on the control qubit followed by the CNOT gate, and the measurement is done in the standard basis. . . . .	13
2.3	Quantum phase estimation circuit with $m$ ancilla qubits. $\text{FFT}^{-1}$ here means inverse fast Fourier transform and $ \Psi\rangle$ is the ground state of the system. . . . .	20
2.4	Circuit for variational quantum eigensolver. . . . .	25
4.1	Dynamical self-energy mapping (DSEM) algorithm to produce a sparse Hamiltonian for a fictitious molecular system. DSEM can be used as a classical-quantum hybrid algorithm for quantum computing, in which case, the high level method will be executed on the quantum machine. . . . .	42
4.2	The imaginary part of the self-energy for $\text{H}_6$ chain in the DZ basis evaluated in FCI with all integrals (denoted here as $\text{FCI}(v)$ ) and FCI with effective, on-site 2-body integrals (denoted as $\text{FCI}(\tilde{v}_{iiii})$ ). Top left: $\text{Im}[\Sigma(i\omega)]_{00}$ element. Bottom left: $\text{Im}[\Sigma(i\omega)]_{01}$ element. Top right: $\text{Im}[\Sigma(i\omega)]_{11}$ element. Bottom right: $\text{Im}[\Sigma(i\omega)]_{03}$ element. . . .	50
5.1	Exact (solid) and approximate (dashed) retarded Green's function for the sparse Hubbard Hamiltonian. The time is in units of $\hbar/H$ . .	66
6.1	The real(top) and imaginary(bottom) part of $G_{00}(i\omega)$ element for $\text{H}_2$ molecule in the STO-6G basis evaluated using FCI and QSE. Inset on respective plots show the difference between Green's function calculated using FCI and QSE. . . . .	77
6.2	The real(top) and imaginary(bottom) part of $G_{00}(i\omega)$ element for $\text{H}_4$ chain with bond length 1.0 Å in the STO-6G basis evaluated using FCI and QSE. Inset on respective plots shows the difference between Green's function calculated using FCI and QSE . . . . .	78

6.3	The real(top) and imaginary(bottom) part of $G_{11}(\omega)$ element for $H_4$ chain with bond length 1.0 Å in the STO-6G basis evaluated using FCI and QSE. Inset on respective plots shows the difference between Green's function calculated using FCI and QSE . . . . .	79
6.4	The real(top) and imaginary(bottom) part of $G_{11}(\omega)$ element for $H_2$ molecule with bond length 1.0 Å in the STO-6G basis evaluated using FCI and QSE done on the QASM simulator. . . . .	80
6.5	The real(top) and imaginary(bottom) parts of $G_{11}(\omega)$ element for $H_2$ molecule with bond length 1.0 Å in the STO-6G basis evaluated using FCI and QSE done on the QASM simulator. QSE results have been post-processed using jackknife for proper error propagation. . .	81
6.6	Distribution of real component of the Green's function element $G_{00}(\omega)$ for the samples taken through the simulator. Top left: For 2000 Samples. Top right: For 4000 Samples. Bottom left: For 8000 Samples. Bottom right: For 16000 Samples. . . . .	82
6.7	Distribution of imaginary component of the Green's function element $G_{00}(\omega)$ for the samples taken through the simulator. Top left: For 2000 Samples. Top right: For 4000 Samples. Bottom left: For 8000 Samples. Bottom right: For 16000 Samples. . . . .	83
6.8	Error distribution obtained from the crude data(without using any resampling technique) as the sample size increases with respect to $1/M^2$ where M is the total number of samples . . . . .	84
6.9	Error distribution obtained after the jackknife analysis as the sample size increases with respect to $1/M^2$ where M is the total number of samples . . . . .	85

## LIST OF TABLES

### Table

1.1	Computational cost of many of the approximate wavefunction based methods. Here N is the number of orbitals in the system in a given basis. . . . .	6
2.1	List of Quantum Logic Gates. . . . .	15
4.1	Energy values obtained using GF2, FCI and parameterized FCI( $\tilde{v}$ ) for H <sub>6</sub> ring with interatomic distance R=0.95 Å in the STO-6G basis. The second row lists 2-body integrals that were used in the evaluation of self-energies. All values of energy are listed in a.u. In case of FCI( $\tilde{v}$ ), $\tilde{v}_{iii}$ denotes the value of the 2-body on-site integral for $i = 1, \dots, 6$ , all other 2-body integrals are equal to zero. . . . .	48
4.2	Energy values obtained using GF2, FCI and parameterized FCI( $\tilde{v}$ ) for H <sub>6</sub> ring with interatomic distance R=0.95 Å in the DZ basis. The second row lists 2-body integrals that were used in the evaluation of self-energies. All values of energy are listed in a.u. In case of FCI( $\tilde{v}$ ), $\tilde{v}_{iii}$ denotes the value of the 2-body on-site integral for 1s $i = 1, \dots, 6$ , $\tilde{v}_{jjj}$ denotes the value of the 2-body on-site integral for 2s, all other 2-body integrals are equal to zero. . . . .	49
4.3	Energy values obtained using GF2, parameterized GF2, FCI, and parameterized FCI. Symbol p1 stands for a parameterization using $\langle ii ii \rangle$ integrals. Symbol p2 stands for a parameterization using $\langle ii ii \rangle$ , $\langle ij ij \rangle$ , $\langle ij ji \rangle$ groups of the effective integrals. Symbol p3 stands for a parameterization that uses all the integrals from the p2 group as well as $\langle ij jj \rangle$ effective integrals. All values of energy are listed in a.u.	51
4.4	Energy values obtained using GF2, parameterized GF2, FCI, and parameterized FCI. Symbol p1 stands for a parameterization using $\langle ii ii \rangle$ integrals. Symbol p2 stands for a parameterization using $\langle ii ii \rangle$ , $\langle ij ij \rangle$ , $\langle ij ji \rangle$ groups of the effective integrals. Symbol p3 stands for a parameterization that uses all the integrals from the p2 group as well as $\langle ij jj \rangle$ effective integrals. All values of energy are listed in a.u.	52

4.5	Energy values obtained using GF2, and parameterized GF2. Symbol p1 stands for a parameterization using $\langle ii ii \rangle$ integrals. Symbol p2 stands for a parameterization using $\langle ij ij \rangle$ , $\langle ij ji \rangle$ groups of the effective integrals. Symbol p3 stands for a parameterization that uses all the integrals from the p2 group as well as $\langle ij jj \rangle$ effective integrals. All values of energy are listed in a.u. . . . . .	52
4.6	Energy values obtained using GF2, and parameterized GF2. Symbol p1 stands for a parameterization using $\langle ii ii \rangle$ integrals. Symbol p2 stands for a parameterization using $\langle ij ij \rangle$ , $\langle ij ji \rangle$ groups of the effective integrals. Symbol p3 stands for a parameterization that uses all the integrals from the p2 group as well as $\langle ij jj \rangle$ effective integrals. All values of energy are listed in a.u. . . . . .	53
4.7	Number of single qubit (SQG) gates and CNOT gates required to exponentiate the full and fictitious Hamiltonian under various parameterizations for both Jordan-Wigner(JW) and Bravyi-Kitaev(BK) transformations. Symbol p1 stands for a parameterization using $\langle ii ii \rangle$ integrals. Symbol p2 stands for a parameterization using $\langle ii ii \rangle$ , $\langle ij ij \rangle$ , $\langle ij ji \rangle$ groups of the effective integrals. Symbol p3 stands for a parameterization that uses all the integrals from the p2 group as well as $\langle ij jj \rangle$ effective integrals. . . . .	53
5.1	Parameters for the sparse Hubbard Hamiltonian that represents the four-site hydrogen ring. ll parameters are in Hartrees. . . . .	63
5.2	Doubles unitary coupled-cluster operators used in creating the approximate ground state. The operators are applied in order according to the rows of the table. . . . .	64
5.3	General form and final numerical values of the coefficients of the approximate ground state after applying the doubles-only excitations, with $c_i \equiv \cos \theta_i$ and $s_i \equiv \sin \theta_i$ . . . . .	65

## LIST OF ABBREVIATIONS

<b>NISQ</b>	Noisy Intermediate Scale Quantum
<b>HF</b>	Hartree Fock
<b>FCI</b>	Full Configuration Interaction
<b>MP2</b>	Second order Moller Plesset Perturbation
<b>DFT</b>	Density Functional Theory
<b>CIS</b>	Configuration Interaction Singles
<b>CISD</b>	Configuration Interaction Singles and Doubles
<b>CISDT</b>	Configuration Interaction Singles, Doubles and Triples
<b>CCSDT</b>	Couple Cluster Singles, Doubles and Triples
<b>LDA</b>	Local Density Approximation
<b>GGA</b>	Generalized Gradient Approximation
<b>CASSCF</b>	Complete Active Space Self-Consistent Field
<b>CASPT2</b>	Complete Active Space Second-Order Perturbation Theory
<b>NEVPT2</b>	n-Electron Valence State Second-Order Perturbation Theory
<b>RASSCF</b>	Restricted Active Space Self-Consistent Field
<b>GFCC</b>	Green's Function Coupled Cluster
<b>DMFT</b>	Dynamic Mean Field Theory
<b>DMET</b>	Density Matrix Embedding Theory
<b>SEET</b>	Self Energy Embedding Theory
<b>CNOT</b>	Controlled-NOT

**QPE** Quantum Phase Estimation  
**VQE** Variational Quantum Eigensolver  
**ASP** Adiabatic State Preparation  
**FFT** Fast Fourier Transform  
**UCC** Unitary Coupled Cluster  
**ADAPT** Adaptive Derivative Assembled Pseudo-Trotter  
**PQE** Projective Quantum Eigensolver  
**DSEM** Dynamic Self-Energy Mapping  
**QSE** Quantum Subspace Expansion

## ABSTRACT

The accurate and efficient simulation of many body systems has been a long-standing challenge for quantum chemists and physicists. At the heart of this challenge lies the correlation between quantum particles, which is crucial in understanding various physical phenomena, but is numerically hard to calculate. Over the decades, there has been remarkable progress in simplifying this problem aided by mathematical and chemical approximations and the availability of powerful computers. However, an exact solution to the problem still remains intractable as it requires exponential resources with respect to the system size.

Recent advances in the field of quantum computing have shown promise in Feynman's idea of simulating quantum mechanics on quantum computers. It has been proposed that an ideal fault-tolerant quantum computer can reduce the scaling of these simulations from exponential to polynomial. However, initial quantum algorithms have shown that there is a large gap between the capabilities of current hardware and the resources required for simulating quantum systems of interest. The work of this thesis focuses on reducing this gap by introducing two novel algorithms for quantum chemistry simulations, which are suitable for near-term hardware. First, we introduce a hybrid algorithm to decrease the total number of operations required for the quantum simulations. We use a classical computer to generate an effective Hamiltonian containing  $O(n^2)$  terms compared to the  $O(n^4)$  terms of the full Hamiltonian, where  $n$  is the number of orbitals. This sparse Hamiltonian can then be used with

a high-level method to recover the ground state energies. We demonstrate that this sparsification of the Hamiltonian reduces the number of quantum operations required for the simulation by an order of magnitude, thus making it accessible for the near-term Hardware. Our second algorithm aims to make the calculation of dynamic correlation functions (Green's functions) more feasible on these quantum machines. This algorithm is designed with the motive of avoiding the use of time-evolution and reduced use of two-qubit gates. We demonstrate that we can reproduce the Green's function within reasonable error limits using this approach. We have also discussed the use of re-sampling techniques for proper error-propagation of the stochastic data obtained from the quantum machines.

The general structure of this thesis is as follows. We begin by motivating this work in Chapter 1. Chapters 2 and 3 provide a general introduction of quantum computing and Green's function based methods, respectively. In chapter 4, the development of effective Hamiltonian is discussed in detail. Chapter 5 demonstrates the use of these effective Hamiltonians on the quantum machine for time evolution. In chapter 6, we have discussed the algorithm to calculate Green's functions on a quantum machine. This is followed by conclusions and future directions in Chapters 7 and 8, respectively.



# CHAPTER I

## Introduction

Recent advances in material sciences have led to major breakthroughs in technology with increasing demand for new and environment-friendly materials. These range from high-temperature superconductors for low-cost electricity transmission to lightweight materials for spacecraft and satellites and low-cost and high absorptivity materials for solar panels. A combined experimental and theoretical effort is necessary to efficiently explore these materials and enhance our understanding of the mechanism behind their properties. Since the 1960s, there have been many developments and innovations in the field of theoretical chemistry parallel to the evolution of computational power. One can now investigate a lot of things theoretically, from structural properties to reactivity, simple reactions to reactions in complex biological systems, conformational changes, reaction mechanisms, and many biological phenomena.

Theoretical chemistry research is governed by principles of quantum mechanics and classical mechanics. The nature of the problem under study is the deciding factor between the two methods. For example, spectroscopic studies involve the interaction of matter with electromagnetic waves, which depends on the motion of subatomic particles and can be described by quantum mechanics. On the other hand, properties like the dielectric field, enthalpy of phase change, density, etc are dependent on the atomic motion and therefore can be predicted by classical mechanics.

In classical mechanics, the evolution of a system in time is described by Newton's second law.

$$-\frac{dV}{dr} = m \frac{d^2r}{dt^2} \quad (1.1)$$

where V is the potential, m is mass, t is time and r is the displacement. However, for the description of microscopic systems, we need quantum mechanics and the time evolution of a quantum system is described by the time-dependent Schrodinger equation.

$$\hat{H}\Psi(x, t) = -\frac{\hbar}{i} \frac{d\Psi(x, t)}{dt} \quad (1.2)$$

This equation can be solved by separating the time and space variables, which gives rise to two separate differential equations.

$$\frac{1}{\Psi(t)} \frac{d\Psi(t)}{dt} = -\frac{iE}{\hbar} \quad (1.3)$$

$$\hat{H}\Psi(x) = E\Psi(x) \quad (1.4)$$

The former equation is solved easily to yield

$$\Psi(t) = \exp\left\{\frac{-iEt}{\hbar}\right\} \quad (1.5)$$

Whereas solving the latter equation is one of the central challenges of non-relativistic quantum chemistry. In Equation 1.2, H is the Hamiltonian operator,  $\Psi$  is the wavefunction, x represents electronic and nuclear coordinates collectively, and E is electronic energy. Hamiltonian operator for a molecular system with N electrons and M nuclei is given by

$$\hat{H} = -\sum_{i=1}^N \frac{1}{2} \nabla_i^2 - \sum_{A=1}^M \frac{1}{2M_A} \nabla_A^2 - \sum_{i=1}^N \sum_{A=1}^M \frac{Z_A}{r_{iA}} + \sum_{i=1}^N \sum_{j>i}^N \frac{1}{r_{ij}} + \sum_{A=1}^M \sum_{B>A}^M \frac{Z_A Z_B}{R_{AB}} \quad (1.6)$$

where  $Z_A$  is the nuclear charge of nucleus A,  $\nabla_i^2$  and  $\nabla_A^2$  involve differentiation with respect to electronic and nuclear coordinates respectively. The first and second terms in Eq. 1.6 are the kinetic energy operators for electrons and nuclei, the third term represents the coulomb attraction between electrons and nuclei and the last two terms represent the repulsion between electrons and between nuclei respectively. According to the Born-Oppenheimer approximation, we can consider the electrons to be moving in the field of fixed nuclei because of the slow motion of nuclei compared to electrons. This allows us to separate the electronic and nuclear Hamiltonian. Electronic part of the Hamiltonian is

$$\hat{H}_{elec} = - \sum_{i=1}^N \frac{1}{2} \nabla_i^2 - \sum_{i=1}^N \sum_{A=1}^M \frac{Z_A}{r_{iA}} + \sum_{i=1}^N \sum_{j>i}^N \frac{1}{r_{ij}} \quad (1.7)$$

The solution to the Schrödinger equation involving only the electronic motion gives us the electronic wavefunction and the electronic energy. These explicitly depend on the electronic coordinates while parametrically depending on the nuclear coordinates. However, solving the Schrödinger equation for multiple particles is non-trivial because of the presence of electron-electron interactions[1].

## 1.1 Electron Correlation

One way to approximately treat these electron-electron interactions is through mean-field theories like Hartree-Fock, where in an n-electron system, the impact of n-1 electrons on the nth electron is approximated in an average manner.

Hartree-Fock theory approximates the wavefunction of the system as an antisymmetrized product of n orthonormal spin orbitals,  $\chi(x)$ , which can be represented by

the Slater determinant

$$\psi(x_1, x_2, \dots, x_n) = \frac{1}{\sqrt{n!}} \begin{vmatrix} \chi_1(x_1) & \chi_2(x_1) & \dots & \chi_n(x_1) \\ \chi_1(x_2) & \chi_2(x_2) & \dots & \chi_n(x_2) \\ \vdots & \vdots & \ddots & \vdots \\ \chi_1(x_n) & \chi_2(x_n) & \dots & \chi_n(x_n) \end{vmatrix} \quad (1.8)$$

The variation principle is then used to identify the best possible wavefunction of the above functional form that minimizes the expectation value of the energy

$$E_0 = \langle \psi_0 | \hat{H} | \psi_0 \rangle \quad (1.9)$$

The above determinant is only one of the possible forms that could be obtained from  $n$  spin orbitals. Therefore, Hartree-Fock energy is always higher than the exact ground state energy of the system. The difference between the exact energy of the system and Hartree-Fock energy gives us correlation energy. Correlation can be divided into two major categories; dynamic and static[2]. It is defined as dynamic if the contribution of the Hartree-Fock Slater determinant to the FCI wavefunction is large, that is  $c_0 \gg c_a^r, c_{ab}^{rs}, \dots$ . The dynamic correlation arises because of small non-zero occupancies of virtual orbitals. Whereas static correlation is the result of degeneracies between multiple determinants. Mathematically, static correlation occurs when the Hartree-Fock contribution is comparable to or smaller than one of the other determinants, for example  $c_0 \approx c_a^r > c_{ab}^{rs}$ . The exact wavefunction which contains information about both static and dynamic correlation can be obtained by taking a linear combination of all the possible Slater determinants formed from a complete set of spin orbitals. This exact wavefunction with reference to the Hartree-Fock determinant is

given by

$$|\Phi\rangle = c_0 |\psi_0\rangle + \sum_{ra} c_a^r |\psi_a^r\rangle + \sum_{\substack{a|b \\ r|s}} c_{ab}^{rs} |\psi_{ab}^{rs}\rangle + \sum_{\substack{a|b|c \\ r|s|t}} c_{abc}^{rst} |\psi_{abc}^{rst}\rangle + \dots \quad (1.10)$$

where indices a,b,... denote the occupied set of orbitals and indices r,s,... denote unoccupied/virtual orbitals. This procedure of including all the spin-orbital configurations is called full configuration interaction(FCI). Unfortunately, implementing this method in practice is computationally infeasible because of the exponential increase in the number of determinants as the system size grows. Therefore, to study the chemical systems of interest, one has to make a trade-off between accuracy and computational cost. We need theoretical methods which can capture the electronic correlation in a chemically reliable, computationally efficient, and systematically improvable way.

## 1.2 Electronic Structure Theory Formalisms

### 1.2.1 Wavefunction Theories

In the wavefunction domain, many other approximations beyond the level of Hartree-Fock approximation have been made. Most of these approximations tend to capture one of the two types of nature of electron correlation, static or weak correlation and dynamic or strong correlation. Methods that capture weak correlations are classified as single reference methods, and those that capture strong correlations are classified as multi-reference methods. Single reference methods include perturbative methods (MP2 [3], MP3 [4], ...), configuration interaction methods (CIS, CISD, CISDT, ...)[5] and couple-cluster methods (CCSD, CCSDT, CCSD(T), CCSDTQ, ...) [6, 7]. Table 1.1 provides an estimate of the cost of all these methods with respect

	Cost	Method
	$N^4$	HF
	$N^5$	MP2
!bth	$N^6$	MP3, CISD, MP4, CCSDQ CCSD, QCISD
	$N^7$	MP4, CCSD(T) QCISD(T)
	$N^8$	MP5, CISDT, CCSDT
	$N^9$	MP6
	$N^{10}$	MP7, CISDTQ, CCSDTQ

Table 1.1: Computational cost of many of the approximate wavefunction based methods. Here  $N$  is the number of orbitals in the system in a given basis.

to system size. Active space based methods like complete active space self-consistent field(CASSCF)[8], complete active space second order perturbation(CASPT2)[9],  $n$ -electron valence second order perturbation(NEVPT2)[10, 11], restricted active space self-consistent field(RASSCF)[12], etc can capture some fraction of the strong correlation but they are limited by how big the active space can be. Moreover, wavefunction based methods are mostly used for zero temperature calculations, including temperature dependence in these methods is very expensive.

### 1.2.2 Density Based Theories

Frameworks other than the wavefunction framework have also been explored. One such example is density functional theory(DFT)[13, 14, 15, 16]. DFT works with electronic density,  $n(\vec{r})$  instead of the wavefunction,

$$n(\vec{r}) = N \int d^3r_2 \dots \int d^3r_N \Psi^*(\vec{r}, \vec{r}_2, \dots, \vec{r}_N) \Psi(\vec{r}, \vec{r}_2, \dots, \vec{r}_N) \quad (1.11)$$

hence reducing the number of coordinates from  $3N$  of wavefunction to 3. It is in essence the mapping of many electron interacting system to a non-interacting Kohn-Sham system that has the same electronic density as the actual system. In principle, it is an exact theory if one can find a universal functional to describe exchange and correlation in all physical systems but finding such a functional remains a challenge

till date. Various approximations to this functional have been made over the years which include local density approximation(LDA)[17, 18], generalized gradient approximation(GGA) [19, 20], hybrid functional [21, 22] etc. DFT can be used to obtain an accurate energetic and structural description of many materials with reasonable computational effort, but it can sometimes lead to qualitatively wrong results when used for calculating quantities like band gaps. For example, DFT underestimates the band gaps for low-gap semiconductors like Si, Ge, etc, thus predicting a metallic ground state [23]. Another difficulty with DFT is the semi-empirical nature of DFT functionals and the absence of a universal functional which can be used for all the systems.

### 1.2.3 Green's Function Theories

A slightly different and less explored electronic structure theory framework is in terms of one-particle Green's function. In quantum chemistry, Green's functions can be described as response functions when a particle is added or removed from an n-electron system. In this thesis, we work with the Green's function formalism. We choose this method because of the convenience associated with multiple unique features of Green's functions. Most importantly, Green's function language makes it easier to study the contribution of the nth order perturbation theory compared to other field operators[24]. Moreover, they contain information about the excited state spectra along with the ground state properties of the system. We can also access thermodynamic properties at various temperatures using certain Green's function formalism. The spectral function can also be calculated from Green's function, which describes the dispersion relation of quasi-particle excitation of a system and helps study the mechanism behind high-temperature superconductivity, magnetic materials, etc. However, Green's function is a complex quantity to compute. Various approximate Green's function theories include perturbation theories[25, 26, 27] like GF2, GF3, etc,

coupled cluster theories like Green’s function coupled cluster(GFCC)[28, 29, 30, 31], and embedding theories like dynamic mean field theory(DMFT)[32, 33], self-energy embedding theory(SEET)[34, 35, 36, 37], etc.

Despite its advantages over other formalisms, Green’s function theories suffer from the same problem of exponential computational scaling. Therefore, we propose the use of quantum computers for calculating Green’s function.

### 1.3 Quantum Chemistry on Quantum Computers

In 1982, Feynman came up with the idea of using quantum machines instead of classical machines for the simulation of quantum mechanics[38]. Quantum computers reduce the scaling of classical algorithms from exponential to polynomial by leveraging the superposition and entanglement between the quantum bits.

Feynman’s idea was followed by various quantum algorithms such as Shor’s algorithm[39] for factorization of integers, Grover’s algorithm[40] for unstructured search, etc. All these algorithms showed a reduction in computational complexity compared to their classical counterparts. The first quantum algorithm for the simulation of quantum mechanics was proposed by Lloyd in 1996 [41]. And the first realization of a quantum simulation on a quantum machine was achieved in 1999 [42] on an NMR-based quantum information processor [43, 44]. More information on this early history can be found in ref [45]. Since then, there has been steady progress in the field both in terms of hardware development as well as quantum algorithms. The most recent hardware implementations include a 127-qubit quantum processor based on superconducting technology [46]. And  $BeH_2$  and  $N_2$  are the largest molecules to be simulated on quantum hardware [47, 48, 49].

In theory, quantum computing has shown promise in solving exponentially scaling algorithms in polynomial time[50, 51] but there are multiple challenges associated



with the physical realization of those theories. The most obvious limitation is the number of qubits on a machine, however, that is not the only thing we care about. The current machines have limited interconnectivity between the qubits and suffer from environmental noise. They are also plagued by shorter coherence times and the noise associated with each quantum operation, thus limiting the length of calculations that can be performed on them. Error-correction codes [52, 53, 54, 55, 56, 57, 58, 59] have been suggested to tackle the problems of noise and decoherence, but they are far from realization in practice. While these difficulties seem disconcerting, we should realize that the field of quantum computing is still in its budding stage and classical computing had to face these challenges as well and that classical algorithms were already being studied before the field was fully developed. Moreover, working with existing technology, which was coined as noisy intermediate scaling quantum (NISQ) technology [60], might enhance our understanding of the principles of quantum mechanics. This motivates us to develop algorithms that are suitable for these NISQ machines so that we can study more complex systems with the current or near-term hardware.

The work of this thesis primarily focuses on developing the above-mentioned algorithms i.e. which require a low circuit depth and can be executed within a limited coherence time. The general framework of this dissertation is as follows. I will start by giving a brief overview of existing quantum algorithms in chapter 2, followed by a discussion on Green's function based methods necessary for understanding this work in chapter 3. Chapters 4 and 5 of this thesis are based on our published articles [61, 62]. Chapter 6 is based on the manuscript under preparation.

## CHAPTER II

# Quantum Computing

The advent of quantum computers has revolutionized the field of physics and chemistry simulations. It has been proposed that quantum computers can attain a reduction in scaling of certain algorithms by leveraging the principles of quantum mechanics, namely superposition and entanglement. This is achieved through quantum bits. Analogous to the way bits are fundamental units of classical computers, quantum bits or qubits are the units of a quantum computer. Unlike classical bits which are binary in nature, qubits can exist in a superposition of two states before being measured. For instance, while a classical bit can be in only 0 or 1 state at a time, a qubit can exist in any superposition of the basis states  $|0\rangle$  and  $|1\rangle$ ,

$$\alpha_0 |0\rangle + \alpha_1 |1\rangle \tag{2.1}$$

where  $\alpha_0$  and  $\alpha_1$  are complex numbers satisfying  $|\alpha_0|^2 + |\alpha_1|^2 = 1$  and  $|0\rangle = \begin{pmatrix} 1 \\ 0 \end{pmatrix}$  and  $|1\rangle = \begin{pmatrix} 0 \\ 1 \end{pmatrix}$  are vectors in the 2 dimensional Hilbert space. Similarly, the state of an n-qubit register can exist as a statevector of  $2^n$  dimensional Hilbert space.

## 2.1 Experimental Realization

A lot of effort is directed toward building quantum computers these days. The first question that arises while building such systems is what kind of systems can be used to physically realize the qubits. Although it is very hard to find the technology that provides us with the required level of control over quantized 2-level systems, we list here the physical systems that have shown potential in their ability to construct scalable, fault-tolerant quantum computers:

- **Superconducting Qubits:** There are three types of superconducting qubits: flux, charge, and phase. The two quantum states in these qubits are characterized by different states of the superconducting circuit concerning the respective properties[63, 64]. For the flux qubits, it is the different number of flux quanta trapped in the circuit, for the charge qubits, it is the number of cooper pairs of electrons and for the phase qubits, the two states correspond to different charge oscillation amplitudes. These qubits have been used to construct the largest known quantum computers including IBM's 127-qubit eagle processor [46], Google's 53-qubit machine used to show quantum supremacy [65], and 62-qubit computer at the University of Science and Technology of China [66]. Superconducting qubits have low error rates associated with the gates and are easier to implement, thus making them scalable but they suffer from shorter coherence times.
- **Trapped-ion Qubits:** Ions trapped in free space by an electromagnetic field can also be used to encode qubits. The two quantum states are achieved through the different energy states of the ions and coupling can be induced by lasers[67, 68]. Trapped-ion qubits are extremely stable and have longer coherence times, however, they are very hard to implement. The largest trapped ion quantum machine has 32 qubits [69].

Apart from the above-discussed technologies, many other physical systems are being studied, for example, spin qubits, linear optical system, etc. It is still a matter of debate on which one is better as most of these technologies are in their early experimental stages.

## 2.2 Qubit States and Operations

A single qubit can be visualized as a point on the surface of the Bloch sphere as in Fig. 2.1 and any single qubit gate can be defined as the operation that can cause these changes in the qubit [70]. Using the spherical coordinates, a general qubit state can be written as

$$|\Psi\rangle = \cos\left(\frac{\theta}{2}\right)|0\rangle + e^{i\phi}\sin\left(\frac{\theta}{2}\right)|1\rangle \quad (2.2)$$

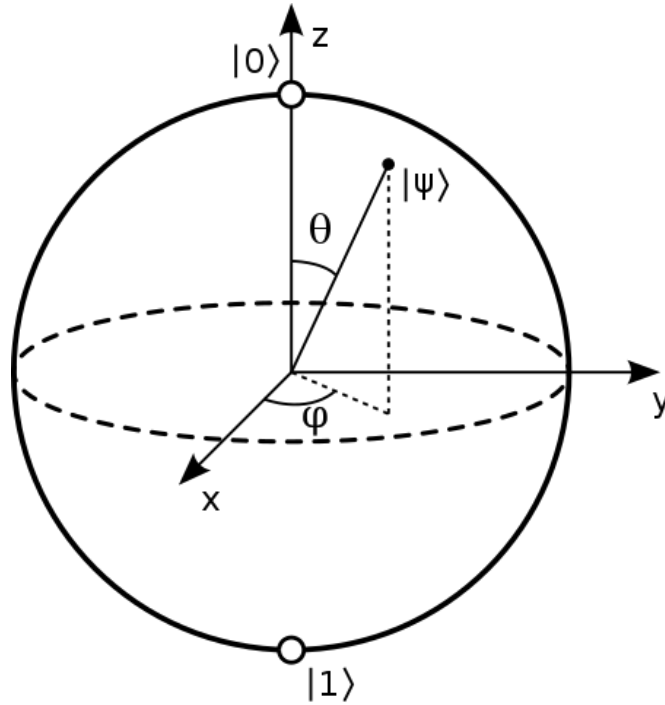


Figure 2.1: Bloch Sphere representing the state of a single qubit geometrically

Systems with more than one qubit cannot be represented using this sphere and exist in the tensor product state of the basis states of qubits. For example, a system

with two qubits has 4 possible states,  $|0\rangle \otimes |0\rangle$ ,  $|1\rangle \otimes |1\rangle$ ,  $|0\rangle \otimes |1\rangle$  and  $|1\rangle \otimes |0\rangle$ . More generally speaking, a system with n-qubits has  $2^n$  basis states of the form  $|\Psi_1\rangle \otimes |\Psi_2\rangle \otimes \dots \otimes |\Psi_n\rangle$ .

Quantum computations are performed by circuits of quantum logic gates. An example of a very basic quantum circuit that creates and measures an entangled state can be seen in Figure 2.2.

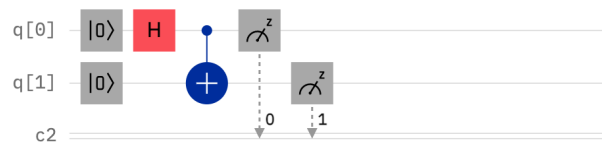

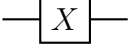
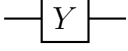

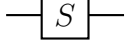
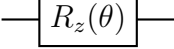
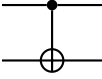


Figure 2.2: Quantum circuit for creation and measurement of bell state. Here the initial states of two qubits are  $|0\rangle$  and  $|1\rangle$ , entanglement is being produced by the application of the Hadamard gate on the control qubit followed by the CNOT gate, and the measurement is done in the standard basis.

A quantum circuit is read from left to right and the horizontal lines in the circuit represent the flow of information. And the quantum gates can be represented using a  $2^n \times 2^n$  matrix for any n qubit operation. Some of the most common quantum gates are listed in table 2.1 along with their symbols and matrices [71]. One important feature of quantum gates unlike many classical gates is that they need to be reversible in nature, that is the matrix representing them should be unitary. This follows directly from Landauer's principle which states that when some information is erased it leads to energy dissipation. This dissipated energy or extra information can disturb the functioning of a quantum computer [71]. This reversible model of computation can be achieved using extra qubits whose values are known apriori, called ancilla qubits and by using the controlled gates mentioned in table 2.1.

Operation	Gate Symbol	Matrix
Single Qubit Gates		
Hadamard		$\begin{bmatrix} 1 & 1 \\ 1 & -1 \end{bmatrix}$
Pauli-X		$\begin{bmatrix} 0 & 1 \\ 1 & 0 \end{bmatrix}$
Pauli-Y		$\begin{bmatrix} 0 & -i \\ i & 0 \end{bmatrix}$
Pauli-Z		$\begin{bmatrix} 1 & 0 \\ 0 & -1 \end{bmatrix}$
Phase		$\begin{bmatrix} 1 & 0 \\ 0 & i \end{bmatrix}$
Rotation		$\begin{bmatrix} 1 & 0 \\ 0 & e^{i\theta} \end{bmatrix}$
Two Qubit Gates		
CNOT		$\begin{bmatrix} 1 & 0 & 0 & 0 \\ 0 & 1 & 0 & 0 \\ 0 & 0 & 0 & 1 \\ 0 & 0 & 1 & 0 \end{bmatrix}$

SWAP		$\begin{bmatrix} 1 & 0 & 0 & 0 \\ 0 & 0 & 1 & 0 \\ 0 & 1 & 0 & 0 \\ 0 & 0 & 0 & 1 \end{bmatrix}$
Multi Qubit Gates		
Toffoli(CCNOT)		$\begin{bmatrix} 1 & 0 & 0 & 0 & 0 & 0 & 0 & 0 \\ 0 & 1 & 0 & 0 & 0 & 0 & 0 & 0 \\ 0 & 0 & 1 & 0 & 0 & 0 & 0 & 0 \\ 0 & 0 & 0 & 1 & 0 & 0 & 0 & 0 \\ 0 & 0 & 0 & 0 & 1 & 0 & 0 & 0 \\ 0 & 0 & 0 & 0 & 0 & 1 & 0 & 0 \\ 0 & 0 & 0 & 0 & 0 & 0 & 0 & 1 \\ 0 & 0 & 0 & 0 & 0 & 0 & 1 & 0 \end{bmatrix}$

Table 2.1: List of Quantum Logic Gates.

## 2.3 Early Quantum Algorithms For Quantum Chemistry

Quantum chemistry simulation is considered one potential area where one could achieve quantum advantage[72]. The first step to simulating quantum systems on quantum machines is representing the quantum problem on the machine. Therefore, before discussing the quantum simulation algorithms, we would like to discuss some of the popular mapping techniques. The idea is to transform the Hamiltonian repre-

senting fermionic interactions into qubit Hamiltonian, which is a more natural form for quantum simulation.

### 2.3.1 Fermionic Hamiltonian to Qubit Hamiltonian

- **Jordan-Wigner Mapping:** This is the most straightforward form of mapping where the occupation of  $i^{th}$  spin orbital is represented by the state of  $i^{th}$  qubit [73]. The qubit state  $|1\rangle$  indicates an occupied spin-orbital whereas state  $|0\rangle$  indicates an unoccupied one, thus there is a one-to-one correspondence between the Slater determinants and the qubit states. We then require a way to represent the electronic creation and annihilation operators in terms of the qubit operators, which can perform the following operations:

$$\hat{Q}^\dagger |0\rangle = |1\rangle; \quad \hat{Q}^\dagger |1\rangle = 0; \quad \hat{Q} |0\rangle = 0; \quad \hat{Q} |1\rangle = |0\rangle \quad (2.3)$$

and follow the anti-commutation relations:  $\{a_i^\dagger, a_j^\dagger\} = \{a_i, a_j\} = 0$  and  $\{a_i^\dagger, a_j\} = \delta_{ij}I$ . This is accomplished by performing a sequence of Pauli Z operations on the preceding qubits

$$a_i^\dagger = \frac{1}{2}(X_i - \iota Y_i) \otimes_{(j<i)} Z_j; \quad a_i = \frac{1}{2}(X_i + \iota Y_i) \otimes_{(j<i)} Z_j \quad (2.4)$$

The purpose of this operation is to introduce a phase shift of -1 if the parity of the qubits before index  $j$  is odd and to not make a change if the parity is even. Using the Jordan-Wigner encoding, fermionic Hamiltonian can be expressed as a linear combination of products of Pauli operators

$$H = \sum_j h_j P_j = \sum_j h_j \prod_{i=0}^{N-1} \sigma_i^j \quad (2.5)$$



where  $\sigma_i^j$  represents the Pauli operator acting on the  $i^{\text{th}}$  qubit and  $N$  is the number of spin-orbitals.  $h_j$  are real scalar coefficients and should not be confused with the 1-electron and 2-electron integrals.

- **Parity Mapping:** Parity mapping is an alternative form of mapping which differs from Jordan-Wigner mapping in terms of how the occupation number and parity are stored. In Jordan-Wigner, occupation number is stored locally whereas parity is stored non-locally i.e. one needs to measure all the preceding qubits to determine the parity. Whereas in parity mapping, instead of using qubit  $j$  to store the parity of only  $j^{\text{th}}$  orbital, we use it to store the parity of all the orbitals up to  $j$  [74]. However, now we cannot represent the creation and annihilation operators by using  $\hat{Q}^\dagger$  and  $\hat{Q}$ , because  $j^{\text{th}}$  qubit doesn't hold information about the orbital occupation but about the parity of qubits up to  $j$ . The operator equivalent to  $\hat{Q}^\dagger$  and  $\hat{Q}$  in the parity basis is given by a two-qubit operator acting on qubits  $j$  and  $j-1$ :

$$\begin{aligned}\hat{P}_j^\dagger &= \hat{Q}_j^\dagger \otimes |0\rangle \langle 0|_{j-1} - \hat{Q}_j \otimes |1\rangle \langle 1|_{j-1} = \frac{1}{2}(X_j \otimes Z_{j-1} - \iota Y_j); \\ \hat{P}_j &= \hat{Q}_j \otimes |0\rangle \langle 0|_{j-1} - \hat{Q}_j^\dagger \otimes |1\rangle \langle 1|_{j-1} = \frac{1}{2}(X_j \otimes Z_{j-1} + \iota Y_j)\end{aligned}\quad (2.6)$$

It is important to realize here that the creation or annihilation of a particle will change the parity data and thus we must update that by the application of  $\sigma_x$  to all the qubits after  $j$ . Parity equivalent of creation and annihilation operators is thus given by:

$$\begin{aligned}\hat{a}_j^\dagger &= \frac{1}{2}((\prod_{j+1}^N \sigma_x) \otimes X_j \otimes Z_{j-1} - (\prod_{j+1}^N \sigma_x) \otimes \iota Y_j); \\ \hat{a}_j &= \frac{1}{2}((\prod_{j+1}^N \sigma_x) \otimes X_j \otimes Z_{j-1} + (\prod_{j+1}^N \sigma_x) \otimes \iota Y_j)\end{aligned}\quad (2.7)$$

Note that we do not improve on the efficiency of the mapping by using this alternative scheme, since, we are just trading the string of  $\sigma_z$ s with the string of  $\sigma_x$ s.

- **Bravyi-Kitaev Mapping:** Bravyi-Kitaev mapping attempts to improve the scaling of both Jordan-Wigner and parity mappings by balancing the local storage of parity and occupation [75, 76]. The information stored locally depends on the index of the orbital, when  $j$  is even, qubit  $j$  stores the occupation number of orbital  $j$  and when  $j$  is odd, qubit  $j$  stores the parity of a particular set of orbitals. The qubit equivalents of creation and annihilation operators in this transformation are given by:

$$\begin{aligned} a_j^\dagger &= \frac{1}{2}(X_{U(j)} \otimes X_j \otimes Z_{p(j)} - \iota X_{U(j)} \otimes X_j \otimes Z_{p(j)}) \\ a_j &= \frac{1}{2}(X_{U(j)} \otimes X_j \otimes Z_{p(j)} + \iota X_{U(j)} \otimes X_j \otimes Z_{p(j)}) \end{aligned} \quad (2.8)$$

where  $U(j)$  and  $P(j)$  represent the update and parity sets of qubit  $j$ . These sets are explained in more detail in reference [76]. Bravyi-Kitaev mapping thus provides an alternative fermion to qubit mapping that balances the storage of occupation number and parity with the complexity of  $O(\log(N))$ , where  $N$  is the number of orbitals.

The first quantum system was simulated on a quantum computer by Seth Lloyd in the year 1996 [41], using Kitaev's algorithm [77] for estimating the eigenvalues of unitary operators. Subsequent works by Lloyd and Abrams [51] implemented these techniques for the fermionic systems. This algorithm is now widely known as Quantum Phase Estimation(QPE) and a brief description of the algorithm follows in the next section.

### 2.3.2 Quantum Phase Estimation(QPE)

In quantum chemistry, QPE is a quantum algorithm used for estimating the eigenvalues of the Hamiltonian operator. It works under the assumption that we have access to the exact ground state  $|\Psi\rangle$  of operator  $H$ . The general algorithm for QPE is as follows:

1. Represent the Hamiltonian operator in the form of unitary operator such that  $\hat{U} = e^{iH\tau}$  and  $\hat{U}|\Psi\rangle = e^{i2\pi\phi}|\Psi\rangle$ . Here, the eigenvalue of  $H$  is mapped to the phase of  $U$ ,  $E = 2\pi\phi/\tau$ .
2. Prepare two-qubit registers as shown in Fig. 2.3, readout register(top) containing  $m$  ancilla qubits in the state  $|0\rangle^{\otimes m}$  and the state register(bottom) containing  $N$  qubits to represent the wavefunction of the system under study. The initial state of the system is in state:  $|\Phi\rangle = |0\rangle|\Psi\rangle$
3. Apply Hadamard gates to the readout register, this puts the circuit in a superimposed state given by  $|\Phi_1\rangle = \frac{1}{\sqrt{2^m}} \sum_{x=0}^{2^m-1} |x\rangle|\Psi\rangle$ .
4. Apply the controlled unitary gates shown in Fig. 2.3 to time evolve the state register. Controlled application of  $U$  when the ancilla is in  $|1\rangle$  state, helps accumulate the phase between  $|0\rangle$  and  $|1\rangle$  state of ancilla. Time evolved state of the system is  $|\Phi_2\rangle = \frac{1}{\sqrt{2^m}} |\Psi\rangle \sum_{x=0}^{2^m-1} e^{2\pi i x E} |x\rangle$
5. Perform a Fourier transform on the readout register to record the phase, which in turn will give us the eigenvalue with a precision that scales linearly with the number of ancilla qubits.

The efficiency of QPE is governed by two factors. One is the construction and implementation of the unitary operators for time-evolving the state and the other is access to a wavefunction with significant overlap with ground state. We begin by discussing the time evolution followed by the description of a method for generating

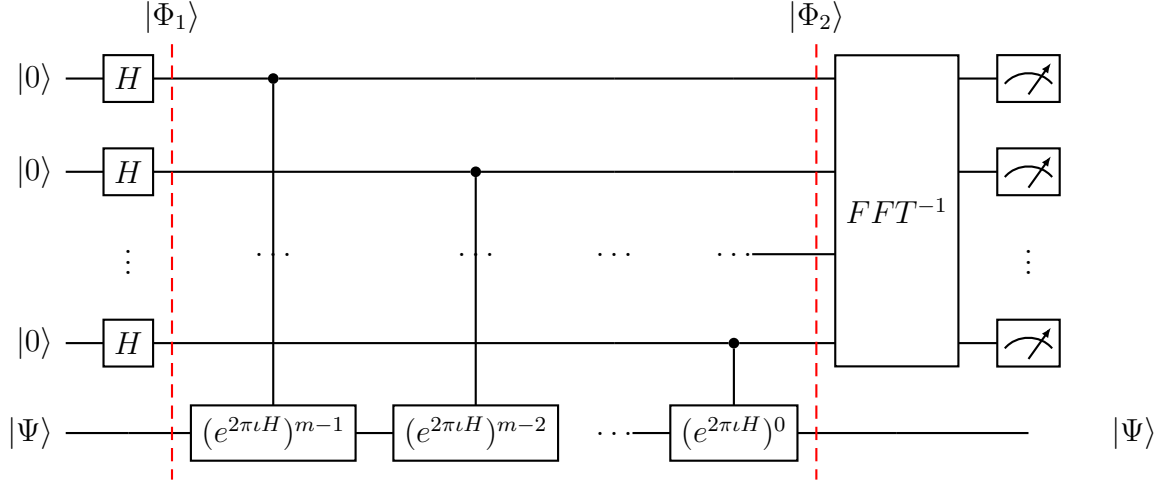


Figure 2.3: Quantum phase estimation circuit with  $m$  ancilla qubits.  $FFT^{-1}$  here means inverse fast Fourier transform and  $|\Psi\rangle$  is the ground state of the system.

such wavefunctions.

The general idea of the time evolution is to represent the unitary matrix as a product of quantum logic gates,  $U = e^{Ht} = e^{t \sum_j H_j t}$ . Note that this cannot be written as a product of exponential operators because the  $H_j$ s don't necessarily commute. Early approximations in this direction are focused on using Trotter-based expansions [78, 79]. Alternative approaches to approximating the unitary operator can be found in references [80, 81, 82, 83, 84].

QPE scales polynomially with the number of orbitals thus providing us with the exponential speedup[50, 51]. Some of the most efficient simulations of QPE have shown a complexity of  $O(N^5 t)$  and  $O(n^2 N^3 t)$ , where  $N$  is the number of spin orbitals and  $n$  is the number of electrons[85]. Further improvements to QPE have been introduced over the years. One of them is iterative phase estimation, where the number of ancilla qubits required to achieve the required precision was decreased [86]. Wiebe and Granade developed Bayesian phase estimation [87], where bayesian inference helps keep track of time-dependent properties and helps increase the algorithm's resilience towards noise and decoherence.

As mentioned earlier, QPE must have access to a wavefunction that has significant overlap with the exact ground state of the system. This problem was addressed with the introduction of adiabatic quantum computing in 2000 [88], which was used by Aspuru-Guzik et al.[89] to prepare the ground state of the fermionic Hamiltonians. QPE and adiabatic state preparation were then combined to study the ground state of chemical systems on the quantum machines.

### 2.3.3 Adiabatic State Preparation

Adiabatic state preparation (ASP) works on the principles of the adiabatic theorem to generate a correlated wavefunction for a given Hamiltonian,  $H_F$ . The adiabatic theorem states that a system will remain in its ground state if its Hamiltonian is evolved slowly enough and if there is a non-zero gap between the ground state and excited state of the given Hamiltonian. Therefore, a correlated wavefunction can be generated by starting from an initial Hamiltonian, say the Hartree-Fock Hamiltonian  $H_{HF}$  and Hartree-Fock wavefunction,  $|\Psi_{HF}\rangle$  and slowly varying the Hamiltonian using a scheduling function,  $s(t)$  from 0 to 1 as shown in Eq. 2.9

$$H(t) = (1 - s(t))H_{HF} + s(t)H_{CI} \quad (2.9)$$

where  $s(t)$  is often defined as  $t/T$ , and  $T$  is the total time of evolution. The efficiency of ASP depends on how fast we can vary the time, which is decided based on the magnitude of the gap between the ground state and excited state energies along the path from  $H_{HF}$  to  $H_{CI}$ . A detailed discussion on the time evolution and choosing the adiabatic path can be found in references [89, 49]

While these algorithms show that quantum problems can be simulated on quantum machines with polynomial scaling. Such scaling is not sufficient to make them practical for the near-term machines, as the exponents and constants for these polynomials

can be quite high. It is also important to emphasize that there are multiple sources of errors which can disturb the functioning of these quantum circuits.

## 2.4 Quantum Noise

Alike early classical computers, quantum machines also suffer from many errors. Classical systems were developed over the years to avoid this noise in most processes while the error-correction codes were used for the rest. Building quantum systems without any errors is a formidable task, quantum computations, therefore, depend majorly on error-correcting codes to protect against noise. The quantum error correcting codes work by using many physical qubits to store the logical information redundantly. Quantum error correction is designed based on the principles of classical error correction but is much more difficult. The reasons behind this are as follows:

- Observing a quantum state destroys the state under observation. Although we need to avoid any interactions of the quantum system with the environment, it is also imperative to control the system from outside to observe the results.
- A quantum state cannot be duplicated as per the no-cloning theorem [90, 91], making it impossible to study and correct the errors by using repetitive code.
- Quantum errors are continuous and accumulate over a large circuit.

The noise associated with a quantum computer can be categorized as coherent and decoherent noise. Decoherent errors occur when a quantum state gets destroyed because of its interaction with the environment. This is often termed decoherence and can arise because of fluctuations in the environment such as temperature changes or external electromagnetic fields. Coherent noise is defined as the slight disturbance to the quantum state as the system progresses through multiple operations. Errors

in quantum gates, measurement errors, and imperfect control of the pulse can all add to coherent noise. This noise doesn't destroy the state of the qubit entirely but leads to accumulation of the errors and thus limits the depth of a quantum circuit. Coherent errors are not as fatal as decoherent errors and can be controlled using error-mitigation techniques.

In theory [92], it is possible to build quantum computers with error-corrected logical qubits, composed of numerous physical qubits, but we are decades away from the hardware required to achieve this. We are now in the era of devices that are beyond the limit of classical simulation but are not yet able to do fully fault-tolerant computations. Preskill [60] used the term "Noisy Intermediate Scaling Quantum(NISQ)" to describe the devices which fall in this gap.

## **2.5 Algorithms For Noisy Intermediate Scaling Quantum(NISQ) Machines**

The algorithms discussed in the previous section are based on the time evolution of a quantum state, and hence require a large number of time steps to reach chemical accuracy, which puts these algorithms out of the reach of near-term computers. In this section, we will discuss algorithms that are more practically suited for NISQ devices. One such set of algorithms which follow the above criteria is hybrid quantum-classical algorithms, where computational tasks are divided between classical and quantum computers based on their inherent advantages. A major workhorse of these hybrid algorithms is the variational quantum eigensolver(VQE).

### **2.5.1 Variational Quantum Eigensolver(VQE)**

Variational quantum eigensolver is a hybrid algorithm based on the variational principle. The variation principle is the basis of various classical quantum chemistry

algorithms and states that given a normalized wave function  $|\Psi\rangle$  which satisfies the boundary conditions, then the expectation value of Hamiltonian is an upper bound to the exact ground state energy[1]. VQE variationally minimizes the eigenvalue of the Hamiltonian operator by optimizing the trial wavefunction. Figure 2.4 shows the schematics of the VQE algorithm and it proceeds as follows:

1. Prepare a trial wavefunction  $|\Psi(\theta)\rangle$  on the quantum computer, where  $\theta$  are the variational parameters
2. Calculate the expectation value,  $E(\theta)$ , of Hamiltonian operator for this trial wavefunction. This is done through a Hamiltonian averaging procedure, where multiple measurements of tensor products of Pauli terms replace the longer coherence time required for QPE.
3. Optimize the parameters,  $\theta$  to minimize the energy eigenvalue using a classical optimizer.
4. Repeat step 1 and 2 until  $E(\theta)$  converges to a given threshold.

The major component of VQE is identifying the ansatz suitable for the trial wavefunction mentioned in step 1, results of VQE depend on how good an ansatz is for a particular problem at hand. One of the most commonly used ansatz for VQE calculations is the unitary couple-cluster(UCC) ansatz [93]. Coupled cluster wavefunctions are parameterized by an exponential ansatz,

$$|\Psi\rangle = e^T |\phi\rangle \tag{2.10}$$

where  $|\phi\rangle$  is a reference state, usually the Hartree-Fock state, and T is a linear combination of excitation operators. The UCC ansatz is a chemically motivated ansatz that preserves the properties of the system. However, this ansatz leads to unfavorably



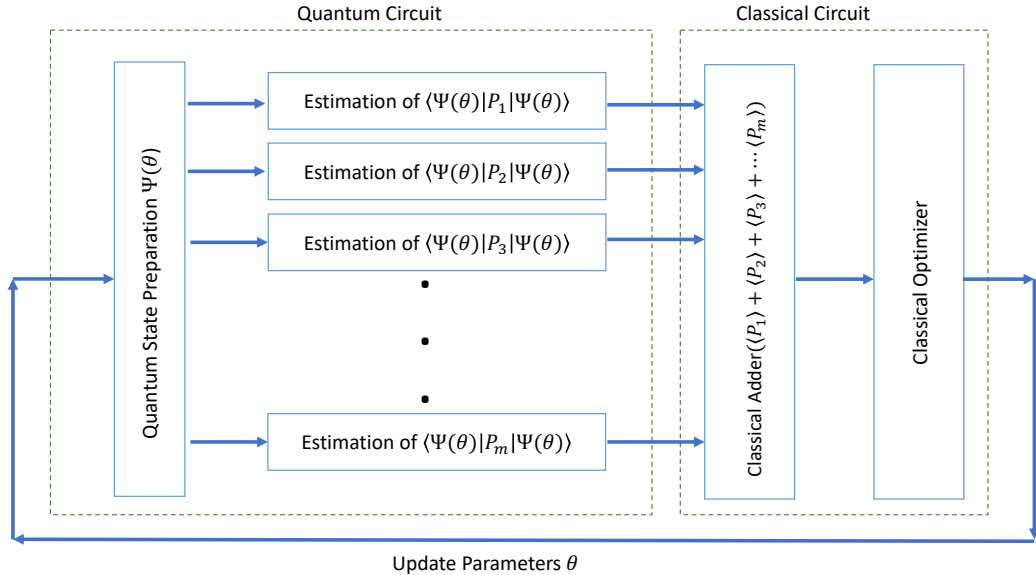


Figure 2.4: Circuit for variational quantum eigensolver.

deep circuits as the number of electrons and spin orbitals in the system increase. Another common ansatz is a hardware efficient ansatz [47] which is built to prepare the ground state in as few gates as possible. They are well adapted to the hardware by design but since they lack the chemical motivation, it can lead to failures beyond some smaller molecules [94]. Several methods [95, 96, 97, 98] have been proposed to mitigate this issue but there is further work required to improve this approach. Therefore, choosing the right kind of ansatz acts as the bottleneck for these VQE algorithms. The chemically motivated and variationally flexible ansatzes require deeper quantum circuits for the state preparation whereas the hardware efficient ansatzes are more system specific.

Alternative approaches to implement VQE have also been explored. The Adaptive Derivative Assembled Pseudo-Trotter (ADAPT) VQE is one such approach, where the ansatz is constructed dynamically from a predetermined pool of operators. The operators that lead to major changes in energy are iteratively added to the ansatz. More details about this method can be found in reference [99]. The projective quan-

tum eigensolver (PQE)[100] is another such example, where the authors make use of projective measurements instead of using the variational principle to minimize the ground state energy. Another alternative implementation VQE is through analog quantum computations, where the parameterized quantum circuit is replaced by direct optimization of a pulse based ansatz. A complete description of this ctrl-VQE approach can be found in reference[101]. Although all these approaches have shown a promise in finding the VQE ansatzes suitable for NISQ machine, investigating more efficient ways to generate a VQE ansatz which minimizes the circuit depth while maximizing the accuracy and universality is an open research question.

All of the above-discussed algorithms work toward finding the correlated wavefunction and the expectation values of the Hamiltonian operator. Quantum algorithms for calculating Green's functions are based on the same principles as these algorithms. In the next chapter, we will discuss these quantum Green's function algorithms in more detail.

## CHAPTER III

# Green's Function on Quantum Computers

Green's function theories play a fundamental role in our treatment of many particle systems as they can be used to study many experimental phenomena theoretically. They are directly related to the experimental quantities, since the response of a system to external probes can be determined through Green's functions. There are two components of Green's functions, one containing information about the cationic states, that is the elimination of a particle from the system and the other contains information about all the anionic states, that is through the addition of a particle to the system. Let us consider a grand-canonical ensemble of  $n$  particles, i.e. the system can exchange energy and particles with the environment. If an electron is added to this  $n$  particle state  $|\Psi_I(t')\rangle$  at a point  $(x', t')$  and propagated in time, the propagation amplitude of a state containing an additional particle for time  $t < t'$  is given by

$$\langle \Psi_I(t) | \hat{a}_{I\alpha}(xt) \hat{U}(t, t') \hat{a}_{I\beta}^\dagger(x't') | \Psi_I(t') \rangle = \langle \Psi_0 | \hat{a}_{H\alpha}(xt) \hat{a}_{H\beta}^\dagger(x't') | \Psi_0 \rangle \quad (3.1)$$

where  $\hat{a}_{I\beta}^\dagger(x't')$  and  $\hat{a}_{I\alpha}(xt)$  are time-dependent fermionic creation and annihilation operators. Similarly, we can obtain the propagator for a state containing an additional hole. Since there can be multiple possibilities of  $|\Psi\rangle$  with an added electron or hole, the one-particle green's function is given by the ensemble average of all these

amplitudes.

$$\iota G_{\alpha\beta}(xt, x't') = \langle \tau \hat{a}_{H\alpha}(xt) \hat{a}_{H\beta}^\dagger(x't') \rangle = \begin{cases} \langle \hat{a}_{H\alpha}(xt) \hat{a}_{H\beta}^\dagger(x't') \rangle & t > t' \\ \pm \langle \hat{a}_{H\beta}^\dagger(x't') \hat{a}_{H\alpha}(xt) \rangle & t' > t \end{cases} \quad (3.2)$$

where  $\langle \dots \rangle$  stands for the grand canonical ensemble average

$$\langle \dots \rangle = \frac{1}{Z} Tr[e^{-\beta H}] \quad (3.3)$$

$Z$  is the partition function for the grand canonical ensemble.  $\tau$  is a time ordering operator which orders the operators in increasing order of time from right to left, while taking into consideration any fermionic exchange through a negative sign. Two separate pairs of correlation functions can now be defined as retarded and advanced Green's functions.

$$\iota G_{\alpha\beta}^R(xt, x't') = \langle \{ \hat{a}_{H\alpha}(xt), \hat{a}_{H\beta}^\dagger(x't') \} \rangle \theta(t - t') \quad (3.4)$$

$$\iota G_{\alpha\beta}^A(xt, x't') = -\langle \{ \hat{a}_{H\alpha}(xt), \hat{a}_{H\beta}^\dagger(x't') \} \rangle \theta(t' - t) \quad (3.5)$$

These advanced and retarded correlation functions are equal to the one-particle Green's function except for near singularities. We must note that for time-independent Hamiltonian, Green's function depends only on the variables  $x - x'$  and  $t - t'$  and not on individual time and position variables (A rigorous proof of this statement can be found in [24]). Retarded Green's function can therefore be rewritten as

$$G_{\alpha\beta}^R(t) = -\iota \theta(t) \langle \hat{a}_{H\alpha}(t), \hat{a}_{H\beta}^\dagger(0) \rangle - \iota \theta(t) \langle \hat{a}_{H\beta}^\dagger(0), \hat{a}_{H\alpha}(t) \rangle \quad (3.6)$$

We can go a step further by writing the time dependence more explicitly

$$\begin{aligned}
G_{\alpha\beta}^R(t) &= -\iota\theta(t)\frac{1}{Z}\text{Tr}[e^{-\beta H}e^{\iota Ht}\hat{a}_{H\alpha}e^{-\iota Ht}\hat{a}_{H\beta}^\dagger] - \iota\theta(t)\frac{1}{Z}\text{Tr}[e^{-\beta H}\hat{a}_{H\beta}^\dagger e^{\iota Ht}\hat{a}_{H\alpha}e^{-\iota Ht}] \\
&= -\iota\theta(t)\frac{1}{Z}\sum_n e^{-\beta E_n}[e^{\iota E_n t}\langle A|\hat{a}_{H\alpha}e^{-\iota Ht}\hat{a}_{H\beta}^\dagger|n\rangle - e^{-\iota E_n t}\langle n|\hat{a}_{H\beta}^\dagger e^{\iota Ht}\hat{a}_{H\alpha}|n\rangle] \\
&= -\iota\theta(t)\frac{1}{Z}\sum_{nm} e^{-\beta E_n}[e^{\iota(E_n-E_m)t}\langle n|\hat{a}_{H\alpha}|m\rangle\langle m|\hat{a}_{H\beta}^\dagger|n\rangle \\
&\quad - e^{-\iota(E_n-E_m)t}\langle n|\hat{a}_{H\beta}^\dagger|m\rangle\langle m|\hat{a}_{H\alpha}|n\rangle]
\end{aligned} \tag{3.7}$$

Relabeling the indices in the second term and taking the Fourier transform of Eq.3.7 gives us the spectral representation of Green's function. We can extract information about the spectral density of states from this representation.

$$G_{\alpha\beta}^R(\omega) = \frac{1}{Z}\sum_{nm} \frac{\langle n|A|m\rangle\langle m|B|n\rangle(e^{-\beta E_n} - e^{-\beta E_m})}{\omega - (E_m - E_n)} \tag{3.8}$$

where  $\omega$  is the frequency. For a non-interacting Green's function, the spectral density function provides us with the delta peaks corresponding to the eigenvalues of the Hamiltonian. When interactions are added to the system, it leads to the broadening of these peaks, providing information about excited state energies and lifetimes.

Green's function, however, is a difficult quantity to compute. One way to calculate Green's function is through perturbative expansion. This expansion however is made difficult by the presence of two mismatching exponentials in Eq. 3.7, one of which,  $e^{-\beta H}$ , is real while the other,  $e^{-\iota Ht}$ , is imaginary. A simple solution to this complication is to set the temperature to zero but that restricts the scope of Green's function to only zero temperature calculations. Another way to solve this problem is by replacing real time with imaginary time,  $it \rightarrow \tau$ . This imaginary time formalism helps perform finite temperature calculations, thus providing us access to thermodynamic quantities. Similar to real-time Green's function, the Fourier transform of imaginary

time Green's function is given by

$$G_{ij}(i\omega_n) = \int_0^\beta G_{ij}(i\tau) e^{i\omega_n \tau} d\tau \quad (3.9)$$

where  $\beta = k_B/T$  and  $\omega_n$  is the frequency and is defined as  $\omega_n = (2n + 1)\pi/\beta$ . Real time and frequency retarded Green's functions can be obtained from their imaginary counterparts by analytical continuation. In the scope of this thesis, we will be discussing mostly about Matsubara Green's function. We refer the interested reader to the references [24, 102, 103] for more details on other Green's function formalisms. We can now go back to using perturbation theory to calculate Green's functions. Let us start by dividing the Hamiltonian into two parts,

$$H = H_0 + V \quad (3.10)$$

where  $H_0$  is the non-interacting Hamiltonian and  $V$  describes its interactions with other particles. This way we can construct  $G$  by summing the non-interacting propagator ( $G_0$ ), propagator with one interaction, propagator with two interactions, etc.

$$G = G_0 + G_0 V G_0 + G_0 V G_0 V G_0 + \dots \quad (3.11)$$

This is the Dyson equation, and the sum of interactions between all the particles is referred to as self-energy. Self-energy is the difference between the energy of the free particle and its quasiparticle form. A quasi-particle can be defined as a particle surrounded by a cloud that forms around it as it propagates through the system and interacts with its environment. Self-energy is the measure of the correlation between particles and can be calculated from interacting and non-interacting Green's function using the Dyson equation.

$$\Sigma = G_0^{-1} - G^{-1} \quad (3.12)$$

Calculating exact self-energy is equally hard as calculating exact Green's function and it can be represented in terms of a perturbative expansion as well. A variety of approaches have been used for calculating the Green's function, either by truncating the series at a finite length or by using embedding techniques like DMFT, SEET, etc. We propose the use of quantum computers for calculating Green's function.

### 3.1 Quantum Algorithms For Green's Function

As mentioned earlier, the quantum algorithms for Green's function calculation are built on the same principles as QPE and VQE algorithms. All of these algorithms start by preparing the ground state of the system using conventional QPE or VQE, followed by the representation of Green's function through unitary operators. The real time Green's function for particle and hole is defined as

$$\begin{aligned} G_{\alpha\beta}^p(t) &= \langle \Psi | c_\alpha(t) c_\beta^\dagger(0) | \Psi \rangle \\ G_{\alpha\beta}^h(t) &= \langle \Psi | c_\alpha^\dagger(t) c_\beta(0) | \Psi \rangle \end{aligned} \quad (3.13)$$

Creation and annihilation operators can then be defined in terms of unitary operators.

$$q_1(t) = c(t) + c^\dagger(t); \quad q_2(t) = \iota[c(t) - c^\dagger(t)] \quad (3.14)$$

In this section, we give a brief overview of how these algorithms differ from each other.

#### 3.1.1 Quantum Phase Estimation Based Algorithms

Some of the early algorithms for calculating Green's functions are based on the QPE scheme. In references [104, 105], authors compute the real time Green's function through time evolution after preparing the ground state using QPE. They first represent the Green's function in terms of unitary operators and then introduce a

probe qubit for all product operators. This probe qubit is coupled to the system of interest, yielding the total density operator,  $\rho_{total} = \rho_{sys} \otimes |0\rangle\langle 0|$ . The state of probe qubit after time evolving the system followed by the controlled application of Pauli gates determines the expectation value for the corresponding Pauli product.

In references [106, 107], authors calculate the real time Green’s function on the quantum machine and extract the imaginary time Green’s function by using spectral function. They start by preparing the ground state of the system through QPE and ASP algorithms. Green’s function is then represented in unitary operators as defined above. Expectation values for these can be obtained by entangling an ancilla with the qubits on which the unitary is applied. The output state of ancilla thus provides the corresponding expectation value. Their algorithm requires eight measurements for each Green’s function element at a given  $t$ . A quantum measurement collapses the state of the system. Therefore, to avoid re-preparation of state after every measurement, a coherent measurement procedure was adopted from the reference[108].

We should note that these algorithms require time-evolution in some form. Here, we would like to emphasize again that time evolution requires a large number of trotter steps, thus rendering these algorithms impractical for NISQ machines. A detailed discussion on the complexity of time evolution algorithms for calculating Green’s functions can be found in reference [109].

### 3.1.2 Variational Quantum Eigensolver Based Algorithms

Variational methods provide a good alternative for calculating Green’s functions on these near-term machines. Reference [110] uses two different methods to calculate Green’s functions. The first method uses a modified version of VQE while the second one is based on Lehmann’s representation of Green’s functions. In the first method, they first prepare the ground state of the system using conventional VQE. This is again followed by representing the creation and annihilation operators in the form of



product of Pauli operators

$$a_k = \sum_{n=1}^{N_k} \lambda_n^{(k)} P_n; \quad a_k^\dagger = \sum_{n=1}^{N_k} \lambda_n^{(k)*} P_n \quad (3.15)$$

Particle Green's function can then be defined as

$$G_{\alpha\beta}^p(t) = \sum_{\alpha\beta} \lambda_\alpha^{(k)} \lambda_\beta^{(k)*} \langle \Psi | e^{\iota H t} P_\alpha e^{-\iota H t} P_\beta | \Psi \rangle \quad (3.16)$$

Thus reducing the problem to solving for the expectation value of Pauli products. In their algorithm, they modify the VQE circuit for measuring expectation value so as to reduce the number of low-fidelity CNOT gates. The second method in the same paper uses Lehmann's representation of the spectral function

$$A_k(\omega) = \sum_n \left( \frac{|\langle E_n | a_k^\dagger | \Psi \rangle|^2}{\omega + E_0 - E_n + \iota\eta} + \frac{|\langle E_n | a_k | \Psi \rangle|^2}{\omega - E_0 + E_n + \iota\eta} \right) \quad (3.17)$$

Energy eigenstates and transition amplitudes of fermion operators are then computed based on subspace search VQE (SSVQE)[111] and multistate contracted VQE(MCVQE)[112] methods. These VQE based methods are an efficient way of calculating the Green's functions but they need quantum circuits with a large number of ancilla qubits and CNOT gates. Both ancilla qubits and CNOT gates are known to decrease the efficiency of quantum calculations because of the large error rates associated with them. Another major challenge associated with variational algorithms is the accurate preparation of wavefunctions on a parameterized quantum circuit.

### 3.1.3 Quantum Subspace Expansion Based Algorithms

Recent work by Rungger[113] and coworkers explores the use of a new class of algorithms, called quantum subspace expansion for Green's function calculations. Quantum subspace expansion(QSE) algorithms work by representing the wavefunc-

tion as a linear combination of basis states instead of preparing it directly on the quantum computer. These basis states can be prepared on the quantum computer individually. The main advantage of QSE algorithms over variational algorithms is that they don't require optimization of circuit parameters, which can be a difficult problem at times. Moreover, QSE can be parallelized over many quantum computers, because each basis state can be prepared on a different machine at the same time. This approach has been used by a lot of algorithms, we direct the interested reader to following references for more details on QSE [114, 115, 116, 117, 118, 112].

The above-mentioned article first prepares the ground state of the system using QSE followed by computation of continued fraction representation of Green's function using Lanczos scheme[119]. They construct an orthogonalized Krylov basis set, starting with  $|\chi_0\rangle = a^\dagger |GS\rangle$ , and iterating to larger  $n$ ,  $|\chi_n\rangle = \hat{H}^n a^\dagger |GS\rangle$ .

We base our quantum algorithm for calculating Green's function on Quantum subspace expansion as well. Our approach however uses QSE to calculate the transition matrix elements, which can then be used to calculate the Green's functions in Lehmann's representation.

We go a step further in making all these algorithms more suitable for NISQ devices by developing an effective Hamiltonian that is sparser in nature. Decreasing the number of terms in the Hamiltonian operator decreases the number of quantum operations, hence making the quantum circuit shallower. This leads to shorter calculations which are good for devices with shorter coherence times. Moreover, a decrease in the number of gates lowers the gate error. We begin by describing this scheme in the next chapter followed by our algorithm for calculating Green's functions.

## CHAPTER IV

# Dynamical Self-energy Mapping (DSEM) for creation of sparse Hamiltonians suitable for quantum computing

Diksha Dhawan<sup>1</sup>, Mekena Metcalf<sup>2</sup>, Dominika Zgid<sup>1,3</sup>

1 – Department of Chemistry, University of Michigan, Ann Arbor, Michigan 48109, USA

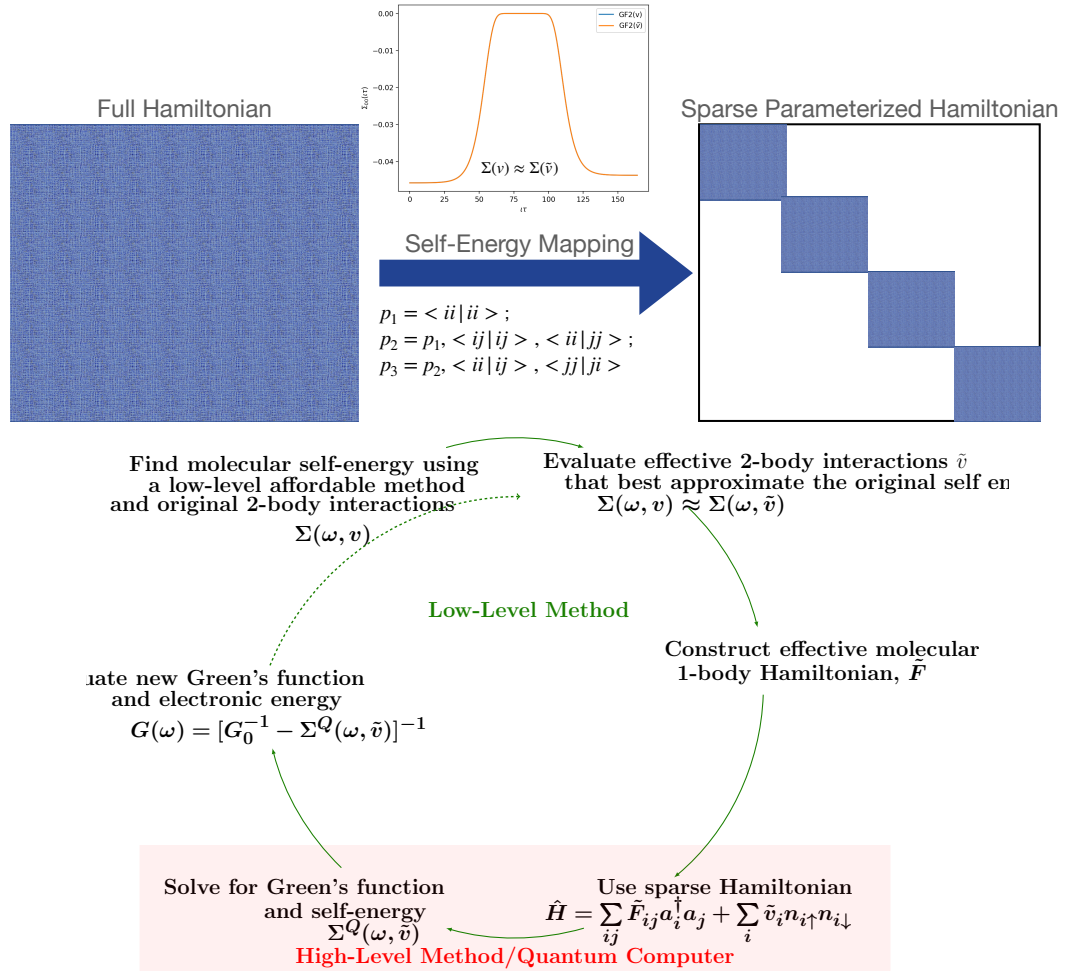
2 – Lawrence Berkeley National Laboratory, 1 Cyclotron Rd, Berkeley, CA 94720

3 – Department of Physics, University of Michigan, Ann Arbor, Michigan 48109, USA

This chapter is adapted from our published article [61].

### 4.1 Abstract

We present a two step procedure called the dynamical self-energy mapping (DSEM) that allows us to find a sparse Hamiltonian representation for molecular problems. In the first part of this procedure, the approximate self-energy of a molecular system is evaluated using a low level method and subsequently a sparse Hamiltonian is found that best recovers this low level dynamic self-energy. In the second step, such a sparse Hamiltonian is used by a high level method that delivers a highly accurate dynamical



part of the self-energy that is employed in later calculations. The tests conducted on small molecular problems show that the sparse Hamiltonian parametrizations lead to very good electronic energies. DSEM has potential to be used as a classical-quantum hybrid algorithm for quantum computing where the sparse Hamiltonian containing only  $\mathcal{O}(n^2)$  terms in a Gaussian orbital basis, where  $n$  is the number of orbitals in the system, could reduce the depth of the quantum circuit by at least an order of magnitude when compared with simulations involving a full Hamiltonian.

## 4.2 Introduction

Creating model Hamiltonians is especially important in condensed matter physics when only a few “important degrees” of freedom need to be modeled at a more accurate level while the remainder of the physical system of interest can be treated approximately. Such effective Hamiltonians can make intractable physical problems accessible to regular classical computations as well as provide a conceptual understanding of the physical processes present in the system. Effective Hamiltonians are commonly used in embedding methods capable of treating strongly correlated problems [120, 121, 122] where many of such Hamiltonians are recovered as a result of a downfolding procedure. In such a procedure, a 1-body Hamiltonian is obtained from a density functional theory (DFT) calculation which is then followed by a projection onto Wannier orbitals [123, 124] and estimation of the lattice model with all the necessary hopping parameters. Subsequently, the 2-body interactions are produced from constrained DFT or random phase approximation (RPA). Effective Hamiltonians can be also obtained as a result of canonical transformation procedure [125, 126, 127], Löwdin orthogonalization method [128], or density matrix downfolding [129, 130]. Effective Hamiltonian formalism has a long history, especially in the context of multi-reference coupled cluster methods (both in Fock as well as in Hilbert space formulations) that result in some form of effective Hamiltonians. This continues to be an active area of development and some important research papers are cited in Refs. [131, 132, 133, 134, 135, 136, 137, 138, 139, 140, 141, 142, 143, 144, 145, 146, 147, 148, 149, 150, 151, 152, 10, 153, 154] In all these methods, a full, computationally demanding solution of a problem is replaced by a computationally less demanding two step procedure involving the construction of a model Hamiltonian and accurate computation with the resulting Hamiltonian.

It is straightforward to envision that a variant of such a procedure could be used in quantum chemistry computations involving quantum computers and here in partic-

ular calculations on noisy intermediate-scale quantum (NISQ) devices [60]. Since in quantum computing applications the number of measurements scales with the number of non-zero terms in the Hamiltonian, handling the full Hamiltonian containing  $n^4$  2-body terms, where  $n$  is the number of orbitals present in a molecular problem is very challenging particularly for NISQ devices, where the number of accessible qubits, gates, and circuits depths are very limited. Consequently, classical–quantum hybrid algorithms resulting in sparse Hamiltonians are naturally best suited computing solutions [155, 156, 157]. The advent of classical-quantum hybrid algorithms has resulted recently in multiple algorithms suitable for this mode of execution, most notably a subspace VQE methods by Takeshita et al. [158], coupled-cluster downfolding methods by Bauman et al. [159, 160, 161], and algorithms by Somma et al. for Hamiltonian simulations in the low energy subspaces [162].

In this paper, we discuss a two step procedure that we call the dynamical self-energy mapping (DSEM) that can in the future be employed as a classical–quantum hybrid algorithm. The first part of this algorithm is using a polynomially scaling algorithm with respect to the number of orbitals present in the problem in order to produce a total approximate Green’s function and self-energy of the molecular problem. The resulting self-energy is then used to parameterize an effective Hamiltonian. This effective Hamiltonian containing only a small parameterized subset of 2-body integrals describes a fictitious system that has the same dynamical part of the self-energy as the parent molecular problem containing all 2-body integrals. Subsequently, this fictitious system described by the sparse Hamiltonian is passed to and solved by an accurate solver yielding non-perturbative dynamical part of the self-energy.

While in this paper, we employ a classical computer to validate this approach, in the future such a solver can be replaced by a quantum machine that produces the self-energy. Since in such a procedure the quantum machine deals only with a very sparse Hamiltonian containing at most  $n^2$  2-body integrals, the number of

gates and the circuit depth are severely reduced as compared to a case when all  $n^4$  2-body interactions are present in the molecular Hamiltonian. Note, that the DSEM algorithm results in a sparse Hamiltonian parameterization for the fictitious system and it gives access to the evaluation of all relevant observables and the electronic energy since it has the same dynamic part of self-energy as the parent system. The ability to rightfully reproduce the self-energy is not always present in the traditional model Hamiltonians that may be designed to reproduce only specific properties.

This paper proceeds as follows. In Sec. 4.3, we explain the basics of the DSEM procedure and discuss how the self-energy necessary for the model Hamiltonian evaluation can be approximated. In Sec. 4.4, we demonstrate the accuracy of our procedure. We conclude in Sec. 4.5.

### 4.3 Method

We define a general Hamiltonian for a chemical system of interest as

$$\hat{H}_{full} = \sum_{ij}^n t_{ij} a_i^\dagger a_j + \frac{1}{2} \sum_{ijkl}^n v_{ijkl} a_i^\dagger a_k^\dagger a_l a_j, \quad (4.1)$$

where  $v_{ijkl}$ , denoted in short as  $\langle ij|kl \rangle$ , are 2-body Coulomb interactions defined as

$$v_{ijkl} = \int \int dr_1 dr_2 \phi_i^*(r_1) \phi_j(r_1) \frac{1}{r_{12}} \phi_k^*(r_2) \phi_l(r_2) \quad (4.2)$$

and containing  $n^4$  terms, where  $n$  is the number of orbitals present in the full molecular problem. The 1-body operator is defined as

$$t_{ij} = \int dr_1 \phi_i^*(r_1) h(r_1) \phi_j(r_1), \quad (4.3)$$

$$h(r_1) = -\frac{1}{2}\nabla_2^2(r_1) - \sum_A \frac{Z_A}{|r_1 - R_A|}. \quad (4.4)$$

For a molecular system of interest the exact Green's function is related to its non-interacting Green's function via Dyson equation

$$\Sigma_\infty + \Sigma(\omega) = [G_0(\omega)]^{-1} - [G(\omega)]^{-1}, \quad (4.5)$$

where  $\Sigma_\infty$  and  $\Sigma(\omega)$  are the static and the dynamical, frequency dependent part of the self-energy, respectively. [1] Both these self-energies arise due to electronic correlations present in the system of interest. The zeroth order Green's function is defined as

$$G_0(\omega) = [(\omega + \mu)S - F]^{-1}, \quad (4.6)$$

where  $\mu$ ,  $S$ , and  $F$  are chemical potential, overlap, and Fock matrix, respectively. Note that here the Fock matrix is defined as

$$F_{ij} = t_{ij} + \sum_{kl} \gamma_{kl}(v_{ijkl} - 0.5v_{ilkj}) \quad (4.7)$$

and can be evaluated using a 1-body density matrix  $\gamma$  that does not necessarily need to come from Hartree-Fock but may come from a correlated method.

The first assumption of the DSEM procedure is that for a molecular system, we will be able to produce an approximate self-energy at a low polynomial cost. In the future when DSEM will be employed as a classical-quantum hybrid algorithm, this approximation to the true self-energy will be produced in the classical part of the algorithm and it can be evaluated in multiple ways, for details see Sec. 4.3.1. In this paper, we approximated the exact dynamical self-energy either as  $\Sigma_1$ , the first coefficient of the high frequency expansion [163] or as  $\Sigma^{(2)}(\omega)$ , the dynamical second-order self-energy from the second order, finite temperature, fully self-consistent Green's



function method (GF2) [164, 165, 166, 167]. In principle, on a classical machine, the approximate self-energy can be evaluated using any polynomially scaling algorithm capable of treating a large number of orbitals (eq. GW [168], FLEX [169, 170], Møller-Plesset second order (MP2) [16]).

The second assumption of our algorithm is that using this approximate self-energy, a Hamiltonian of the fictitious system,  $H_{\text{fic}}$  can be evaluated in such a way that with only a subset of 2-body integrals (here at most  $n^2$ ) and all 1-body integrals of the original problem it recovers very well the approximate self-energy of the original molecular problem. This sparse  $H_{\text{fic}}$  is then used to produce a Green’s function and subsequently a self-energy using a high level non-perturbative method. When DSEM would be executed as quantum-classical hybrid then this part is performed on a quantum machine. In such a case, the sparse fictitious Hamiltonian  $H_{\text{fic}}$  will result in a shallow quantum circuit requiring only a limited number of qubits due to the sparsity of the 2-body integrals. Note that here, the quantum machine evaluated self-energy is exact for a fictitious, auxiliary system defined using a classical machine, however, it is not an exact self-energy of the Hamiltonian containing all interactions. Nevertheless, we expect that the self-energy of the fictitious system will approximate the exact self-energy of the true molecular system very well as we will show in the subsequent sections. The self-energy evaluated using the high level method can then be used to evaluate the total electronic energy and other desired properties.

Here, we summarize the two part DSEM algorithm. **LLP** denotes a part executed by an approximate perturbative method, while **HLP** is employed to describe an accurate high level, non-perturbative solver. Note that if DSEM was executed as a classical-quantum hybrid algorithm then **LLP** is executed on a classical machine while **HLP** part is employing a quantum machine. A schematic picture showing the DSEM algorithm is presented in Fig. 4.1.

**LLP0** Using the Hamiltonian  $\hat{H}_{\text{full}}$  from Eq. 4.1 containing all interactions perform

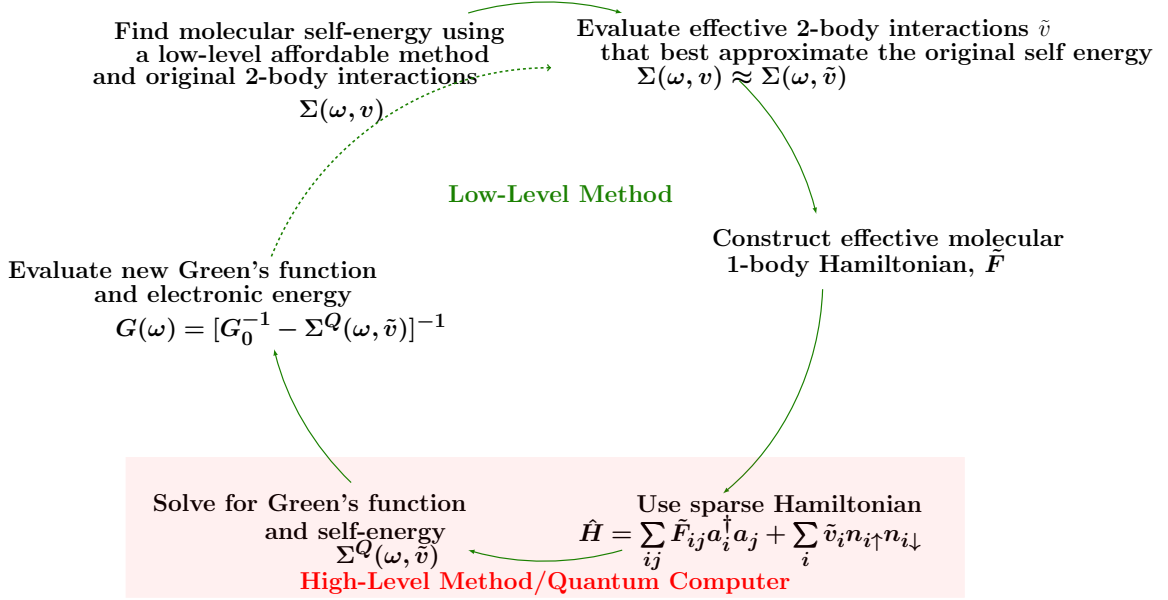


Figure 4.1: Dynamical self-energy mapping (DSEM) algorithm to produce a sparse Hamiltonian for a fictitious molecular system. DSEM can be used as a classical-quantum hybrid algorithm for quantum computing, in which case, the high level method will be executed on the quantum machine.

a HF calculation for the system of interest.

**LLP1** Employ  $\hat{H}_{full}$  to evaluate a self-energy defined as  $\Sigma_\infty(t_{full}, v_{full}) + \Sigma(\omega)(t_{full}, v_{full})$  using a polynomially scaling method (in this paper, we are using GF2). Note, that here we explicitly denote that both parts of the approximate self-energy are evaluated using full 1- and 2-body integrals.

**LLP2** Use the least square fit to find effective integrals  $\tilde{v}$  for which  $\Sigma(\omega)(\tilde{F}, \tilde{v})$  best approximates  $\Sigma(\omega)(t_{full}, v_{full})$  evaluated with full integrals. Note that  $\Sigma(\omega)(\tilde{F}, \tilde{v})$  is evaluated using fictitious Hamiltonian  $H_{fic}$  that contains effective 2-body integrals. For details see Sec. 4.3.1 and 4.3.2.

**HLP0** The fictitious Hamiltonian given by Eq. 4.17 and obtained by a perturbative method is passed to a non-perturbative solver (or a quantum machine).

**HLP1** Evaluate Green's function  $G(\omega)(\tilde{F}, \tilde{v})$  using a high level solver such as exact diagonalization, quantum Monte Carlo, or one of the truncated configuration

interaction (CI) schemes. In a case of quantum execution of this step the Green's function evaluation can be done based on one of the algorithms described in Refs. [171, 172, 110, 105, 173, 174, 107, 175, 176, 108].

**LLP3** Evaluate the self-energy  $\Sigma(\omega)(\tilde{F}, \tilde{v})$  using the Dyson equation.

**LLP4** Employ the self-energy evaluated in **HLP1** to calculate the new Green's function  $G(\omega)$  according to

$$G(\omega) = [(\omega + \mu)S - F - \Sigma(\omega)(\tilde{F}, \tilde{v})]^{-1} \quad (4.8)$$

Note that by writing  $\Sigma(\omega)(\tilde{F}, \tilde{v})$ , we explicitly denote that this self-energy came from the solution of the fictitious problem solved in **HLP1**.

**LLP5** Find chemical potential  $\mu$  yielding a proper number of electrons.

**LLP6** Evaluate a new density matrix  $\gamma$  from the Green's function obtained in **CP4** and a new Fock matrix.

**LLP7** Evaluate 1-body electronic energy as

$$E_{1b} = \frac{1}{2} \sum_{i,j} \gamma_{ij} (t_{ij} + F_{ij}). \quad (4.9)$$

**LLP8** Using the new Green's function and self-energy evaluate 2-body energy according to

$$E_{2b} = \frac{2}{\beta} \sum_{i,j} \text{Re} \left[ \sum_{\omega} G_{ij}(\omega) \Sigma_{ij}(\omega)(\tilde{F}, \tilde{v}) \right]. \quad (4.10)$$

**LLP9** Using the Green's function defined in **LLP4**, it is possible to re-evaluate the self-energy in the **LLP** part of the algorithm and find a new set of effective integrals and continue iterating until electronic energies stop to change

Note that iterations described in **LLP9** are optional, in Sec 4.4, we report results without them. Our observations indicated that the difference between performing only the first iteration and all iterations is small (usually below 1 mE<sub>h</sub>) for the systems studied.

### 4.3.1 Approximating self-energy

Here, we focus on possible approximations to the exact self-energy evaluated in the **LLP** part of the algorithm that can be computed with a polynomial cost. This approximate self-energy is later used to find best effective 2-body integrals for the fictitious Hamiltonian.

#### 4.3.1.1 High frequency expansion of the self-energy

In our previous work [163], we showed that in certain molecular cases, a good approximation to the exact self-energy is obtained by using a high frequency expansion of the self-energy

$$\Sigma(\omega) = \frac{\Sigma_1}{\omega} + \frac{\Sigma_2}{\omega^2} + \frac{\Sigma_3}{\omega^3} + O\left(\frac{1}{\omega^4}\right) \quad (4.11)$$

that is then truncated only to preserve

$$\Sigma(\omega) \approx \frac{\Sigma_1}{\omega}, \quad (4.12)$$

where  $\Sigma_1$  is the first coefficients of the high frequency expansion. This coefficient can be evaluated either in approximate perturbative theories or by employing formulas listed in Ref. [163] that use both 1- and 2-body density matrices. Such a simple approximation for the self-energy can be then employed to evaluate fictitious Hamiltonian containing only on-site 2-body integrals given by the following expression

$$\tilde{v}_{iii} = \sqrt{\frac{2[\Sigma_1]_{ii}}{\gamma_{ii}(1 - \frac{1}{2}\gamma_{ii})}}, \quad (4.13)$$

where  $\gamma_{ii}$  is the on-site 1-body density matrix.

### 4.3.1.2 Frequency dependent self-energy from the second order finite temperature Green’s function perturbation theory (GF2)

For molecular systems, the self-energy obtained in the GF2 method

$$\Sigma_{ij}^{(2)}(\tau) = - \sum_{klmnpq} G_{kl}(\tau)G_{mn}(\tau)G_{pq}(-\tau) \times v_{imqk}(2v_{lprj} - v_{nplj}) \quad (4.14)$$

is a very good approximation to the exact self-energy. Therefore, we evaluate it in a lower level part of the algorithm using the full molecular Hamiltonian. This evaluation scales as  $n^5 n_\tau$ , where  $n$  is the number of orbitals in the molecular problem while  $n_\tau$  is the size of imaginary time grid. Since in this approach, all the elements of the self-energy matrix are produced, we use the least square fitting to find a set of sparse 2-body integrals that yield the best approximation to the second order self-energy, namely

$$\Sigma_{ij}^{(2)}(\tau, t_{full}, v_{full}) \approx \Sigma_{ij}^{(2)}(\tau, \tilde{F}, \tilde{v}). \quad (4.15)$$

We require the sparse 2-body integrals  $\tilde{v}$  depend at most on two indices thus resulting in only  $n^2$  2-body integrals. These optimizations are done in the imaginary time domain. We calculate the distance between the self-energies for a given imaginary time grid point and use the Frobenius norm of the resulting difference matrix as our cost function. All the values for all time grid points were then summed up to create the total objective function

$$f = \sum_{t=\tau_1}^{t=\tau_{max}} \|\Sigma_{ij}^{(2)}(\tau, t_{full}, v_{full}) - \Sigma_{ij}^{(2)}(\tau, \tilde{F}, \tilde{v})\|. \quad (4.16)$$

The optimization is stopped when the desired threshold of 0.001 is reached.

To check the accuracy of this approximation we tested and included multiple

groups of integrals starting from just the on-site integrals and then gradually increasing the set to  $n^2$  integrals containing at most two independent indices.

### 4.3.2 Fictitious Hamiltonian

Note that using the effective integrals obtained either in Sec. 4.3.1.1 or 4.3.1.2, the sparse Hamiltonian that is used subsequently by the high level solver has the following form

$$\hat{H}_{\text{fic}} = \sum_{ij} \tilde{F}_{ij} a_i^\dagger a_j + \frac{1}{2} \sum_{ijkl} \tilde{v}_{ijkl} a_i^\dagger a_j^\dagger a_k a_l, \quad (4.17)$$

where  $\tilde{v}_{ijkl}$  are non-zero only for the chosen integrals groups. The modified Fock matrix  $\tilde{F}_{ij}$  is given by the following equation

$$\tilde{F}_{ij} = t_{ij} + \sum_{kl} \gamma_{kl} (v_{ijkl} - \frac{1}{2} v_{iklj}) - \sum_{kl} \gamma_{kl} (\tilde{v}_{ijkl} - \frac{1}{2} \tilde{v}_{iklj}), \quad (4.18)$$

where  $F_{ij} = t_{ij} + \sum_{kl} \gamma_{kl} (v_{ijkl} - \frac{1}{2} v_{iklj})$  is the Fock matrix produced in GF2, where  $\gamma$  is the 1-body density matrix from GF2 and  $v_{ijkl}$  are the full 2-body integrals. The term  $\sum_{kl} \gamma_{kl} (\tilde{v}_{ijkl} - \frac{1}{2} \tilde{v}_{iklj})$  corresponds to the double counting correction that should be evaluated with the effective 2-body integrals evaluated as discussed either in Sec 4.3.1.1 or 4.3.1.2.

## 4.4 Results

In this section, we will examine our results from different fictitious Hamiltonian parameterizations, namely **(p1)**  $\langle ii|ii \rangle$  on-site 2-body integrals, **(p2)** both on-site integrals as well as  $\langle ii|jj \rangle$ ,  $\langle ij|ij \rangle$  integrals, and **(p3)** on-site integrals and all modified two body integrals with two varying indices out of the total of four indices, namely  $\langle ii|jj \rangle$ ,  $\langle ij|ij \rangle$ , and  $\langle ij|jj \rangle$  integrals. Note that while the DSEM scheme is designed

to be used as a classical–quantum hybrid algorithm, here, to provide validations and benchmarking of this procedure, we performed it entirely on a regular, classical machine. All the parametrizations performed here were done in symmetrized atomic orbitals (SAO). It is an important fact since parametrizations performed in different orbital bases can lead to different structure of the 2-body integrals. To best preserve the existing symmetries, we are retaining all integrals that are equivalent due to symmetry and their final values are made equal.

#### 4.4.1 Hamiltonians with parameterized on-site integrals from high frequency expansion

Initially, we parameterized simple molecular Hamiltonians used for the self-energy evaluation to contain only on-site effective integrals. These integrals can be defined as the 2-body integrals of the form  $\tilde{v}_{iii} = \langle ii|ii \rangle$  where  $i$  is the orbital number. In this paper, to simulate a classical–quantum hybrid computing process, the self-energy was calculated using a polynomially scaling GF2 algorithm. In this section, we focus on the parameterization of the Hamiltonian using only the on-site 2-body integrals coming from the high frequency expansion of the GF2 self-energy.

In Tab. 4.1, for the  $H_6$  ring in the STO-6G basis, we list the 2-body integrals obtained from the high frequency expansion of the GF2 self-energy. The 1-body energies and 2-body energies listed were obtained by employing Eq. 4.9 and Eq. 4.10, respectively. The GF2 and FCI results were evaluated using all  $n^4$  integrals, where  $n$  is the total number of orbitals in the problem. By  $\text{FCI}(\tilde{v})$ , we denote an FCI energy evaluated using effective on-site  $\tilde{v}_{iii}$  2-body integrals parameterized using the GF2 self-energy. We note that the total electronic energy that is recovered by  $\text{FCI}(\tilde{v})$  is very close to the true FCI energy and constitutes 102% of the original correlation energy. The effective on-site integral evaluated in the symmetrized atomic orbital (SAO) basis  $\tilde{v}_{iii} = 0.598096$  is smaller than the bare on-site Coulomb integral  $v_{iii} = 0.9060789$  as

	GF2	FCI	FCI( $\tilde{v}$ )
2-body integrals	all integrals	all integrals	$\tilde{v}_{iii} = 0.598096$
1-body energy	-9.221596	-9.162680	-9.194815
2-body energy	-0.104371	-0.185912	-0.155320
Correlation energy	-0.052695	-0.075320	-0.076999
Electronic energy	-9.325966	-9.348592	-9.350271

Table 4.1: Energy values obtained using GF2, FCI and parameterized FCI( $\tilde{v}$ ) for H<sub>6</sub> ring with interatomic distance R=0.95 Å in the STO-6G basis. The second row lists 2-body integrals that were used in the evaluation of self-energies. All values of energy are listed in a.u. In case of FCI( $\tilde{v}$ ),  $\tilde{v}_{iii}$  denotes the value of the 2-body on-site integral for  $i = 1, \dots, 6$ , all other 2-body integrals are equal to zero.

is expected since it includes the effects of other non-local integrals.

To assess the effect of the basis set increase, we also performed calculations in the DZ basis. In Tab. 4.2, we list results for H<sub>6</sub> ring at R=0.95 Å in the DZ basis. Here, the solution of FCI( $\tilde{v}$ ) with parameterized on-site integrals recovers 94% of correlation energy. Note also the values of the effective integrals  $\tilde{v}_{iii} = 1.001197$  and  $\tilde{v}_{jjjj} = 0.424057$  are smaller than the bare on-site Coulomb integrals  $v_{iii} = 1.20619$  and  $v_{jjjj} = 0.447542$ . Such a difference is expected and it is arising due to inclusion of the non-local effects.

While these results are encouraging, in most cases for more complicated molecular examples, employing only on-site 2-body effective integrals cannot lead to the full recovery of the off-diagonal elements of the self-energy. Since here the off-diagonal elements are only evaluated as a result of the following multiplication  $\Sigma_{ij}^{(2)}(\tau) = -\sum_{ij}[G_{ij}(\tau)]^2 G_{ij}(-\tau) \tilde{v}_{iii} \tilde{v}_{jjjj}$  not enough freedom may be present to find best on-site integrals  $\tilde{v}_{iii}$  that lead to best approximation  $\Sigma_{ij}^{(2)}(\tau, t_{full}, v_{full}) \approx \Sigma_{ij}^{(2)}(\tau, \tilde{F}, \tilde{v}_{iii})$ . We illustrate this observation in Fig. 4.2 by displaying the elements of imaginary part of the self-energy for the H<sub>6</sub> chain in the DZ basis. It is evident that while the diagonal elements of the self-energy are recovered reasonably well, the off-diagonal self-energy elements are not recovered well and are almost equal to zero. Conse-



	GF2	FCI	FCI( $\tilde{v}$ )
2-body integrals	all integrals	all integrals	$\tilde{v}_{iii}=1.001197$ $\tilde{v}_{jjjj}=0.424057$
1-body energy	-9.257054	-9.204537	-9.248869
2-body energy	-0.132880	-0.206746	-0.157235
Correlation energy	-0.066384	-0.087733	-0.082553
Electronic energy	-9.389935	-9.411284	-9.406104

Table 4.2: Energy values obtained using GF2, FCI and parameterized FCI( $\tilde{v}$ ) for H<sub>6</sub> ring with interatomic distance R=0.95 Å in the DZ basis. The second row lists 2-body integrals that were used in the evaluation of self-energies. All values of energy are listed in a.u. In case of FCI( $\tilde{v}$ ),  $\tilde{v}_{iii}$  denotes the value of the 2-body on-site integral for 1s  $i = 1, \dots, 6$ ,  $\tilde{v}_{jjjj}$  denotes the value of the 2-body on-site integral for 2s, all other 2-body integrals are equal to zero.

quently, we conclude that the Hamiltonians with only on-site effective interactions will yield accurate results for systems where the self-energy is majorly diagonal. For other cases a larger number of 2-body integrals is necessary to recover the off-diagonal elements of self-energy.

#### 4.4.2 Modified Hamiltonian parameterization using GF2 self-energy

Here, we focus on parameterization of the fictitious Hamiltonian by finding a small number of effective 2-body integrals that produced a best match between the original GF2 self-energy and the GF2 self-energy evaluated with only the effective  $\tilde{v}$  integrals  $\Sigma_{ij}^{(2)}(\tau, t_{full}, v_{full}) \approx \Sigma_{ij}^{(2)}(\tau, \tilde{F}, \tilde{v})$  as described in Sec. 4.3.1.2. In order to perform these fits we used the least-squares optimization subroutine from `scipy` [177]. We investigate parameterizations with both only on-site and more extensive parameterizations with up to  $n^2$  integrals. Here, we perform the DSEM procedure for several small molecular systems such as H<sub>6</sub> ring, H<sub>6</sub> chain, H<sub>2</sub>O, and Be dimer. We believe that these systems are good examples of molecular problems that at present can be solved using NISQ devices.

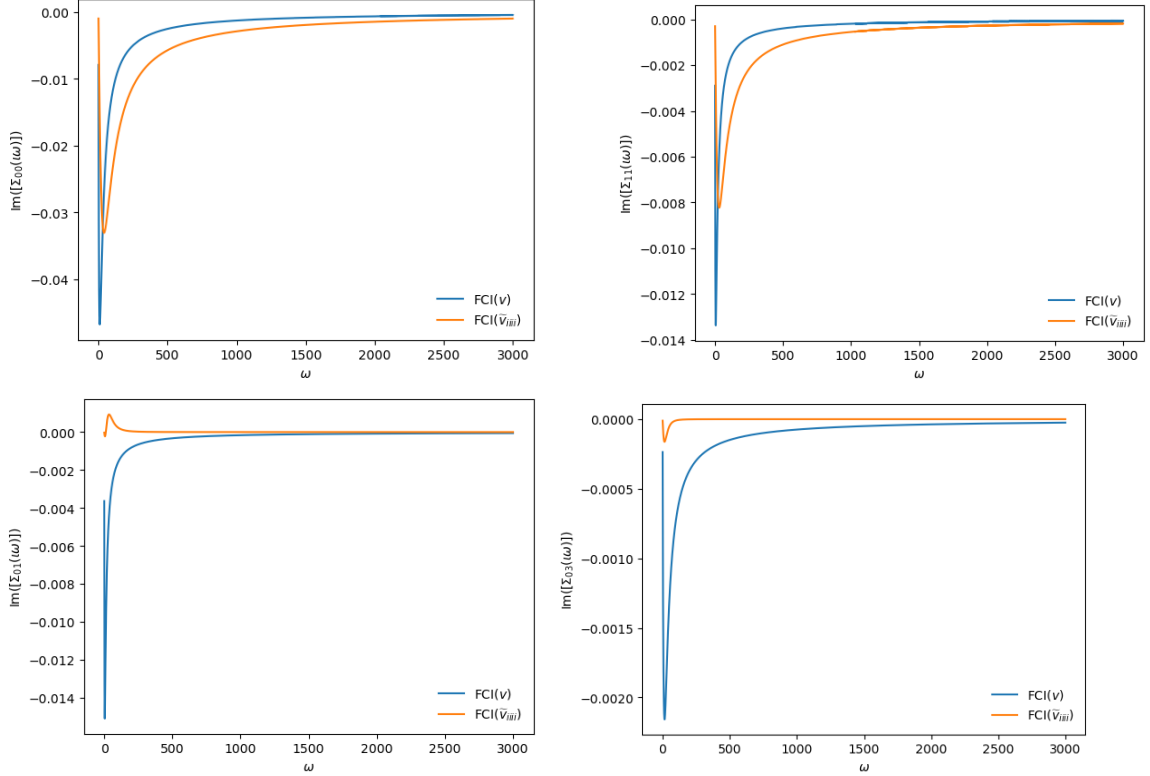


Figure 4.2: The imaginary part of the self-energy for  $H_6$  chain in the DZ basis evaluated in FCI with all integrals (denoted here as  $\text{FCI}(v)$ ) and FCI with effective, on-site 2-body integrals (denoted as  $\text{FCI}(\tilde{v}_{iii})$ ). Top left:  $\text{Im}[\Sigma(i\omega)]_{00}$  element. Bottom left:  $\text{Im}[\Sigma(i\omega)]_{01}$  element. Top right:  $\text{Im}[\Sigma(i\omega)]_{11}$  element. Bottom right:  $\text{Im}[\Sigma(i\omega)]_{03}$  element.

#### 4.4.2.1 $H_6$ ring in the STO-6G basis set

Both the correlation energies and electronic energies for the  $H_6$  ring in the STO-6G basis are presented in Tab. 4.3. We observe that increasing the number of the effective 2-body integrals leads to a significant improvement in the match of the GF2 self-energies  $\Sigma_{ij}^{(2)}(\tau, t_{full}, v_{full}) \approx \Sigma_{ij}^{(2)}(\tau, \tilde{F}, \tilde{v})$  and consequently a significant improvement of GF2 electronic and correlation energies when compared to a GF2 energy evaluated with all the integrals. We analyze three previously mentioned parameterizations p1, p2, and p3. We observed that p2 and p3 parameterizations were completely sufficient to recover the electronic energy beyond 4th digit after decimal point.

In Tab. 4.3, we also list the results of FCI ( $\text{FCI}(p1)$ ,  $\text{FCI}(p2)$ , and  $\text{FCI}(p3)$ )

H <sub>6</sub> ring; Basis: STO-6G								
	GF2(v)	GF2(p1)	GF2(p2)	GF2(p3)	FCI(v)	FCI(p1)	FCI(p2)	FCI(p3)
Correlation energy	-0.05269	-0.06202	-0.05268	-0.05266	-0.07532	-0.06191	-0.08107	-0.06694
Electronic energy(a.u.)	-9.32597	-9.33529	-9.32595	-9.32593	-9.34859	-9.33518	-9.35434	-9.34021

Table 4.3: Energy values obtained using GF2, parameterized GF2, FCI, and parameterized FCI. Symbol p1 stands for a parameterization using  $\langle ii|ii \rangle$  integrals. Symbol p2 stands for a parameterization using  $\langle ii|ii \rangle$ ,  $\langle ij|ij \rangle$ ,  $\langle ij|ji \rangle$  groups of the effective integrals. Symbol p3 stands for a parameterization that uses all the integrals from the p2 group as well as  $\langle ij|jj \rangle$  effective integrals. All values of energy are listed in a.u.

performed using the Hamiltonian parameterized at the GF2 level using the three previously discussed parameterizations. We observe that the results from p2 and p3 parameterizations are around 1 mE<sub>h</sub> per hydrogen away from the FCI energy evaluated with all the integrals. Note also that we only applied a relatively naive fitting where we do not use any sophisticated weighing scheme to differently weigh the diagonal and off-diagonal elements of the self-energy or the low- and high frequency behavior.

#### 4.4.2.2 H<sub>6</sub> chain in the DZ basis set

We investigated how the accuracy of different parameterizations behaves as the number of orbitals in the basis set is increased. In Tab. 4.4, results of these studies for the H<sub>6</sub> chain in the DZ basis are listed. We observe that the GF2 energy evaluated with all the integrals is recovered by parameterization p3 while parameterization p2 is differing only by  $\approx 3$  mE<sub>h</sub>. When Hamiltonian in parameterization p3 is used in FCI, we observe that the result is approximately 1 mE<sub>h</sub> per hydrogen different than the FCI result evaluated with all the integrals.

#### 4.4.2.3 H<sub>2</sub>O in DZ basis set

Studying both the H<sub>6</sub> chain and ring examples in two different basis sets allow us to confirm that when the p3 parameterization in GF2 is very close to the original

H <sub>6</sub> chain; Basis: DZ								
	GF2(v)	GF2(p1)	GF2(p2)	GF2(p3)	FCI(v)	FCI(p1)	FCI(p2)	FCI(p3)
Correlation energy	-0.06677	-0.08606	-0.06958	-0.06623	-0.09584	-0.05678	-0.08102	-0.10139
Electronic energy(a.u.)	-8.13663	-8.15592	-8.13944	-8.13609	-8.16570	-8.12664	-8.15088	-8.17125

Table 4.4: Energy values obtained using GF2, parameterized GF2, FCI, and parameterized FCI. Symbol p1 stands for a parameterization using  $\langle ii|ii \rangle$  integrals. Symbol p2 stands for a parameterization using  $\langle ii|ii \rangle$ ,  $\langle ij|ij \rangle$ ,  $\langle ij|ji \rangle$  groups of the effective integrals. Symbol p3 stands for a parameterization that uses all the integrals from the p2 group as well as  $\langle ij|jj \rangle$  effective integrals. All values of energy are listed in a.u.

H <sub>2</sub> O; Basis: DZ				
	GF2(v)	GF2(p1)	GF2(p2)	GF2(p3)
Correlation energy	-0.13287	-0.19069	-0.13844	-0.13519
Electronic energy(a.u.)	-85.47654	-85.53436	-85.48212	-85.47886

Table 4.5: Energy values obtained using GF2, and parameterized GF2. Symbol p1 stands for a parameterization using  $\langle ii|ii \rangle$  integrals. Symbol p2 stands for a parameterization using  $\langle ii|ii \rangle$ ,  $\langle ij|ij \rangle$ ,  $\langle ij|ji \rangle$  groups of the effective integrals. Symbol p3 stands for a parameterization that uses all the integrals from the p2 group as well as  $\langle ij|jj \rangle$  effective integrals. All values of energy are listed in a.u.

GF2 energy evaluated with all the integrals then the FCI energies recovered from the p3 parameterization is also very close to the original FCI energy. This observation prompts us to analyze examples where calculating the Green’s function in the FCI procedure will result in a significant computational time and memory use. For these cases, we will only examine the systematic improvement present in the p1, p2, and p3 GF2 parameterizations.

In Tab. 4.5, we list GF2 energies resulting from the different parameterizations of the Hamiltonian. Note that both the p2 and p3 parameterizations are only 6 and 2 mE<sub>h</sub> away from the original GF2 energy, respectively.

Be <sub>2</sub> ; Basis: 6-31G				
	GF2(v)	GF2(p1)	GF2(p2)	GF2(p3)
Correlation energy	-0.04814	-0.02047	-0.04463	-0.04651
Electronic energy	-29.18194	-29.15427	-29.17843	-29.18031

Table 4.6: Energy values obtained using GF2, and parameterized GF2. Symbol p1 stands for a parameterization using  $\langle ii|ii \rangle$  integrals. Symbol p2 stands for a parameterization using  $\langle ii|ii \rangle$ ,  $\langle ij|ij \rangle$ ,  $\langle ij|ji \rangle$  groups of the effective integrals. Symbol p3 stands for a parameterization that uses all the integrals from the p2 group as well as  $\langle ij|jj \rangle$  effective integrals. All values of energy are listed in a.u.

#### 4.4.2.4 Be<sub>2</sub> in 6-31G basis set

Finally, in Tab. 4.6, we analyze a small diatomic molecule Be<sub>2</sub> that when calculated in the 6-31G basis set is an ideal test case for calculations on small molecular systems. For this case, similar to the previous cases the GF2 energy coming from the p1 parametrization is not acceptable. However, the p2 parameterization results in energies that are very close to the original GF2 energy. The p3 parameterization yields the energy value with an error as small as 1 mE<sub>h</sub>.

#### 4.4.3 Number of gates for different Hamiltonian parameterizations

		H <sub>6</sub> ring; Basis:STO-6G		H <sub>6</sub> chain; Basis: DZ		H <sub>2</sub> O; Basis: DZ		Be <sub>2</sub> ; Basis: 6-31G	
		JW	BK	JW	BK	JW	BK	JW	BK
2 <sup>8</sup> H(v)	SQG	[3.25×10 <sup>3</sup> ,1.30×10 <sup>4</sup> ]	[4.23×10 <sup>3</sup> ,1.72×10 <sup>4</sup> ]	[1.21×10 <sup>5</sup> ,2.15×10 <sup>5</sup> ]	[1.95×10 <sup>5</sup> ,3.46×10 <sup>5</sup> ]	[2.34×10 <sup>5</sup> ,2.79×10 <sup>5</sup> ]	[3.90×10 <sup>5</sup> ,4.49×10 <sup>5</sup> ]	[2.81×10 <sup>5</sup> , 2.90×10 <sup>5</sup> ]	[4.93×10 <sup>5</sup> , 10.66×10 <sup>5</sup> ]
	CNOT	[5.01×10 <sup>3</sup> ,1.97×10 <sup>4</sup> ]	[4.66×10 <sup>3</sup> ,1.93×10 <sup>4</sup> ]	[3.12×10 <sup>5</sup> ,5.54×10 <sup>5</sup> ]	[2.43×10 <sup>5</sup> ,5.11×10 <sup>5</sup> ]	[7.29×10 <sup>5</sup> ,8.46×10 <sup>5</sup> ]	[4.98×10 <sup>5</sup> ,5.91×10 <sup>5</sup> ]	[10.83×10 <sup>5</sup> ,10.66×10 <sup>5</sup> ]	[6.58×10 <sup>5</sup> , 6.72×10 <sup>5</sup> ]
2 <sup>8</sup> H(p1)	SQG	3.18×10 <sup>2</sup>	5.10×10 <sup>2</sup>	1.35×10 <sup>3</sup>	2.60×10 <sup>3</sup>	1.85×10 <sup>3</sup>	3.65×10 <sup>3</sup>	1.20×10 <sup>3</sup>	2.52×10 <sup>3</sup>
	CNOT	5.72×10 <sup>2</sup>	5.12×10 <sup>2</sup>	4.59×10 <sup>3</sup>	2.96×10 <sup>3</sup>	7.30×10 <sup>3</sup>	4.23×10 <sup>3</sup>	6.39×10 <sup>3</sup>	2.96×10 <sup>3</sup>
2 <sup>8</sup> H(p2)	SQG	9.18×10 <sup>2</sup>	8.70×10 <sup>2</sup>	4.00×10 <sup>3</sup>	4.19×10 <sup>3</sup>	5.02×10 <sup>3</sup>	4.97×10 <sup>3</sup>	7.24×10 <sup>3</sup>	6.15×10 <sup>3</sup>
	CNOT	1.05×10 <sup>3</sup>	1.14×10 <sup>3</sup>	6.71×10 <sup>3</sup>	5.92×10 <sup>3</sup>	8.56×10 <sup>3</sup>	7.18×10 <sup>3</sup>	1.12×10 <sup>4</sup>	9.91×10 <sup>3</sup>
2 <sup>8</sup> H(p3)	SQG	1.53×10 <sup>3</sup>	1.85×10 <sup>3</sup>	6.64×10 <sup>3</sup>	9.32×10 <sup>3</sup>	7.70×10 <sup>3</sup>	1.04×10 <sup>4</sup>	9.56×10 <sup>3</sup>	1.11×10 <sup>4</sup>
	CNOT	2.17×10 <sup>3</sup>	2.07×10 <sup>3</sup>	1.59×10 <sup>4</sup>	1.14×10 <sup>4</sup>	1.98×10 <sup>4</sup>	1.31×10 <sup>4</sup>	2.40×10 <sup>4</sup>	1.54×10 <sup>4</sup>

Table 4.7: Number of single qubit (SQG) gates and CNOT gates required to exponentiate the full and fictitious Hamiltonian under various parameterizations for both Jordan-Wigner(JW) and Bravyi-Kitaev(BK) transformations. Symbol p1 stands for a parameterization using  $\langle ii|ii \rangle$  integrals. Symbol p2 stands for a parameterization using  $\langle ii|ii \rangle$ ,  $\langle ij|ij \rangle$ ,  $\langle ij|ji \rangle$  groups of the effective integrals. Symbol p3 stands for a parameterization that uses all the integrals from the p2 group as well as  $\langle ij|jj \rangle$  effective integrals.

The estimation of the cost of performing molecular calculations on quantum de-

vices is critical to gain insight into the efficiency of such calculations. Such estimations were done most notably for phase estimation in Ref. [178] and subsequently for the VQE formalism [179]. These estimations point to the crucial dependence of the circuit depth on the sparsity of the Hamiltonian. To illustrate that such DSEM simplified Hamiltonian parameterizations will lead to low circuit depths, we calculated the number of gates for the fictitious Hamiltonians constructed in the previous section. Number of gates required for exponentiation of full and fictitious Hamiltonians are listed in Tab. 4.7. We used Jordan-Wigner [180] and Bravyi-Kitaev [181] transformations for expressing the molecular Hamiltonian in terms of Pauli operators. These transformations were obtained using OpenFermion’s [182] practical implementation of these techniques. Number of gates required were calculated using these Pauli representations as described in Ref. [183]. For the parameterized cases ( $H(p1)$ ,  $H(p2)$ ,  $H(p3)$ ), we have worked in SAO basis, while for the full Hamiltonian, we evaluated the number of gates both in SAO and molecular orbitals (MO) representation listing both cases. For the small molecular cases analyzed here, we observe a reduction in the number of gates by about an order of magnitude when using the fictitious Hamiltonian (even within p3 parameterization) in comparison to the full Hamiltonian. Note, however, that as the system size increases, we expect that the difference in the number of gates necessary to perform a single Trotter step will increase for the full Hamiltonian. Consequently, in the limit of a large molecular system, a parameterized Hamiltonian will result in even larger reduction of necessary gates when compared to the full Hamiltonian.

## 4.5 Conclusions

We have presented a DSEM procedure which allows us to find a fictitious, sparse Hamiltonian that recovers the self-energy evaluated with the full, original Hamiltonian containing all 2-body integrals. DSEM procedure is a two step procedure which

employs a polynomially scaling evaluation of the self-energy that is necessary for finding a sparse, fictitious Hamiltonian that is then used to evaluate an exact self-energy using a high level method. The high level solver deals only with the sparse Hamiltonian containing at most  $n^2$  terms. We have compared the GF2 and FCI energies obtained using the DSEM procedure to the original GF2 and FCI energies. From these comparisons, we have demonstrated that the errors can be controlled and are small.

DSEM has a potential to be used as a classical-quantum algorithm in quantum computing. The first part of the DSEM algorithm can be executed on a classical machine while the second part relying on an accurate, non-perturbative solver can be executed on a quantum computer. Since the Hamiltonian present in quantum computation is sparse, the resulting circuit is shallow with many fewer gates than for the circuit necessary to represent the original Hamiltonian. We have shown that the number of necessary gates in order to express the sparse Hamiltonian is at least one order of magnitude smaller, even for small systems, when compared to the gates necessary to express the original Hamiltonian.

There are various other quantum algorithms that leverage the sparsity of the Hamiltonian for a reduced gate count in a quantum circuit. In Ref. [184], Babbush et al. reduced the number of Hamiltonian terms to  $\mathcal{O}(N^2)$ , where  $N$  is the number of basis functions in a plane-wave basis-set. They diagonalize different components of the Hamiltonian operator, namely kinetic operator and potential operator using plane wave and dual plane wave basis respectively. Our method differs from this approach as we perform all our calculations in a Gaussian orbital basis, which requires fewer basis functions to obtain the same level of convergence with respect to the basis set. For regular chemical systems the number of necessary plane waves are thousands times larger than the number of Gaussian orbitals,  $N \gg n$ . However, at the same time, we make approximations to the self-energy in order to reduce the

number of terms in the Hamiltonian which when not done carefully can lead to a loss of accuracy. Further work to improve these approximations is in progress in our lab. The results of Babbush et al. were further extended to Gaussian basis set by M. Motta et al. [185] using two-step decomposition of 2-electron integrals introduced by B. Peng et al. [186]. While this work leads to reduction of  $N$ , this is done at the cost of introducing multiple Givens rotations which ultimately again result in complicated circuits. Such complication does not arise in the DSEM scheme where the number of 2-body integrals is drastically reduced.

We believe that our work opens several new venues of molecular quantum computing research that were not explored before. First, we propose that the quantum machine performs an evaluation for the fictitious Hamiltonian that is used to recover the molecular frequency dependent self-energy. From a mathematical view point, this has several interesting implications. For the “true”, analytical, and exact self-energy there is only one Hamiltonian capable of yielding this self-energy. However, for a self-energy that is numerical and only agrees to a very good numerical accuracy with the “true” exact self-energy, there can be several Hamiltonians reproducing it. These Hamiltonians can be much more suitable for quantum computing than the original Hamiltonian. Additionally, the analytical properties of Green’s functions and self-energies such as the high frequency expansion are well known, thus providing an additional tool in the assessment of the errors arising in computation on NISQ devices. Moreover, these errors can be partially corrected since the analytic limits are known when algorithms such as DSEM are employed. Finally, we would like to mention that DSEM can be naturally extended to work in conjunction with an embedding framework such as dynamical mean field theory (DMFT) [32, 120, 172, 122] or self-energy embedding theory (SEET) [187, 188, 189, 190].



## 4.6 Acknowledgements

D.Z. and D.D. acknowledge National Science Foundation grant number CHE1836497. M. M. was supported by the “Embedding Quantum Computing into Many-body Frameworks for Strongly Correlated Molecular and Materials Systems” project, which is funded by the U.S. Department of Energy(DOE), Office of Science, Office of Basic Energy Sciences, the Division of Chemical Sciences, Geosciences, and Biosciences. D.Z. thanks James Freericks for helpful discussions.

## Author contributions

DD developed the effective Hamiltonian approach and demonstrated how DSEM works in comparison to benchmarking methods, GF2 and FCI. All authors contributed to the writing of the manuscript.

## CHAPTER V

# Sparse-Hamiltonian approach to the time evolution of molecules on quantum computers

Christina Daniel<sup>1</sup>, Diksha Dhawan<sup>2</sup>, Dominika Zgid<sup>2,3</sup>, James Freericks<sup>4</sup>

1 – Department of Physics, Georgetown University, Washington, DC 20057 USA

2 – Department of Chemistry, University of Michigan, Ann Arbor, Michigan 48109, USA

3 – Department of Physics, University of Michigan, Ann Arbor, Michigan 48109, USA

4 – Department of Physics, Georgetown University, Washington, DC 20057 USA

This chapter is adapted from our published article [62]

### 5.1 Abstract

Quantum chemistry has been viewed as one of the potential early applications of quantum computing. Two techniques have been proposed for electronic structure calculations: (i) the variational quantum eigensolver and (ii) the phase-estimation algorithm. In both cases, the complexity of the problem increases for basis sets where either the Hamiltonian is not sparse, or it is sparse, but many orbitals are required to accurately describe the molecule of interest. In this work, we explore the possibility of mapping the molecular problem onto a sparse Hubbard-like Hamiltonian,

which allows a Green’s-function-based approach to electronic structure via a hybrid quantum-classical algorithm. We illustrate the time-evolution aspect of this methodology with a simple four-site hydrogen ring.

## 5.2 Introduction

In the variational quantum eigensolver algorithm [191, 192], one prepares a trial wavefunction and evaluates the expectation values needed to determine the expectation value of the Hamiltonian with respect to that wavefunction. The number of measurements scales with the number of nonzero terms in the Hamiltonian, which typically grows like the fourth power of the number of spin orbitals used in the basis set for the given calculation. The state is usually prepared with a simple strategy like a unitary coupled cluster approach [193]. A self-consistent loop optimizes the parameters in the variational ansatz until the required accuracy is achieved. The phase estimation algorithm [77] instead determines the phase of  $\exp(-i\lambda\hat{\mathcal{H}})$  and requires many operations of the exponential of the Hamiltonian onto the wavefunction, similar to time evolution, to complete the calculation ( $\lambda$  is a scaling factor). If the initial wavefunction has high overlap with the ground state, then the chance to project onto the ground state with the measurement is high.

In both cases, the complexity of the algorithm grows with the number of nonzero terms in the Hamiltonian matrix—for the variational quantum eigensolver, this is seen in the number of measurements required, while in the phase estimation algorithm it is in the number of independent Trotter steps required for each application of the exponential of the Hamiltonian (multiplied by a constant). Given the fact that current noisy intermediate scale quantum (NISQ) computers can only run low depth circuits, this is problematic for running these algorithms on complex molecules. Even when fault-tolerant quantum computers become available, they may still require low-depth circuits due to drift of the tuning of the machine over extended periods of time

(which is not normally corrected by error correction algorithms). This then implies that methods focused on making the Hamiltonian matrix sparse are critical to the success of quantum chemistry applications on quantum computers in the near term.

In this work, we describe the time-evolution piece of the algorithm to do this. It is based on a simple premise that the electron correlations in the molecule can be efficiently encoded in the self-energy of the molecule. Then, if we can construct a sparse Hamiltonian that approximates the self-energy of the molecule well, we can use it to determine the properties of the molecule. We describe just how such a process can be carried out on a quantum computer with a simple example below. We examine the accuracy of using an approximate unitary coupled cluster wavefunction to estimate the zero-temperature Green's function of the sparse Hamiltonian, which is the Hubbard Hamiltonian here.

Of course, this algorithm can be carried out for small systems on conventional computers (essentially those that can be solved with a full configuration interaction approach). The need for quantum computer enters when the number of spin orbitals used in describing the electronic structure of the molecule is more than about 20. Then the mapping to the Hubbard model becomes difficult to employ to calculate the Green's function on a classical computer. But, if the Hamiltonian is sparse enough, time evolution can still be carried out on a quantum computer. If one has a simple (and accurate) ground-state preparation protocol, then this approach can successfully describe molecules that could not be tackled by conventional computers to the same level of accuracy, nor by conventional VQE or QPE, because those circuits would be too deep. This situation is likely to continue to hold even when fault-tolerant quantum computers become available in the future.

### 5.3 Formalism

The retarded Green's function in position space is defined to be

$$G_{ij\sigma}(t) = -i\theta(t)\text{Tr} e^{-\beta\hat{\mathcal{H}}}\{\hat{c}_{i\sigma}(t), \hat{c}_{j\sigma}^\dagger\} \frac{1}{\mathcal{Z}}, \quad (5.1)$$

where  $\mathcal{Z} = \text{Tr} \exp(-\beta\hat{\mathcal{H}})$  is the partition function,  $\beta$  is the inverse temperature and  $\theta(t)$  is the unit step function. Here we have that  $\hat{c}_{i\sigma}$  ( $\hat{c}_{i\sigma}^\dagger$ ) are the annihilation (creation) operators for an electron at site  $i$  with spin  $\sigma$ . The braces denote the anticommutator, and the time-evolution of the operators is given in the Heisenberg representation. The trace is over all many body states with a fixed number of electrons (that is, we are calculating a canonical, not a grand canonical Green's function here). In this work, we focus on  $T = 0$ , where the trace includes just one state, the ground state. We also can work in momentum space (we assume the lattice is periodic), where

$$\hat{c}_{k\sigma} = \frac{1}{\sqrt{V}} \sum_{j=0}^{V-1} e^{-ikj} \hat{c}_{j\sigma}, \quad (5.2)$$

$V$  is the number of lattice sites and we set the lattice constant  $a = 1$ . The allowed  $k$  values are  $0, \pi/2, \pi,$  and  $3\pi/2$  for a four-site lattice.

We will be mapping the hydrogen ring to a sparse Hamiltonian given by the Hubbard model [194], which is

$$\hat{\mathcal{H}} = \sum_{ij\sigma} t_{ij} \hat{c}_{i\sigma}^\dagger \hat{c}_{j\sigma} + U \sum_i \hat{c}_{i\uparrow}^\dagger \hat{c}_{i\uparrow} \hat{c}_{i\downarrow}^\dagger \hat{c}_{i\downarrow}. \quad (5.3)$$

Here,  $t_{ij}$  is the hopping matrix and  $U$  is the on-site Coulomb interaction. The first term is the kinetic energy, and the second term is the potential energy. In this mapping, the hopping matrix is a full matrix, with nonzero coefficients for all hopping terms.

The Hamiltonian can also be written in momentum space as

$$\hat{\mathcal{H}} = \sum_{k,\sigma} \epsilon_k \hat{c}_{k\sigma}^\dagger \hat{c}_{k\sigma} + \frac{U}{V} \sum_{kk'q} \hat{c}_{k\uparrow}^\dagger \hat{c}_{k'\uparrow} \hat{c}_{q\downarrow}^\dagger \hat{c}_{k-k'+q\downarrow} \quad (5.4)$$

and we will be primarily working with this form. Here we have the bandstructure given by  $\epsilon_k = \frac{1}{V} \sum_{jj'} t_{jj'} \exp(ikj)$ , which is independent of  $j'$  due to the translational invariance of the lattice (hydrogen ring). If the molecule is not a translationally invariant ring, a more complicated single-particle term to the Hamiltonian is needed, but we do not discuss this further here. Note that the hopping matrix also includes diagonal terms with  $j = j'$ .

The mapping of the molecular Hamiltonian to the Hubbard Hamiltonian is designed to recover the dynamic part of the finite temperature self-energy of the parent molecular problem with all two-body interactions present. We call such a mapping the dynamical self-energy mapping (DSEM). Such a mapping was described in Ref. [163] where the effective on-site two-body integrals were chosen to recover the first moment of the frequency dependent self-energy. Here, as a proof of principle, the given sparse Hamiltonian is created to recover the first moment of the exact self-energy obtained in the exact-diagonalization procedure. In general, the following scheme of mapping can be used to design quantum-classical hybrid algorithms where a classical computer is used to calculate the sparse Hamiltonian that is then employed by the quantum computer. Details of the preparation of such a mapping are described in Ref. [61].

## 5.4 Results

The fitting procedure produces a diagonal term  $t_0$ , a nearest neighbor hopping  $t_1$  and a second neighbor hopping  $t_2$ , along with the on-site repulsion  $U$  (see Table 5.1).

The exact ground state is found by diagonalizing the Hamiltonian with four elec-

Table 5.1: Parameters for the sparse Hubbard Hamiltonian that represents the four-site hydrogen ring. ll parameters are in Hartrees.

$U$	$t_0$	$t_1$	$t_2$
0.6830907036	-0.3025	-0.380776	0.03035031

trons. It yields

$$\begin{aligned}
 |\Psi_0\rangle = & \alpha(\hat{c}_{0\uparrow}^\dagger\hat{c}_{1\uparrow}^\dagger\hat{c}_{0\downarrow}^\dagger\hat{c}_{1\downarrow}^\dagger|0\rangle - \hat{c}_{0\uparrow}^\dagger\hat{c}_{3\uparrow}^\dagger\hat{c}_{0\downarrow}^\dagger\hat{c}_{3\downarrow}^\dagger|0\rangle) + \beta(\hat{c}_{0\uparrow}^\dagger\hat{c}_{1\uparrow}^\dagger\hat{c}_{2\downarrow}^\dagger\hat{c}_{3\downarrow}^\dagger|0\rangle + \hat{c}_{0\uparrow}^\dagger\hat{c}_{3\uparrow}^\dagger\hat{c}_{1\downarrow}^\dagger\hat{c}_{2\downarrow}^\dagger|0\rangle) \\
 & + \hat{c}_{1\uparrow}^\dagger\hat{c}_{2\uparrow}^\dagger\hat{c}_{0\downarrow}^\dagger\hat{c}_{3\downarrow}^\dagger|0\rangle + \hat{c}_{2\uparrow}^\dagger\hat{c}_{3\uparrow}^\dagger\hat{c}_{0\downarrow}^\dagger\hat{c}_{1\downarrow}^\dagger|0\rangle + 2\hat{c}_{1\uparrow}^\dagger\hat{c}_{3\uparrow}^\dagger\hat{c}_{0\downarrow}^\dagger\hat{c}_{2\downarrow}^\dagger|0\rangle + 2\hat{c}_{0\uparrow}^\dagger\hat{c}_{2\uparrow}^\dagger\hat{c}_{1\downarrow}^\dagger\hat{c}_{3\downarrow}^\dagger|0\rangle) \\
 & + \gamma(\hat{c}_{2\uparrow}^\dagger\hat{c}_{3\uparrow}^\dagger\hat{c}_{2\downarrow}^\dagger\hat{c}_{3\downarrow}^\dagger|0\rangle - \hat{c}_{1\uparrow}^\dagger\hat{c}_{2\uparrow}^\dagger\hat{c}_{1\downarrow}^\dagger\hat{c}_{2\downarrow}^\dagger|0\rangle),
 \end{aligned} \tag{5.5}$$

with  $\alpha = 0.6895316741725$ ,  $\beta = 0.059610737681519$  and  $\gamma = 0.056792869544809$ .

While we could compute the Green's function for the exact ground state, that would not be representative of what a true quantum computation would be that is based on the variational quantum eigensolver, so we instead use an approximate ground state based on a factorized unitary coupled cluster ansatz that uses just doubles excitations from the reference state where both the level with  $k = 0$  and the level with  $k = 1$  are filled. This state was described in Ref. [195], where the excitation operators for a factorized unitary coupled cluster are given. That approach is generalized here and summarized in Tables 5.2 and 5.3.

The factorized form of the unitary coupled cluster approximation applies each doubles excitation (and de-excitation) operator in the order given in Table 5.2 to the initial reference state,  $\hat{c}_{0\uparrow}^\dagger\hat{c}_{1\uparrow}^\dagger\hat{c}_{0\downarrow}^\dagger\hat{c}_{1\downarrow}^\dagger|0\rangle$ . The resulting, approximate ground state in terms of the three angles  $\theta_1$ ,  $\theta_3$ , and  $\theta_4$  is summarized in Table 5.3. We use the same notation as used in Ref. [195], which is why we have no  $\theta_2$ , since that was used for a quad excitation that we do not include here.

Once the analytical coefficients of Table 5.3 are obtained, numerical values are

Table 5.2: Doubles unitary coupled-cluster operators used in creating the approximate ground state. The operators are applied in order according to the rows of the table.

Order	Unitary coupled cluster factor
1	$e^{-\theta_1 \hat{c}_{2\uparrow}^\dagger \hat{c}_{3\downarrow}^\dagger \hat{c}_{0\downarrow} \hat{c}_{1\uparrow} + \theta_1 \hat{c}_{1\uparrow}^\dagger \hat{c}_{0\downarrow}^\dagger \hat{c}_{3\downarrow} \hat{c}_{2\uparrow}}$
2	$e^{-\theta_1 \hat{c}_{3\uparrow}^\dagger \hat{c}_{2\downarrow}^\dagger \hat{c}_{1\downarrow} \hat{c}_{0\uparrow} + \theta_1 \hat{c}_{0\uparrow}^\dagger \hat{c}_{1\downarrow}^\dagger \hat{c}_{2\downarrow} \hat{c}_{3\uparrow}}$
3	$e^{-\frac{\pi}{4} \hat{c}_{3\uparrow}^\dagger \hat{c}_{3\downarrow}^\dagger \hat{c}_{1\downarrow} \hat{c}_{1\uparrow} + \frac{\pi}{4} \hat{c}_{1\uparrow}^\dagger \hat{c}_{1\downarrow}^\dagger \hat{c}_{3\downarrow} \hat{c}_{3\uparrow}}$
4	$e^{+\theta_3 \hat{c}_{2\uparrow}^\dagger \hat{c}_{3\uparrow}^\dagger \hat{c}_{1\uparrow} \hat{c}_{0\uparrow} - \theta_3 \hat{c}_{0\uparrow}^\dagger \hat{c}_{1\uparrow}^\dagger \hat{c}_{3\uparrow} \hat{c}_{2\uparrow}}$
5	$e^{+\theta_3 \hat{c}_{2\downarrow}^\dagger \hat{c}_{3\downarrow}^\dagger \hat{c}_{1\downarrow} \hat{c}_{0\downarrow} - \theta_3 \hat{c}_{0\downarrow}^\dagger \hat{c}_{1\downarrow}^\dagger \hat{c}_{3\downarrow} \hat{c}_{2\downarrow}}$
6	$e^{-\theta_3 \hat{c}_{1\uparrow}^\dagger \hat{c}_{2\uparrow}^\dagger \hat{c}_{3\uparrow} \hat{c}_{0\uparrow} + \theta_3 \hat{c}_{0\uparrow}^\dagger \hat{c}_{3\uparrow}^\dagger \hat{c}_{2\uparrow} \hat{c}_{1\uparrow}}$
7	$e^{-\theta_3 \hat{c}_{1\downarrow}^\dagger \hat{c}_{2\downarrow}^\dagger \hat{c}_{3\downarrow} \hat{c}_{0\downarrow} + \theta_3 \hat{c}_{0\downarrow}^\dagger \hat{c}_{3\downarrow}^\dagger \hat{c}_{2\downarrow} \hat{c}_{1\downarrow}}$
8	$e^{-\theta_4 \hat{c}_{2\uparrow}^\dagger \hat{c}_{2\downarrow}^\dagger \hat{c}_{0\downarrow} \hat{c}_{0\uparrow} + \theta_4 \hat{c}_{0\uparrow}^\dagger \hat{c}_{0\downarrow}^\dagger \hat{c}_{2\downarrow} \hat{c}_{2\uparrow}}$

calculated from the analytical coefficients. To do this, equations for the angles  $\theta_1$ ,  $\theta_3$ , and  $\theta_4$  are needed. These equations are given in Ref. [195] and the angles depend on the values of  $\alpha$ ,  $\beta$ , and  $\gamma$  from the exact ground state. They are

$$\theta_1 = \frac{1}{2} \sin^{-1}(4\beta) \quad (5.6)$$

$$\theta_3 = \frac{1}{2} \sin^{-1} \left( \frac{2\sqrt{2}\beta}{c_1^2} \right) \quad (5.7)$$

$$\theta_4 = \tan^{-1} \left( \frac{\gamma}{\alpha} \right) - \tan^{-1} (\tan^2 \theta_3). \quad (5.8)$$

After substituting the values for  $\alpha$ ,  $\beta$ , and  $\gamma$  into the equations for the angles, the approximate ground state with numerical coefficients is obtained (see Table 5.3). This wavefunction is representative of a generic state that one would obtain after performing a variational quantum eigensolver calculation.

Using this approximate ground state, we compute the (approximate) time-dependent Green's function, where the ground-state wavefunction is replaced by the approximate ground-state, and compare it to the exact Green's function with the exact ground state. Figure 5.1 shows these two results (real and imaginary part). One can see that



Table 5.3: General form and final numerical values of the coefficients of the approximate ground state after applying the doubles-only excitations, with  $c_i \equiv \cos \theta_i$  and  $s_i \equiv \sin \theta_i$ .

State	Analytical Coefficient	Numerical Coefficient
$\hat{c}_{0\uparrow}^\dagger \hat{c}_{1\uparrow}^\dagger \hat{c}_{0\downarrow}^\dagger \hat{c}_{1\downarrow}^\dagger  0\rangle$	$\frac{c_4}{\sqrt{2}}(c_1^2 c_3^2 + s_1^2 s_3^2) + \frac{s_4}{\sqrt{2}}(s_1^2 c_3^2 - c_1^2 s_3^2)$	0.6902877166375496
$\hat{c}_{0\uparrow}^\dagger \hat{c}_{3\uparrow}^\dagger \hat{c}_{0\downarrow}^\dagger \hat{c}_{3\downarrow}^\dagger  0\rangle$	$\frac{c_4}{\sqrt{2}}(s_1^2 s_3^2 - c_1^2 c_3^2) + \frac{s_4}{\sqrt{2}}(s_1^2 c_3^2 + c_1^2 s_3^2)$	-0.6886258223794277
$\hat{c}_{0\uparrow}^\dagger \hat{c}_{1\uparrow}^\dagger \hat{c}_{2\downarrow}^\dagger \hat{c}_{3\downarrow}^\dagger  0\rangle$	$\frac{c_1^2}{\sqrt{2}} s_3 c_3 - \frac{s_1^2}{\sqrt{2}} s_3 c_3$	0.05873846703927717
$\hat{c}_{0\uparrow}^\dagger \hat{c}_{3\uparrow}^\dagger \hat{c}_{1\downarrow}^\dagger \hat{c}_{2\downarrow}^\dagger  0\rangle$	$\frac{c_3 s_3}{\sqrt{2}}$	0.06048300832376081
$\hat{c}_{1\uparrow}^\dagger \hat{c}_{2\uparrow}^\dagger \hat{c}_{0\downarrow}^\dagger \hat{c}_{3\downarrow}^\dagger  0\rangle$	$\frac{c_3 s_3}{\sqrt{2}}$	0.06048300832376081
$\hat{c}_{2\uparrow}^\dagger \hat{c}_{3\uparrow}^\dagger \hat{c}_{0\downarrow}^\dagger \hat{c}_{1\downarrow}^\dagger  0\rangle$	$\frac{c_1^2}{\sqrt{2}} s_3 c_3 - \frac{s_1^2}{\sqrt{2}} s_3 c_3$	0.05873846703927717
$\hat{c}_{1\uparrow}^\dagger \hat{c}_{3\uparrow}^\dagger \hat{c}_{0\downarrow}^\dagger \hat{c}_{2\downarrow}^\dagger  0\rangle$	$c_1 s_1$	0.11922147536303802
$\hat{c}_{0\uparrow}^\dagger \hat{c}_{2\uparrow}^\dagger \hat{c}_{1\downarrow}^\dagger \hat{c}_{3\downarrow}^\dagger  0\rangle$	$c_1 s_1$	0.11922147536303802
$\hat{c}_{2\uparrow}^\dagger \hat{c}_{3\uparrow}^\dagger \hat{c}_{2\downarrow}^\dagger \hat{c}_{3\downarrow}^\dagger  0\rangle$	$\frac{c_4}{\sqrt{2}}(s_1^2 c_3^2 + c_1^2 s_3^2) + \frac{s_4}{\sqrt{2}}(c_1^2 c_3^2 - s_1^2 s_3^2)$	0.06687536735226934
$\hat{c}_{1\uparrow}^\dagger \hat{c}_{2\uparrow}^\dagger \hat{c}_{1\downarrow}^\dagger \hat{c}_{2\downarrow}^\dagger  0\rangle$	$\frac{c_4}{\sqrt{2}}(s_1^2 c_3^2 - c_1^2 s_3^2) - \frac{s_4}{\sqrt{2}}(c_1^2 c_3^2 + s_1^2 s_3^2)$	-0.04669803278042805

the two Green's functions are nearly identical; their differences are on the order of  $10^{-4}$ . The reason why is that the square of the overlap of the approximate state with the ground state is very high (the fidelity is 0.99979). This value is surprising given that the approximate ground state differs from the exact one with coefficients that are on the order of 0.01, but there is a cancellation leading to a higher fidelity.

Unfortunately, for such a small system, it does not make sense to use Dyson's equation to extract the frequency-dependent self-energy, because the data is truncated to too short of a time. This leads to inaccuracies here, because the system is finite and the Fourier transform of the Green's function yields a sum over delta functions. But if the Green's function is cut-off too early in the time domain, the results of the Fourier transform would be significantly distorted. This becomes less of a concern for larger molecules because they have so many frequencies that they tend to dephase and create a decaying Green's function in the time domain, which can be cut off,

resulting in just a small broadening of the delta functions, so the calculations can proceed more normally for larger systems. Most molecules will fall into this category.

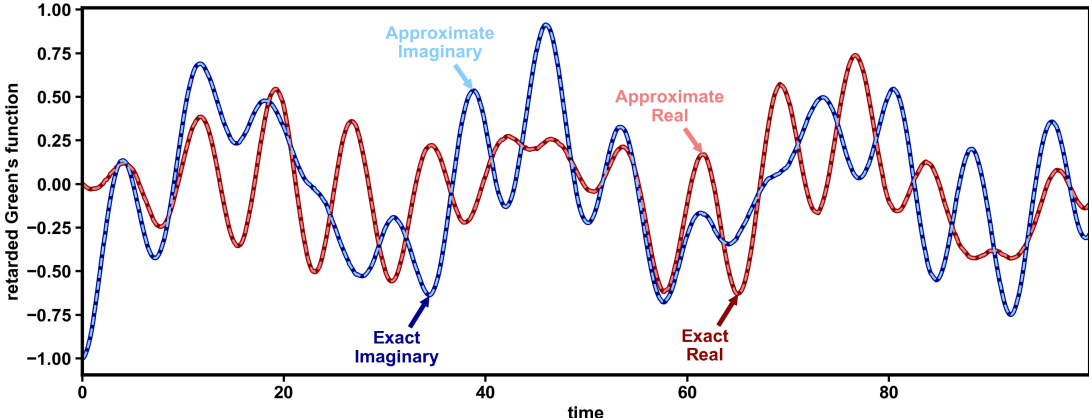


Figure 5.1: Exact (solid) and approximate (dashed) retarded Green’s function for the sparse Hubbard Hamiltonian. The time is in units of  $\hbar/H$ .

## 5.5 Discussion

The algorithm on the quantum computer is now straightforward. After mapping the problem from the molecule to the sparse Hubbard Hamiltonian, we use the factorized form of the unitary coupled cluster ansatz to create an approximate ground state. In general, such an approach will involve many different types of excitations, but in this simple example, it involves only doubles excitations. The lower the order of the excitation, the lower the depth of the circuit for the quantum computer, so it is likely that many calculations will opt to only use singles and doubles, if possible. Then we would invoke the algorithm from the Los Alamos group [196, 108] to calculate the Green’s function by measuring the  $x$  or  $y$  Pauli spin operator on the ancilla qubit to determine the real and imaginary parts of  $G$ . Both of these steps can be carried out with relatively low-depth circuits due to the sparsity of the effective Hamiltonian, but they do still require time evolution, which is still beyond the capability of currently

available NISQ machines (see Ref. [110] for a discussion of strategies to determine Green’s functions on NISQ machines). Once one has determined the Green’s function to far enough time on the quantum computer, then we would take the Fourier transform, extract the self-energy from Dyson’s equation, and employ it to describe the Green’s function of the molecule. This then allows the ground-state energy of the molecule to be determined. Alternatively, one can extract the self-energy from imaginary axis calculations at the Matsubara frequencies, which may be numerically more stable.

## 5.6 Conclusions

In this work, we described an approach to use on near-term quantum computers that will allow us to calculate the electronic structure of more complex molecules sooner. The approach maps the molecule onto a sparse Hamiltonian that has a full single-particle hopping matrix, but only local interactions. Due to the significant reduction in the number of nonzero matrix elements, this sparse Hamiltonian becomes much easier to simulate on a quantum computer and one should be able to determine its Green’s function once time evolution becomes possible; this may occur in near-term NISQ machines or may need to wait until fault-tolerant computers are available. Once the Green’s function for the sparse Hamiltonian is found on the quantum computer, we extract the self-energy and use it as the self-energy for the molecule in the full molecular problem. We showed how using an approximate form for the ground state leads to an accurate approximation to the exact result for a relatively long period of time. Hence, this makes it promising that such an approach can lead to accurate and efficient ways to perform electronic structure calculations on quantum computers.

In terms of quantum computing complexity, a factorized form of UCC state preparation uses only doubles excitations here, and the time-evolution needed to compute

the Green's function requires only control operations for the application of the creation or annihilation operators, but not for the time evolution. This is contrary to the quantum phase estimation algorithm, which requires controlled application of the Hamiltonian. Hence, the approach described here has the potential to be quite efficient for implementation on both near-term and fault-tolerant quantum computers.

## 5.7 Acknowledgement

This work is supported from the National Science Foundation under grant number CHE-1836497. JKF is also funded by the McDevitt bequest at Georgetown University. We thank Manuel Weber for useful discussions.

## Author contributions

JKF and DZ conceived the project. CD wrote the codes to calculate the Green's functions by exact diagonalization. DD fit the molecular electronic structure for the  $H_4$  ring to the sparse Hubbard Hamiltonian, providing the parameters used in this work. All authors contributed to the writing of the manuscript.

## CHAPTER VI

# Quantum Subspace Expansion Based Approach for Calculating Green's Functions

Diksha Dhawan<sup>1</sup>, Mario Motta<sup>2</sup>, Dominika Zgid<sup>3</sup>

1 – Department of Chemistry, University of Michigan, Ann Arbor, Michigan 48109, USA

2 – IBM Quantum, IBM Research Almaden, 650 Harry Road, San Jose, CA 95120, USA

3 – Department of Physics, University of Michigan, Ann Arbor, Michigan 48109, USA

This chapter is adapted from our manuscript which is under preparation.

### 6.1 Introduction

The solution of the time-independent Schrodinger equation continues to be one of the central challenges to non-relativistic quantum mechanics. This solution provides us access to multiple properties of the system such as optimized geometries, excitation energies, ionization potentials, etc. One powerful tool to solve this type of difficult differential equations is through Green's functions. In quantum mechanics, Green's functions are defined as correlation functions, from which we can extract information about the system, such as the density of states, relaxation times and

response functions, etc. Moreover, Green's function formalism provides us direct access to thermodynamic quantities while naturally including temperature dependence. Despite its versatility, it is computationally intensive to compute.

Calculation of exact one-particle Green's function is computationally infeasible because of the exponential increase in cost as the system size increases. Over the years, many approximate methods to compute Green's functions have been proposed, for example, GW [197, 198, 199], GF2 [25, 26, 27], GFCC [28, 200, 31, 30]. These approximations provide us with accurate results in the weakly and moderated correlated regimes. However, many systems of interest fall outside the regime of validity of these approximations. Embedding methods like DMFT [32, 33], DMET[201, 202, 203], and SEET[34, 35, 36, 37], have also been proposed to overcome this challenge. Most of these methods are based on using exact diagonalization(ED) as the impurity solver, which again limits the size of impurity orbitals because of ED's exponential scaling. Recent developments in the field of quantum computing have shown that we can overcome this limitation by using quantum machines. Several quantum algorithms have been proposed for obtaining Green's function from quantum machines. Bauer et al [106] calculate the green's function by time evolving the Hamiltonian in the real time domain and Fourier transform it to obtain it in the frequency domain. Despite their accuracy and scalability, time evolution algorithms require longer coherence times, thus making them a bad choice for noisy intermediate scaling quantum (NISQ) machines. On the other hand, Variational quantum algorithms are noise resilient and require only a moderate number of qubits. Nakagawa and coworkers [110] propose the use of variational quantum eigensolver(VQE) to evaluate the Green's function. They also use Lehmann's representation [24] of the Green's function, for which they obtain the excited states using subspace-search variational quantum eigensolver(SSVQE). In references [110, 204], green's function was calculated using McLachlan variational principle. In another recent work, the continued frac-

tion representation of Green's function was calculated in the Krylov subspace using quantum subspace expansion(QSE) [113].

In this work, we propose the use of QSE to calculate green's function in Lehmann's representation. We use a hybrid algorithm, where QSE is used to calculate the transition matrix elements on the quantum machine. Green's function is then calculated on the classical computer through post-processing.

## 6.2 Method

### 6.2.1 Green's Function Formulation

The Hamiltonian for a fermionic system is given by

$$H = \sum_{ij} h_{ij} c_i^\dagger c_j + \frac{1}{2} \sum_{ijkl} v_{ijkl} c_i^\dagger c_j^\dagger c_l c_k \quad (6.1)$$

where  $h_{ij}$  are  $v_{ijkl}$  are one-body and two-body integrals, and  $c_i^\dagger$  and  $c_i$  are fermionic creation and annihilation operators respectively. Green's function of such a system characterizes the propagation of a state containing an additional particle or hole. The exact Green's function is given by

$$\iota G_{ij}(t, t') = \langle \Psi_0 | T [c_{H\alpha}(t) c_{H\beta}^\dagger(t')] | \Psi_0 \rangle \quad (6.2)$$

where  $|\Psi_0\rangle$  is the Heisenberg ground state of the system,  $c_{H\alpha}(t)$  is the field operator in Heisenberg representation and T stands for the time-ordered product of operators. In this equation, time ordering only makes a difference in the convergence factor which doesn't affect the Green's function value at any finite value of time, therefore, we can rewrite Eq 6.2 as

$$\iota G_{ij}(t, t') = \langle \Psi_0 | \{c_{H\alpha}(t), c_{H\beta}^\dagger(t')\} | \Psi_0 \rangle \Theta(t - t') \quad (6.3)$$

where  $\Theta$  is the Heaviside step function. Matsubara Green's function is then obtained by taking the Fourier transform as

$$G_{ij}(\iota\omega_n) = \langle \Psi_0 | c_i \frac{1}{\iota\omega_n + E_0 - H} c_j^\dagger | \Psi_0 \rangle + \langle \Psi_0 | c_j^\dagger \frac{1}{\iota\omega_n + H - E_0} c_i | \Psi_0 \rangle \quad (6.4)$$

where  $\omega_n$  are the Matsubara frequencies. Then, we introduce the resolution of identities in the N-1 and N+1 particle subspaces to obtain the Green's function as

$$G_{ij}(\iota\omega_n) = \sum_{\mu} \langle \Psi_0 | c_i | \Phi_{\mu}^+ \rangle \frac{1}{\iota\omega_n + E_0 - E_{\mu}^+} \langle \Phi_{\mu}^+ | c_j^\dagger | \Psi_0 \rangle + \sum_{\mu} \langle \Psi_0 | c_j^\dagger | \Phi_{\mu}^- \rangle \frac{1}{\iota\omega_n + E_{\mu}^- - E_0} \langle \Phi_{\mu}^- | c_i | \Psi_0 \rangle \quad (6.5)$$

The first and second parts of G describe the attachment of an electron to the system and the elimination of an electron from the system, respectively. The latter contains all cationic states and exhibits explicitly as poles the ionization potentials (IP) of the system. Analogously, the electron affinities (EA) appear as poles of the former which is associated with anionic states. Now let us define the transition matrix elements as

$$X_{\mu j}^+ = \langle \Phi_{\mu}^+ | c_j^\dagger | \Psi_0 \rangle; \quad (X_{\mu j}^+)^* = \langle \Psi_0 | c_j | \Phi_{\mu}^+ \rangle \\ X_{\mu i}^- = \langle \Phi_{\mu}^- | c_i | \Psi_0 \rangle; \quad (X_{\mu i}^-)^* = \langle \Psi_0 | c_i^\dagger | \Phi_{\mu}^- \rangle \quad (6.6)$$

Substituting these matrix elements into Eq 6.5 gives us

$$G_{ij}(\iota\omega_n) = \sum_{\mu} \frac{(X_{\mu i}^+)^* X_{\mu j}^+}{\iota\omega_n + E_0 - E_{\mu}^+} + \sum_{\mu} \frac{(X_{\mu j}^-)^* X_{\mu i}^-}{\iota\omega_n + E_{\mu}^- - E_0} \langle \Phi_{\mu}^- | c_i | \Psi_0 \rangle \quad (6.7)$$



After representing the Green's function in this form, the major challenge that remains is to calculate the transition matrix elements, for this purpose, we employ QSE.

### 6.2.2 Quantum Subspace Expansion

Quantum subspace expansion(QSE) based methods provide us with a new way of solving the eigenvalue problem on a quantum computer. In these methods, the wavefunction is represented as a linear combination of basis states instead of preparing it directly on a quantum computer, thus avoiding the need to have an approximate ansatz. The general idea of QSE is to obtain the entire eigenspectrum of a system in a subspace defined from the reference state,  $|\Psi\rangle$ . The ansatz for such a subspace can be defined as

$$|\Phi_i\rangle = \hat{R}_i |\Psi\rangle \quad (6.8)$$

where  $\Psi$  is the VQE ground state and  $\hat{R}_i$  is an excitation operator with  $i$  specifying different levels of excitation. Then the eigenspectrum can be computed by diagonalizing the Hamiltonian defined in the subspace spanned by  $\{|\Phi_i\rangle\}$ , essentially reducing the problem to a generalized eigenvalue problem.

$$H^{sub}C = S^{sub}CE \quad (6.9)$$

where  $H^{sub}$  is the Hamiltonian in truncated Hilbert space,  $C$  are eigenvectors,  $S^{sub}$  gives overlap and  $E$  is the eigenvalues matrix.  $H^{sub}$  and  $S^{sub}$  matrices are defined as

$$H_{ij}^{sub} = \langle \Phi_i | H | \Phi_j \rangle, \quad S_{ij}^{sub} = \langle \Phi_i | \Phi_j \rangle \quad (6.10)$$

Here,  $H$  and  $S$  matrices are computed on a quantum machine and then Eq 6.9 is solved to obtain eigenvectors and eigenenergies.

### 6.2.3 Green's Function Calculation Using QSE

As discussed in Section A, we can use QSE to calculate the transition matrix elements and then Green's function can be obtained from Eq 6.5. For the sake of simplicity, here we give a detailed description for calculation of only one of the transition matrix element, the procedure is similar for all the other terms. Our implementation of QSE to calculate transition matrix elements is as follows:

- Prepare ground state of the system. We note that this step is independent of rest of the algorithm. We can use QPE, QSE or any other quantum algorithm for ground state preparation. For this paper, we use VQE.
- Choose an ansatz for N+1 subspace.

$$|\Phi_{mu}^+\rangle = \sum_i V_{i\mu} c_i^\dagger |\Psi_0\rangle \quad (6.11)$$

- Calculate H and S matrices in N+1 subspace on the quantum machine.

$$H_{ij}^{N+1} = \langle \Psi_0 | c_i H c_j^\dagger | \Psi_0 \rangle, \quad S_{ij}^{N+1} = \langle \Psi_0 | c_i c_j^\dagger | \Psi_0 \rangle \quad (6.12)$$

- Solve the eigenvalue equation.

$$H^{N+1}C = S^{N+1}CE \quad (6.13)$$

- Compute transition matrix elements as

$$\begin{aligned} X_{\mu j}^+ &= \langle \Phi_{\mu}^+ | c_j^\dagger | \Psi_0 \rangle = \sum_i V_{i\mu} \langle \Psi_0 | c_i c_j^\dagger | \Psi_0 \rangle \\ &= \sum_i V_{i\mu} S_{ij} \end{aligned} \quad (6.14)$$

- Substitute the value of transition matrix elements in Eq 6.7 to compute Green's function on classical computer.

#### 6.2.4 Statistical Analysis

Green's function calculated on a quantum computer includes some quantum noise as well as statistical error. Statistical errors are intrinsic to the calculations performed on quantum computers. Ideally, these errors can be reduced by increasing the number of measurements as the magnitude of error is inversely proportional to the square of number of measurements. However, when normally distributed data goes through non-linear transformations, it loses its normality. In such cases, standard error propagation techniques may not be of great help as there is a certain bias in this new set of data. The best way to deal with such non-traditional datasets is using resampling techniques like jackknife, bootstrap etc. For this paper, we use jackknife for the error propagation. Jackknife method works by systematically redistributing the samples to form sub-samples, and estimating the statistics of each of these sub-samples separately. The general procedure for jackknife is as follows:

- Distribute the samples into  $M$  bins.
- Form a sub-sample  $M_i$  of  $M-1$  bins, where  $M_i$  contains all the bins except the  $i^{th}$  bin
- Evaluate the mean,  $U_i$ , in each of the  $M$  bins and obtain an error estimate from the variance of these estimates.
- Jackknife mean of the complete set of data is then given by

$$U = U_0 - (M - 1)(\bar{U} - U_0) \tag{6.15}$$

where  $U_0$  is the average of complete dataset, and  $\bar{U}$  is given by taking an average over all  $U_i$ .

- Error estimate is given by

$$\Delta U = \sqrt{M-1} \left( \frac{1}{M} \sum_{i=1}^M (U_i)^2 - \bar{U}^2 \right)^{1/2} \quad (6.16)$$

In section 6.3, we show how the use of jackknife analysis improves the statistics of our results.

### 6.3 Results

In this section, we show some results from our experiments to examine the above-described method. We test our method on  $H_2$  and  $H_4$  chains in STO-6G basis. We have performed all our calculations using Qiskit[205]. We used Jordan-Wigner [73] type mapping to map our Hamiltonian from fermionic to qubit Hamiltonian. We systematically analyze our results by slowly adding different sources of error to our calculations, thus helping us differentiate between the error from quantum hardware and the method itself.

#### 6.3.1 Green's Function from QSE and FCI

At first, we compare the results from QSE calculation performed on statevector simulator [205] to FCI results. The results from the simulator are deterministic, this helps us track the errors arising because of approximations used in the QSE algorithm. Fig. 6.1 shows the real and imaginary part of  $G_{00}(i\omega)$  element for  $H_2$  molecule computed at equilibrium bond length using QSE and FCI. These values were computed on a Matsubara frequency grid.

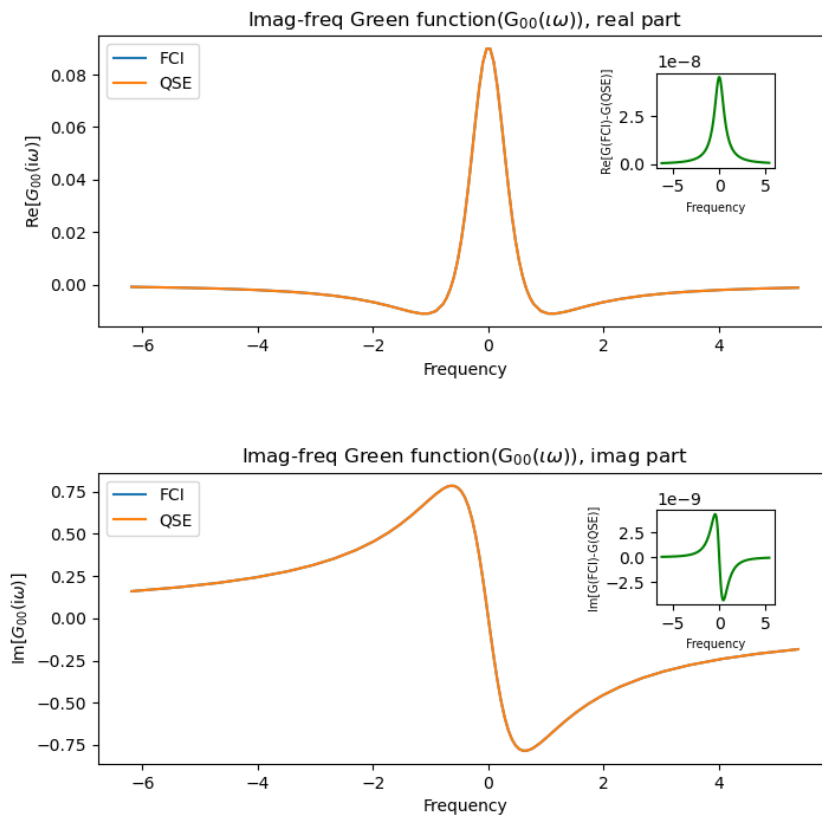


Figure 6.1: The real(top) and imaginary(bottom) part of  $G_{00}(i\omega)$  element for  $\text{H}_2$  molecule in the STO-6G basis evaluated using FCI and QSE. Inset on respective plots show the difference between Green’s function calculated using FCI and QSE.

Next, we performed the similar calculations on a  $\text{H}_4$  chain with each Hydrogen separated by 1 Å. Fig. 6.2 and 6.3 show the  $G_{00}(i\omega)$  and  $G_{11}(i\omega)$  elements from both QSE and FCI. Inset in the plot shows the actual difference between the elements at different frequency points.

### 6.3.1.1 Statistical Errors

The results obtained from quantum machines are not deterministic but stochastic in nature and therefore, some post-processing is required to propagate the numbers

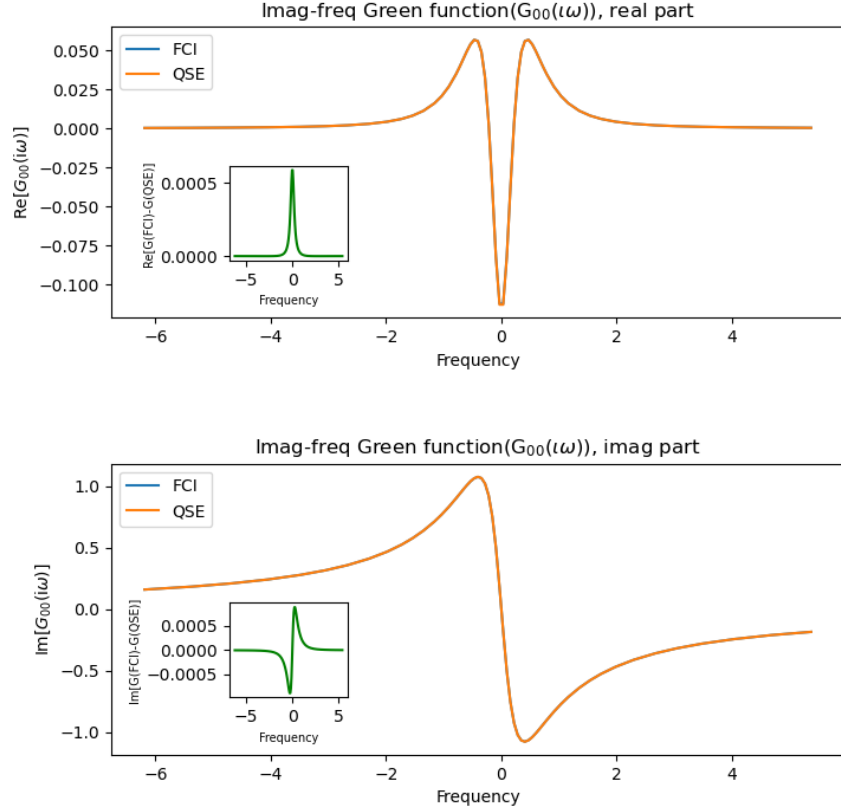


Figure 6.2: The real(top) and imaginary(bottom) part of  $G_{00}(i\omega)$  element for  $\text{H}_4$  chain with bond length  $1.0 \text{ \AA}$  in the STO-6G basis evaluated using FCI and QSE. Inset on respective plots shows the difference between Green's function calculated using FCI and QSE

through multiple calculations. Here, we describe these post-processing procedures and how QSE will behave on a fault-tolerant error-corrected quantum machine. We can do so by performing our calculations on the QASM simulator without any noise model. The results obtained from the simulator are shown in Figure 6.4. The data obtained from the simulator is expected to be normally distributed. However, as mentioned in the earlier section, non-linear operations on those results renders the distribution non-normal. This can be observed in Fig 6.6 and Fig 6.7, showing the distribution of real and imaginary parts of  $G_{00}(i\omega)$  element for different sample sizes, where the histograms are deviating slightly from the normal behavior. This is further

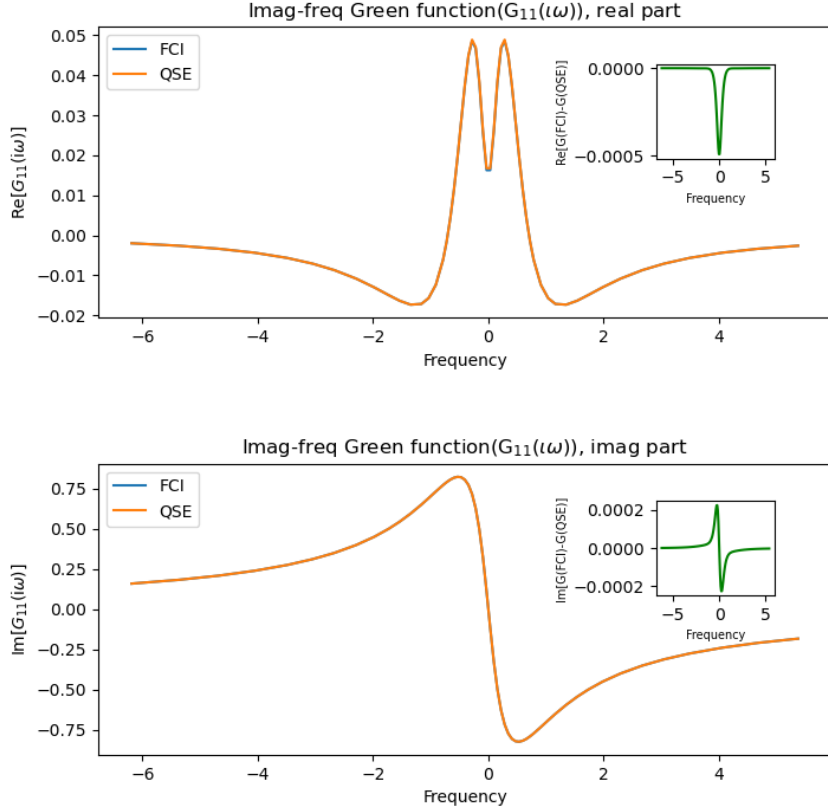


Figure 6.3: The real(top) and imaginary(bottom) part of  $G_{11}(i\omega)$  element for  $\text{H}_4$  chain with bond length  $1.0 \text{ \AA}$  in the STO-6G basis evaluated using FCI and QSE. Inset on respective plots shows the difference between Green's function calculated using FCI and QSE

made clear by the behavior of standard deviation with respect to sample size as shown in Fig. 6.8. The standard deviation is expected to be inversely proportional to  $M^2$  where  $M$  is the sample size, however, we observe that the standard deviation doesn't change with the increasing number of samples. Therefore, we resample our results using jackknife, leading to the expected decrease in the error as the sample size increases, Fig. 6.9. In Fig. 6.5, we compare the QSE Green's function calculated on the statevector simulator to the Green's function calculated on the QASM simulator without any noise after the jackknife.

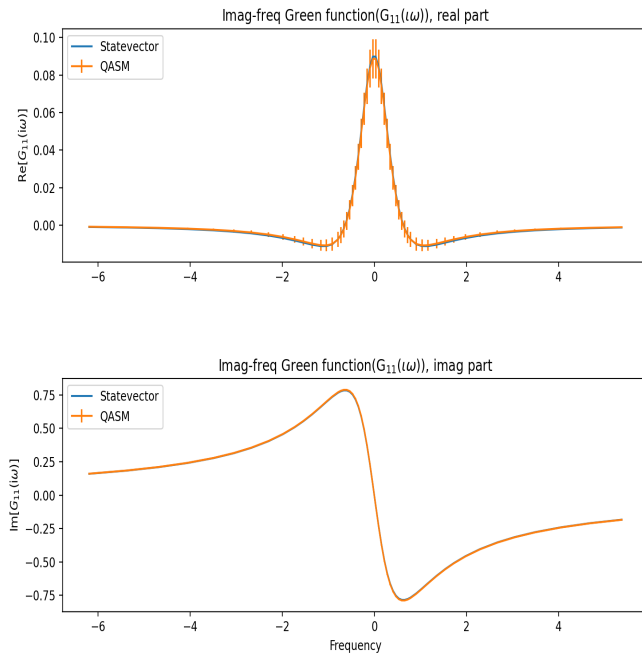


Figure 6.4: The real(top) and imaginary(bottom) part of  $G_{11}(i\omega)$  element for  $H_2$  molecule with bond length 1.0 Å in the STO-6G basis evaluated using FCI and QSE done on the QASM simulator.

## 6.4 Conclusions

In this work, we described a hybrid quantum-classical approach for calculating Green’s functions on quantum computers. We start by preparing the ground state of the system using VQE. We expand the subspace around this VQE ground state to obtain transition matrix elements for  $n+1$  and  $n-1$  states, where  $n$  is the number of spin orbitals. These transition matrix elements are then used on a classical machine to calculate the Green’s function using Lehmann’s representation of the spectral function. We successfully demonstrated that our algorithm produces the Green’s function within reasonable error limits of the FCI Green’s function. We further used the re-sampling approach to propagate the statistical noise from the quantum simulator. There are other algorithms that use quantum subspace expansion to study excited state properties. In ref. [113], authors use QSE to calculate Green’s functions. Our



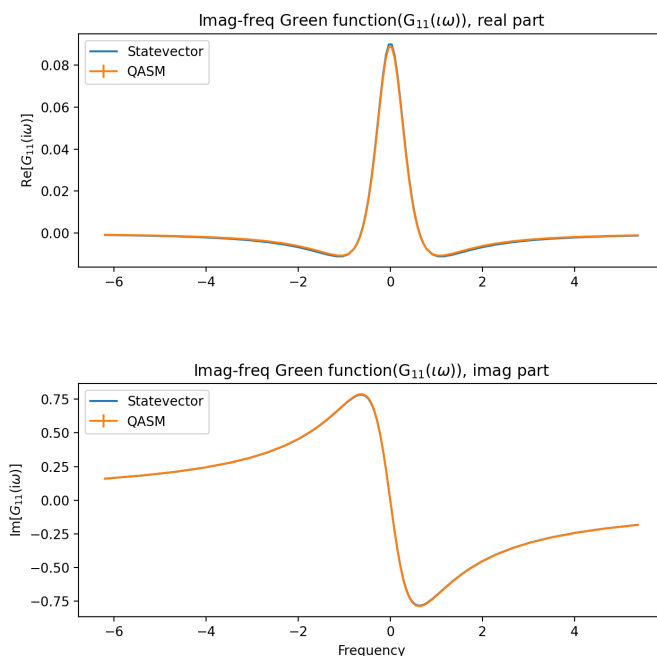


Figure 6.5: The real(top) and imaginary(bottom) parts of  $G_{11}(i\omega)$  element for  $H_2$  molecule with bond length 1.0 Å in the STO-6G basis evaluated using FCI and QSE done on the QASM simulator. QSE results have been post-processed using jackknife for proper error propagation.

approach differs from this work as they calculate the continued fraction representation of Green’s function using the Lanczos scheme.

We believe that the ability to calculate Green’s functions on near-term quantum computers is an opportunity to study chemical systems in more detail. With Green’s function based approaches, we can calculate the thermodynamic properties and have access to some of the excited state properties without the need to obtain excited states. We can use this in embedding theories like DMFT, SEET, etc. We must mention that this approach can also be used in conjunction with dynamic self-energy mapping to calculate the Green’s functions on near-term quantum devices.

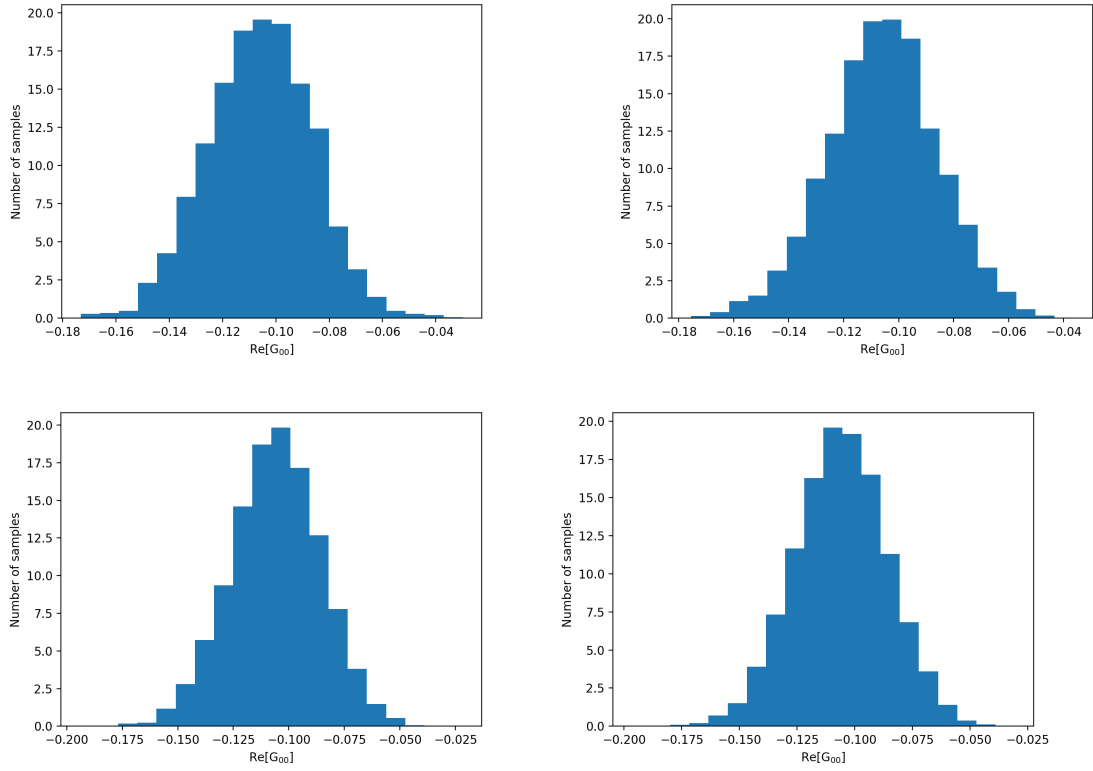


Figure 6.6: Distribution of real component of the Green's function element  $G_{00}(\omega)$  for the samples taken through the simulator. Top left: For 2000 Samples. Top right: For 4000 Samples. Bottom left: For 8000 Samples. Bottom right: For 16000 Samples.

## Author contributions

DD developed the code for calculating the Green's functions and analyzed the errors.

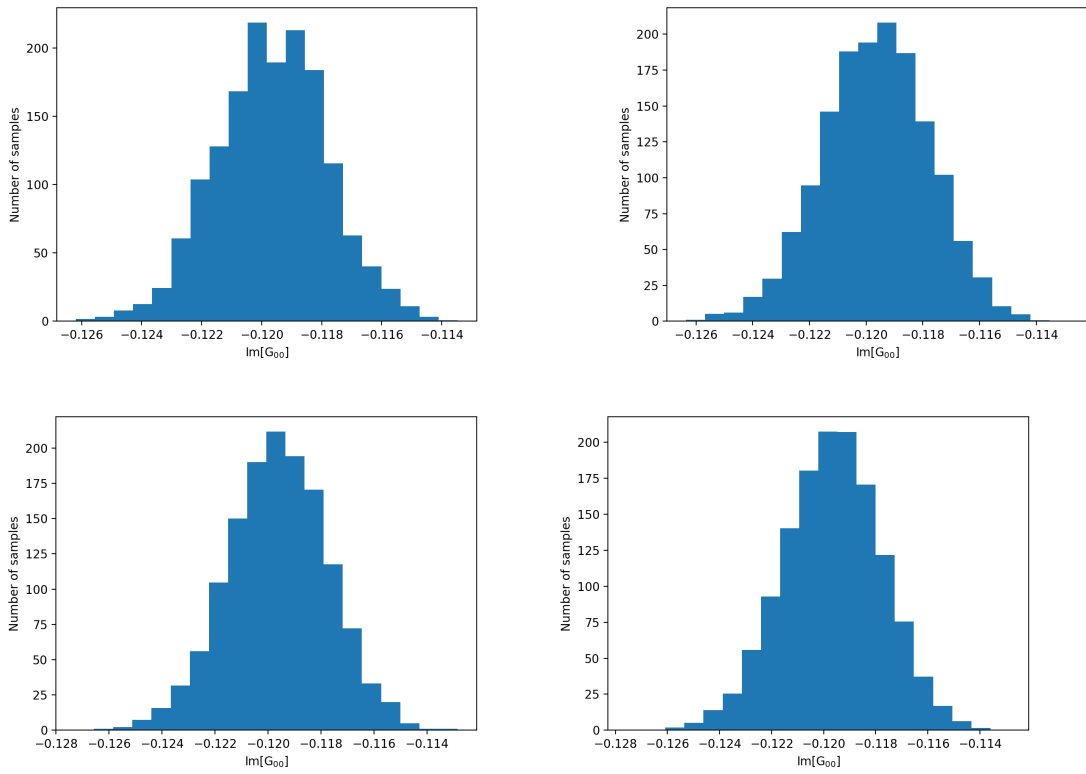


Figure 6.7: Distribution of imaginary component of the Green's function element  $G_{00}(i\omega)$  for the samples taken through the simulator. Top left: For 2000 Samples. Top right: For 4000 Samples. Bottom left: For 8000 Samples. Bottom right: For 16000 Samples.

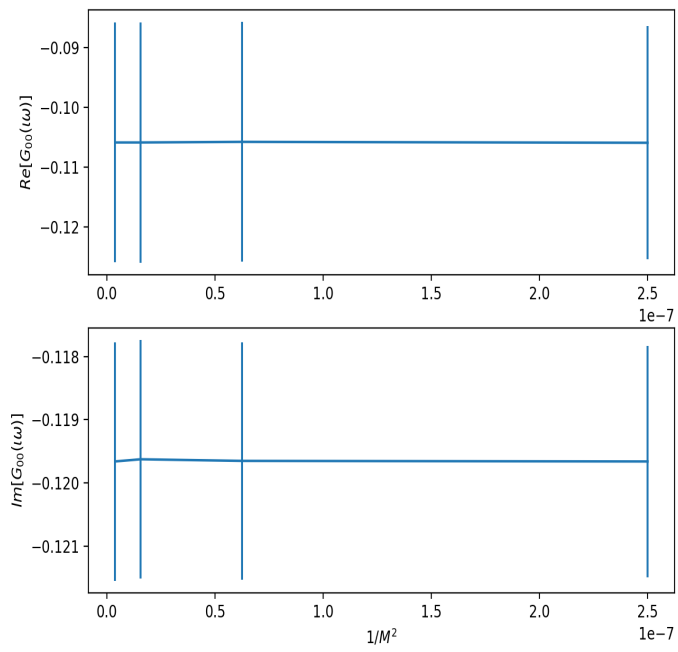


Figure 6.8: Error distribution obtained from the crude data (without using any re-sampling technique) as the sample size increases with respect to  $1/M^2$  where  $M$  is the total number of samples

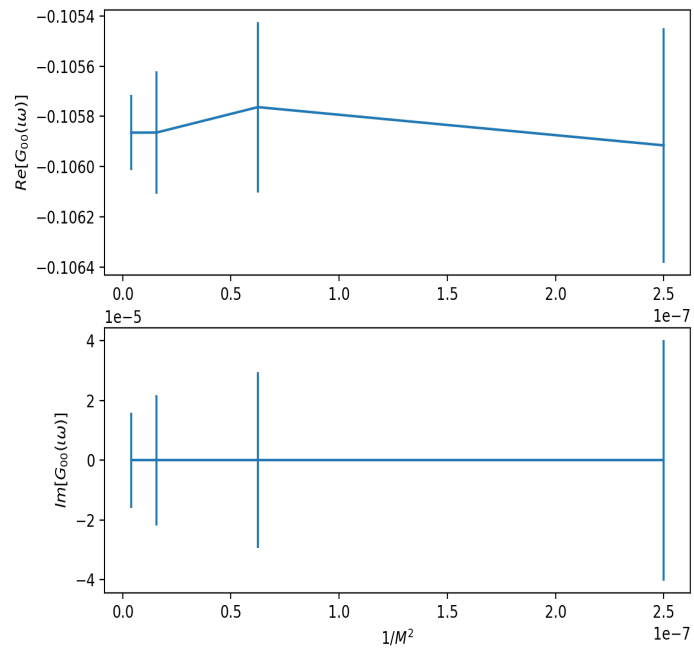


Figure 6.9: Error distribution obtained after the jackknife analysis as the sample size increases with respect to  $1/M^2$  where  $M$  is the total number of samples

## CHAPTER VII

### Conclusions

We would like to conclude this dissertation by summarizing our contribution to the field of finite temperature electronic structure theory methods. In this work, we have introduced two hybrid quantum-classical algorithms that are suitable for calculating Green's functions using NISQ devices.

In Chapter 4, We have successfully devised an effective Hamiltonian approach called DSEM. DSEM is a two-step procedure where we first sparsify the Hamiltonian using a polynomially scaling low-level method. This sparsified Hamiltonian containing a maximum of  $n^2$  terms compared to the  $n^4$  terms of full Hamiltonian ( $n$  = number of orbitals) is then used for high-level calculations, we use ED here. We show that the GF2 and ED energies obtained using the effective Hamiltonian are in good agreement with the original GF2 and ED energies. We propose to use DSEM as a hybrid classical-quantum algorithm. The first part of the algorithm can be executed on the classical machine while the quantum machine can be used for more exact calculations. The sparse nature of the Hamiltonian helps decrease the depth of the quantum circuit, thus making it suitable for NISQ machines. We have shown that we achieve an order of magnitude reduction in the number of gates required for mapping of sparse Hamiltonian when compared to the full Hamiltonian. We must note that in the presented work, we use a classical solver to show proof of principle. This suggests that

DSEM can be used even if the quantum machines are inaccessible, effective Hamiltonian approaches have shown a lot of promise in the history of quantum simulations. In Chapter 5, we use this sparse Hamiltonian approach to study the Hubbard model. In this work, we show how an approximate form of ground state Hamiltonian can lead us to more accurate results by using this approach.

Chapter 6 introduces a quantum algorithm based on quantum subspace expansion for the calculation of Green's functions. We use QSE to calculate the transition matrix elements which are used to calculate Green's function on the classical computer through post-processing. QSE provides us with the option of making our calculations parallel over multiple quantum machines and the structure of circuits makes it resilient against some of the quantum noise. We have demonstrated that the Green's function calculated using QSE is approximately equal to the one calculated using FCI within reasonable error limits. We also calculate the Green's function using a simulator that mimics an ideal fault-tolerant quantum machine, which helps us understand the statistical noise associated with a quantum machine. A proper way to treat this statistical noise has also been discussed in this work. We also try to understand the impact of quantum noise on QSE by running some calculations on quantum hardware. Although we have demonstrated both the algorithms in a stand-alone fashion, the goal of our work is to use them together, so that the sparse Hamiltonians from DSEM can help decrease the circuit depth of QSE.

The current quantum computers cannot outperform the classical computers but this thesis is a small effort to make the quantum algorithms practically useful in the near future. We believe that through these hybrid algorithms, one can leverage the best from both classical and quantum computers.

## CHAPTER VIII

### Future Directions

In this thesis, we have introduced two novel algorithms for Green's function based methods on near term quantum machines. This work opens the path to a number of promising directions. The most apparent one is to study how these two algorithms will perform together. It would be interesting to see the difference in circuit depth of the QSE algorithm as we use DSEM Hamiltonian instead of full Hamiltonian of the system.

We would also like to explore different parameterization schemes for the DSEM procedure such that we can find a systematically improvable way to generate the effective Hamiltonians. This work can also be extended to the embedding theories such as DMFT, SEET, DMET etc. We hypothesize that the use of DSEM procedure to generate the impurity Hamiltonian will provide us the option to study larger impurities on near term quantum hardware.

We understand that quantum computers have limitations and there is still a long way to go in understanding what quantum computers can and cannot do. We must also acknowledge that it is possible that the actual applications of quantum machines do not match the enthusiastic expectations. But we believe that the algorithms we have developed contribute to the field of classical electronic structure theory as well. For example, the DSEM algorithm can be used for generating effective sparse



Hamiltonians which can decrease the scaling of existing classical methods, thus making them tractable for classical machines. This comes from the long history of model Hamiltonians in quantum physics and chemistry for studying systems of interest more accurately while the environment is treated in an approximate fashion.

It is also interesting to see how the quest of building and using the quantum hardware can help enhance our understanding of quantum physics and chemistry in general. One example of such a realization is that different quantum phases of matter can be distinguished according to the structure of their long-range quantum entanglement [206].

Finally, we should realize that the quantum technology is still in its infancy and that the NISQ devices do not aim to change the world on their own but they are a step toward the quantum technology we hope to attain.

# Bibliography

- [1] Attila Szabo and Neil S Ostlund. *Modern quantum chemistry: introduction to advanced electronic structure theory*. Courier Corporation, 2012.
- [2] Trygve Helgaker, Poul Jorgensen, and Jeppe Olsen. *Molecular electronic-structure theory*. John Wiley & Sons, 2014.
- [3] Martin Head-Gordon, John A Pople, and Michael J Frisch. Mp2 energy evaluation by direct methods. *Chemical physics letters*, 153(6):503–506, 1988.
- [4] Stefan Grimme. Improved third-order møller–plesset perturbation theory. *Journal of computational chemistry*, 24(13):1529–1537, 2003.
- [5] Isaiah Shavitt. The history and evolution of configuration interaction. *Molecular Physics*, 94(1):3–17, 1998.
- [6] Rodney J Bartlett. Many-body perturbation theory and coupled cluster theory for electron correlation in molecules. *Annual review of physical chemistry*, 32(1):359–401, 1981.
- [7] Rodney J Bartlett and Monika Musiał. Coupled-cluster theory in quantum chemistry. *Reviews of Modern Physics*, 79(1):291, 2007.
- [8] Per-Åke Malmqvist and Björn O Roos. The casscf state interaction method. *Chemical physics letters*, 155(2):189–194, 1989.

- [9] Kerstin Andersson, Per Aake Malmqvist, Bjoern O Roos, Andrzej J Sadlej, and Krzysztof Wolinski. Second-order perturbation theory with a casscf reference function. *Journal of Physical Chemistry*, 94(14):5483–5488, 1990.
- [10] Celestino Angeli, Renzo Cimiraglia, S Evangelisti, T Leininger, and J-P Malrieu. Introduction of n-electron valence states for multireference perturbation theory. *The Journal of Chemical Physics*, 114(23):10252–10264, 2001.
- [11] Sheng Guo, Mark A Watson, Weifeng Hu, Qiming Sun, and Garnet Kin-Lic Chan. N-electron valence state perturbation theory based on a density matrix renormalization group reference function, with applications to the chromium dimer and a trimer model of poly (p-phenylenevinylene). *Journal of chemical theory and computation*, 12(4):1583–1591, 2016.
- [12] David Casanova and Martin Head-Gordon. Restricted active space spin-flip configuration interaction approach: theory, implementation and examples. *Physical Chemistry Chemical Physics*, 11(42):9779–9790, 2009.
- [13] Aron J Cohen, Paula Mori-Sánchez, and Weitao Yang. Challenges for density functional theory. *Chemical reviews*, 112(1):289–320, 2012.
- [14] Robert G Parr. Density functional theory. *Annual Review of Physical Chemistry*, 34(1):631–656, 1983.
- [15] Walter Kohn. Density functional theory. *Introductory Quantum Mechanics with MATLAB: For Atoms, Molecules, Clusters, and Nanocrystals*, 2019.
- [16] John A Pople, J Stephen Binkley, and Rolf Seeger. Theoretical models incorporating electron correlation. *International Journal of Quantum Chemistry*, 10(S10):1–19, 1976.

- [17] Viraht Sahni, K-P Bohnen, and Manoj K Harbola. Analysis of the local-density approximation of density-functional theory. *Physical Review A*, 37(6):1895, 1988.
- [18] EKH Gross and Walter Kohn. Local density-functional theory of frequency-dependent linear response. *Physical review letters*, 55(26):2850, 1985.
- [19] Andrea Dal Corso, Alfredo Pasquarello, Alfonso Baldereschi, and Roberto Car. Generalized-gradient approximations to density-functional theory: A comparative study for atoms and solids. *Physical Review B*, 53(3):1180, 1996.
- [20] Xinlei Hua, Xiaojie Chen, and WA Goddard. Generalized generalized gradient approximation: An improved density-functional theory for accurate orbital eigenvalues. *Physical Review B*, 55(24):16103, 1997.
- [21] Jochen Heyd and Gustavo E Scuseria. Efficient hybrid density functional calculations in solids: Assessment of the heyd–scuseria–ernzerhof screened coulomb hybrid functional. *The Journal of chemical physics*, 121(3):1187–1192, 2004.
- [22] Ayako Nakata, Yutaka Imamura, Takao Otsuka, and Hiromi Nakai. Time-dependent density functional theory calculations for core-excited states: Assessment of standard exchange-correlation functionals and development of a novel hybrid functional. *The Journal of chemical physics*, 124(9):094105, 2006.
- [23] Vladimir I Anisimov. *Strong coulomb correlations in electronic structure calculations*. CRC Press, 2000.
- [24] Alexander L Fetter and John Dirk Walecka. *Quantum theory of many-particle systems*. Courier Corporation, 2012.
- [25] LJ Holleboom and JG Snijders. A comparison between the mo/ller–plesset and green’s function perturbative approaches to the calculation of the corre-

- lation energy in the many-electron problem. *The Journal of chemical physics*, 93(8):5826–5837, 1990.
- [26] Nils Erik Dahlen and Robert van Leeuwen. Self-consistent solution of the dyson equation for atoms and molecules within a conserving approximation. *The Journal of chemical physics*, 122(16):164102, 2005.
- [27] Jordan J Phillips and Dominika Zgid. Communication: The description of strong correlation within self-consistent green’s function second-order perturbation theory. *The Journal of chemical physics*, 140(24):241101, 2014.
- [28] Marcel Nooijen and Jaap G Snijders. Coupled cluster approach to the single-particle green’s function. *International Journal of Quantum Chemistry*, 44(S26):55–83, 1992.
- [29] Marcel Nooijen and Jaap G Snijders. Coupled cluster green’s function method: Working equations and applications. *International journal of quantum chemistry*, 48(1):15–48, 1993.
- [30] Avijit Shee and Dominika Zgid. Coupled cluster as an impurity solver for green’s function embedding methods. *Journal of chemical theory and computation*, 15(11):6010–6024, 2019.
- [31] Tianyu Zhu, Carlos A Jiménez-Hoyos, James McClain, Timothy C Berkelbach, and Garnet Kin-Lic Chan. Coupled-cluster impurity solvers for dynamical mean-field theory. *Physical Review B*, 100(11):115154, 2019.
- [32] Antoine Georges and Gabriel Kotliar. Hubbard model in infinite dimensions. *Physical Review B*, 45(12):6479, 1992.
- [33] Gabriel Kotliar, Sergej Y Savrasov, Kristjan Haule, Viktor S Oudovenko, O Par-

- collet, and CA Marianetti. Electronic structure calculations with dynamical mean-field theory. *Reviews of Modern Physics*, 78(3):865, 2006.
- [34] Tran Nguyen Lan, Alexei A Kananenka, and Dominika Zgid. Communication: Towards ab initio self-energy embedding theory in quantum chemistry. *The Journal of chemical physics*, 143(24):241102, 2015.
- [35] Lan Nguyen Tran, Sergei Iskakov, and Dominika Zgid. Spin-unrestricted self-energy embedding theory. *The Journal of Physical Chemistry Letters*, 9(15):4444–4450, 2018.
- [36] Tran Nguyen Lan, Alexei A Kananenka, and Dominika Zgid. Rigorous ab initio quantum embedding for quantum chemistry using green’s function theory: Screened interaction, nonlocal self-energy relaxation, orbital basis, and chemical accuracy. *Journal of Chemical Theory and Computation*, 12(10):4856–4870, 2016.
- [37] Tran Nguyen Lan and Dominika Zgid. Generalized self-energy embedding theory. *The Journal of Physical Chemistry Letters*, 8(10):2200–2205, 2017.
- [38] Richard P Feynman. Quantum mechanical computers. *Found. Phys.*, 16(6):507–532, 1986.
- [39] Peter W Shor. Algorithms for quantum computation: discrete logarithms and factoring. In *Proceedings 35th annual symposium on foundations of computer science*, pages 124–134. Ieee, 1994.
- [40] Lov K Grover. A fast quantum mechanical algorithm for database search. In *Proceedings of the twenty-eighth annual ACM symposium on Theory of computing*, pages 212–219, 1996.
- [41] Seth Lloyd. Universal quantum simulators. *Science*, 273(5278):1073–1078, 1996.

- [42] S Somaroo, CH Tseng, TF Havel, Raymond Laflamme, and David G Cory. Quantum simulations on a quantum computer. *Physical review letters*, 82(26):5381, 1999.
- [43] Neil A Gershenfeld and Isaac L Chuang. Bulk spin-resonance quantum computation. *science*, 275(5298):350–356, 1997.
- [44] Timothy F Havel, David G Cory, and Amr F Fahmy. Ensemble quantum computing by nuclear magnetic resonance spectroscopy. In *Harvard University Center for*. Citeseer, 1997.
- [45] John Preskill. Quantum computing 40 years later. *arXiv preprint arXiv:2106.10522*, 2021.
- [46] Jerry Chow, Oliver Dial, and Jay Gambetta. Ibm quantum breaks the 100-qubit processor barrier, Nov 2021.
- [47] Abhinav Kandala, Antonio Mezzacapo, Kristan Temme, Maika Takita, Markus Brink, Jerry M Chow, and Jay M Gambetta. Hardware-efficient variational quantum eigensolver for small molecules and quantum magnets. *Nature*, 549(7671):242–246, 2017.
- [48] Joonho Lee, William J Huggins, Martin Head-Gordon, and K Birgitta Whaley. Generalized unitary coupled cluster wave functions for quantum computation. *Journal of chemical theory and computation*, 15(1):311–324, 2018.
- [49] Kenji Sugisaki, Kazuo Toyota, Kazunobu Sato, Daisuke Shiomi, and Takeji Takui. Adiabatic state preparation of correlated wave functions with nonlinear scheduling functions and broken-symmetry wave functions. *Communications Chemistry*, 5(1):1–13, 2022.

- [50] Daniel S Abrams and Seth Lloyd. Simulation of many-body fermi systems on a universal quantum computer. *Physical Review Letters*, 79(13):2586, 1997.
- [51] Daniel S Abrams and Seth Lloyd. Quantum algorithm providing exponential speed increase for finding eigenvalues and eigenvectors. *Physical Review Letters*, 83(24):5162, 1999.
- [52] Andrew M Steane. Error correcting codes in quantum theory. *Physical Review Letters*, 77(5):793, 1996.
- [53] Andrew M Steane. Simple quantum error-correcting codes. *Physical Review A*, 54(6):4741, 1996.
- [54] Daniel Gottesman. An introduction to quantum error correction. In *Proceedings of Symposia in Applied Mathematics*, volume 58, pages 221–236, 2002.
- [55] Emanuel Knill and Raymond Laflamme. Theory of quantum error-correcting codes. *Physical Review A*, 55(2):900, 1997.
- [56] A Robert Calderbank and Peter W Shor. Good quantum error-correcting codes exist. *Physical Review A*, 54(2):1098, 1996.
- [57] Emanuel Knill, Raymond Laflamme, and Lorenza Viola. Theory of quantum error correction for general noise. *Physical Review Letters*, 84(11):2525, 2000.
- [58] Fernando Pastawski, Beni Yoshida, Daniel Harlow, and John Preskill. Holographic quantum error-correcting codes: Toy models for the bulk/boundary correspondence. *Journal of High Energy Physics*, 2015(6):1–55, 2015.
- [59] Peter D Johnson, Jonathan Romero, Jonathan Olson, Yudong Cao, and Alán Aspuru-Guzik. Qvector: an algorithm for device-tailored quantum error correction. *arXiv preprint arXiv:1711.02249*, 2017.



- [60] John Preskill. Quantum computing in the nisc era and beyond. *Quantum*, 2:79, 2018.
- [61] Diksha Dhawan, Mekena Metcalf, and Dominika Zgid. Dynamical self-energy mapping (dsem) for creation of sparse hamiltonians suitable for quantum computing. *Journal of Chemical Theory and Computation*, 17(12):7622–7631, 2021.
- [62] Christina Daniel, Diksha Dhawan, Dominika Zgid, and James K Freericks. Sparse-hamiltonian approach to the time-evolution of molecules on quantum computers. *The European Physical Journal Special Topics*, 230(4):1067–1071, 2021.
- [63] Michel H Devoret, Andreas Wallraff, and John M Martinis. Superconducting qubits: A short review. *arXiv preprint cond-mat/0411174*, 2004.
- [64] Johannes Majer, JM Chow, JM Gambetta, Jens Koch, BR Johnson, JA Schreier, L Frunzio, DI Schuster, Andrew Addison Houck, Andreas Wallraff, et al. Coupling superconducting qubits via a cavity bus. *Nature*, 449(7161):443–447, 2007.
- [65] Frank Arute, Kunal Arya, Ryan Babbush, Dave Bacon, Joseph C Bardin, Rami Barends, Rupak Biswas, Sergio Boixo, Fernando GSL Brandao, David A Buell, et al. Quantum supremacy using a programmable superconducting processor. *Nature*, 574(7779):505–510, 2019.
- [66] Ming Gong, Shiyu Wang, Chen Zha, Ming-Cheng Chen, He-Liang Huang, Yulin Wu, Qingling Zhu, Youwei Zhao, Shaowei Li, Shaojun Guo, et al. Quantum walks on a programmable two-dimensional 62-qubit superconducting processor. *Science*, 372(6545):948–952, 2021.
- [67] David Kielpinski, Chris Monroe, and David J Wineland. Architecture for a large-scale ion-trap quantum computer. *Nature*, 417(6890):709–711, 2002.

- [68] Christopher Monroe and Jungsang Kim. Scaling the ion trap quantum processor. *Science*, 339(6124):1164–1169, 2013.
- [69] Peter Chapman. Introducing the world’s most powerful quantum computer. *Accessed on*, 10:2021, 2020.
- [70] Tony Lu, Xiyue Miao, and Harold Metcalf. Bloch theorem on the bloch sphere. *Physical Review A*, 71(6):061405, 2005.
- [71] Michael A Nielsen and Isaac Chuang. Quantum computation and quantum information, 2002.
- [72] Christof Zalka. Simulating quantum systems on a quantum computer. *Proceedings of the Royal Society of London. Series A: Mathematical, Physical and Engineering Sciences*, 454(1969):313–322, 1998.
- [73] Eugene Paul Wigner. *The Collected Works of Eugene Paul Wigner*, volume 1. Springer Science & Business Media, 1993.
- [74] Andrew Tranter, Peter J Love, Florian Mintert, and Peter V Coveney. A comparison of the bravyi–kitaev and jordan–wigner transformations for the quantum simulation of quantum chemistry. *Journal of chemical theory and computation*, 14(11):5617–5630, 2018.
- [75] Sergey B Bravyi and Alexei Yu Kitaev. Fermionic quantum computation. *Annals of Physics*, 298(1):210–226, 2002.
- [76] Jacob T Seeley, Martin J Richard, and Peter J Love. The bravyi-kitaev transformation for quantum computation of electronic structure. *The Journal of chemical physics*, 137(22):224109, 2012.
- [77] A Yu Kitaev. Quantum measurements and the abelian stabilizer problem. *arXiv preprint quant-ph/9511026*, 1995.

- [78] Hale F Trotter. On the product of semi-groups of operators. *Proceedings of the American Mathematical Society*, 10(4):545–551, 1959.
- [79] Masuo Suzuki. Generalized trotter’s formula and systematic approximants of exponential operators and inner derivations with applications to many-body problems. *Communications in Mathematical Physics*, 51(2):183–190, 1976.
- [80] Nathan Wiebe and Andrew Childs. Hamiltonian simulation using linear combinations of unitary operations. In *APS March Meeting Abstracts*, volume 2012, pages T30–003, 2012.
- [81] Dominic W Berry and Andrew M Childs. Black-box hamiltonian simulation and unitary implementation. *arXiv preprint arXiv:0910.4157*, 2009.
- [82] Anmer Daskin and Sabre Kais. Decomposition of unitary matrices for finding quantum circuits: application to molecular hamiltonians. *The Journal of chemical physics*, 134(14):144112, 2011.
- [83] Dominic W Berry, Andrew M Childs, Richard Cleve, Robin Kothari, and Rolando D Somma. Exponential improvement in precision for simulating sparse hamiltonians. In *Forum of Mathematics, Sigma*, volume 5. Cambridge University Press, 2017.
- [84] Guang Hao Low and Isaac L Chuang. Hamiltonian simulation by qubitization. *Quantum*, 3:163, 2019.
- [85] Ryan Babbush, Dominic W Berry, Ian D Kivlichan, Annie Y Wei, Peter J Love, and Alán Aspuru-Guzik. Exponentially more precise quantum simulation of fermions in second quantization. *New Journal of Physics*, 18(3):033032, 2016.
- [86] Benjamin P Lanyon, James D Whitfield, Geoff G Gillett, Michael E Goggin, Marcelo P Almeida, Ivan Kassal, Jacob D Biamonte, Masoud Mohseni, Ben J

- Powell, Marco Barbieri, et al. Towards quantum chemistry on a quantum computer. *Nature chemistry*, 2(2):106–111, 2010.
- [87] Nathan Wiebe and Chris Granade. Efficient bayesian phase estimation. *Physical review letters*, 117(1):010503, 2016.
- [88] Edward Farhi, Jeffrey Goldstone, Sam Gutmann, and Michael Sipser. Quantum computation by adiabatic evolution. *arXiv preprint quant-ph/0001106*, 2000.
- [89] Alán Aspuru-Guzik, Anthony D Dutoi, Peter J Love, and Martin Head-Gordon. Simulated quantum computation of molecular energies. *Science*, 309(5741):1704–1707, 2005.
- [90] Vladimir Bužek and Mark Hillery. Quantum copying: Beyond the no-cloning theorem. *Physical Review A*, 54(3):1844, 1996.
- [91] Göran Lindblad. A general no-cloning theorem. *Letters in Mathematical Physics*, 47(2):189–196, 1999.
- [92] Dorit Aharonov and Michael Ben-Or. Fault-tolerant quantum computation with constant error rate. *SIAM Journal on Computing*, 2008.
- [93] Jarrod R McClean, Jonathan Romero, Ryan Babbush, and Alán Aspuru-Guzik. The theory of variational hybrid quantum-classical algorithms. *New Journal of Physics*, 18(2):023023, 2016.
- [94] Jarrod R McClean, Sergio Boixo, Vadim N Smelyanskiy, Ryan Babbush, and Hartmut Neven. Barren plateaus in quantum neural network training landscapes. *Nature communications*, 9(1):1–6, 2018.
- [95] Panagiotis Kl Barkoutsos, Jerome F Gonthier, Igor Sokolov, Nikolaj Moll, Gian Salis, Andreas Fuhrer, Marc Ganzhorn, Daniel J Egger, Matthias Troyer, Antonio Mezzacapo, et al. Quantum algorithms for electronic structure calculations:

- Particle-hole hamiltonian and optimized wave-function expansions. *Physical Review A*, 98(2):022322, 2018.
- [96] Marc Ganzhorn, Daniel J Egger, Panagiotis Barkoutsos, Pauline Ollitrault, Gian Salis, Nikolaj Moll, Marco Roth, A Fuhrer, P Mueller, Stefan Woerner, et al. Gate-efficient simulation of molecular eigenstates on a quantum computer. *Physical Review Applied*, 11(4):044092, 2019.
- [97] Edward Grant, Leonard Wossnig, Mateusz Ostaszewski, and Marcello Benedetti. Una estrategia de inicialización para abordar mesetas estériles en circuitos cuánticos parametrizados. *Quantum*, 3(214):10–22331, 2019.
- [98] Tyler Volkoff and Patrick J Coles. Large gradients via correlation in random parameterized quantum circuits. *Quantum Science and Technology*, 6(2):025008, 2021.
- [99] Harper R Grimsley, Sophia E Economou, Edwin Barnes, and Nicholas J Mayhall. An adaptive variational algorithm for exact molecular simulations on a quantum computer. *Nature communications*, 10(1):1–9, 2019.
- [100] Nicholas H Stair and Francesco A Evangelista. Simulating many-body systems with a projective quantum eigensolver. *PRX Quantum*, 2(3):030301, 2021.
- [101] Oinam Romesh Meitei, Bryan T Gard, George S Barron, David P Pappas, Sophia E Economou, Edwin Barnes, and Nicholas J Mayhall. Gate-free state preparation for fast variational quantum eigensolver simulations: ctrl-vqe. *arXiv preprint arXiv:2008.04302*, 2020.
- [102] Radi A Jishi. *Feynman diagram techniques in condensed matter physics*. Cambridge University Press, 2013.

- [103] Gianluca Stefanucci and Robert Van Leeuwen. *Nonequilibrium many-body theory of quantum systems: a modern introduction*. Cambridge University Press, 2013.
- [104] Juha M Kreula, Laura García-Álvarez, Lucas Lamata, Stephen R Clark, Enrique Solano, and Dieter Jaksch. Few-qubit quantum-classical simulation of strongly correlated lattice fermions. *EPJ Quantum Technology*, 3(1):1–19, 2016.
- [105] JM Kreula, Stephen R Clark, and D Jaksch. Non-linear quantum-classical scheme to simulate non-equilibrium strongly correlated fermionic many-body dynamics. *Scientific reports*, 6(1):1–7, 2016.
- [106] Bela Bauer, Dave Wecker, Andrew J Millis, Matthew B Hastings, and Matthias Troyer. Hybrid quantum-classical approach to correlated materials. *Physical Review X*, 6(3):031045, 2016.
- [107] Ben Jaderberg, Abhishek Agarwal, Karsten Leonhardt, Martin Kiffner, and Dieter Jaksch. Minimum hardware requirements for hybrid quantum–classical dmft. *Quantum Science and Technology*, 5(3):034015, 2020.
- [108] Dave Wecker, Matthew B Hastings, Nathan Wiebe, Bryan K Clark, Chetan Nayak, and Matthias Troyer. Solving strongly correlated electron models on a quantum computer. *Physical Review A*, 92(6):062318, 2015.
- [109] Yu Tong, Dong An, Nathan Wiebe, and Lin Lin. Fast inversion, preconditioned quantum linear system solvers, fast green’s-function computation, and fast evaluation of matrix functions. *Physical Review A*, 104(3):032422, 2021.
- [110] Suguru Endo, Iori Kurata, and Yuya O Nakagawa. Calculation of the green’s function on near-term quantum computers. *Physical Review Research*, 2(3):033281, 2020.

- [111] Ken M Nakanishi, Kosuke Mitarai, and Keisuke Fujii. Subspace-search variational quantum eigensolver for excited states. *Physical Review Research*, 1(3):033062, 2019.
- [112] Robert M Parrish, Edward G Hohenstein, Peter L McMahon, and Todd J Martínez. Quantum computation of electronic transitions using a variational quantum eigensolver. *Physical review letters*, 122(23):230401, 2019.
- [113] Francois Jamet, Abhishek Agarwal, and Ivan Rungger. Quantum subspace expansion algorithm for green’s functions. *arXiv preprint arXiv:2205.00094*, 2022.
- [114] Mario Motta, Chong Sun, Adrian TK Tan, Matthew J O’Rourke, Erika Ye, Austin J Minnich, Fernando GSL Brandão, and Garnet Kin Chan. Determining eigenstates and thermal states on a quantum computer using quantum imaginary time evolution. *Nature Physics*, 16(2):205–210, 2020.
- [115] Jarrod R McClean, Mollie E Kimchi-Schwartz, Jonathan Carter, and Wibe A De Jong. Hybrid quantum-classical hierarchy for mitigation of decoherence and determination of excited states. *Physical Review A*, 95(4):042308, 2017.
- [116] William J Huggins, Joonho Lee, Unpil Baek, Bryan O’Gorman, and K Birgitta Whaley. A non-orthogonal variational quantum eigensolver. *New Journal of Physics*, 22(7):073009, 2020.
- [117] Katherine Klymko, Carlos Mejuto-Zaera, Stephen J Cotton, Filip Wudarski, Miroslav Urbanek, Diptarka Hait, Martin Head-Gordon, K Birgitta Whaley, Jonathan Moussa, Nathan Wiebe, et al. Real-time evolution for ultracompact hamiltonian eigenstates on quantum hardware. *PRX Quantum*, 3(2):020323, 2022.

- [118] Ethan N Epperly, Lin Lin, and Yuji Nakatsukasa. A theory of quantum subspace diagonalization. *SIAM Journal on Matrix Analysis and Applications*, 43(3):1263–1290, 2022.
- [119] HQ Lin, JE Gubernatis, Harvey Gould, and Jan Tobochnik. Exact diagonalization methods for quantum systems. *Computers in Physics*, 7(4):400–407, 1993.
- [120] Antoine Georges, Gabriel Kotliar, Werner Krauth, and Marcelo J. Rozenberg. Dynamical mean-field theory of strongly correlated fermion systems and the limit of infinite dimensions. *Rev. Mod. Phys.*, 68:13–125, Jan 1996.
- [121] K Held. Electronic structure calculations using dynamical mean field theory. *Advances in physics*, 56(6):829–926, 2007.
- [122] G. Kotliar, S. Y. Savrasov, K. Haule, V. S. Oudovenko, O. Parcollet, and C. A. Marianetti. Electronic structure calculations with dynamical mean-field theory. *Rev. Mod. Phys.*, 78:865–951, Aug 2006.
- [123] Gregory H. Wannier. The structure of electronic excitation levels in insulating crystals. *Phys. Rev.*, 52:191–197, Aug 1937.
- [124] Nicola Marzari, Arash A. Mostofi, Jonathan R. Yates, Ivo Souza, and David Vanderbilt. Maximally localized wannier functions: Theory and applications. *Rev. Mod. Phys.*, 84:1419–1475, Oct 2012.
- [125] Takeshi Yanai and Garnet Kin-Lic Chan. Canonical transformation theory for multireference problems. *The Journal of chemical physics*, 124(19):194106, 2006.
- [126] Takeshi Yanai and Garnet Kin-Lic Chan. Canonical transformation theory from



- extended normal ordering. *The Journal of chemical physics*, 127(10):104107, 2007.
- [127] Garnet Kin Chan and Takeshi Yanai. Canonical transformation theory for dynamic correlations in multireference problems. *Advances in Chemical Physics*, 134:343, 2007.
- [128] R Sakuma, T Miyake, and F Aryasetiawan. Effective quasiparticle hamiltonian based on löwdin’s orthogonalization. *Physical Review B*, 80(23):235128, 2009.
- [129] Huihuo Zheng, Hitesh J Changlani, Kiel T Williams, Brian Busemeyer, and Lucas K Wagner. From real materials to model hamiltonians with density matrix downfolding. *Frontiers in Physics*, 6:43, 2018.
- [130] Hitesh J Changlani, Huihuo Zheng, and Lucas K Wagner. Density-matrix based determination of low-energy model hamiltonians from ab initio wavefunctions. *The Journal of chemical physics*, 143(10):102814, 2015.
- [131] Claude Bloch. Sur la théorie des perturbations des états liés. *Nuclear Physics*, 6:329–347, 1958.
- [132] Jacques Des Cloizeaux. Extension d’une formule de lagrange à des problèmes de valeurs propres. *Nuclear Physics*, 20:321–346, 1960.
- [133] John R Schrieffer and Peter A Wolff. Relation between the anderson and kondo hamiltonians. *Physical Review*, 149(2):491, 1966.
- [134] Baird H Brandow. Linked-cluster expansions for the nuclear many-body problem. *Reviews of Modern Physics*, 39(4):771, 1967.
- [135] CE Soliverez. An effective hamiltonian and time-independent perturbation theory. *Journal of Physics C: Solid State Physics*, 2(12):2161, 1969.

- [136] TH Schucan and HA Weidenmüller. The effective interaction in nuclei and its perturbation expansion: An algebraic approach. *Annals of Physics*, 73(1):108–135, 1972.
- [137] Flemming Jørgensen. Effective hamiltonians. *Molecular Physics*, 29(4):1137–1164, 1975.
- [138] Debashis Mukherjee, Raj Kumar Moitra, and Atri Mukhopadhyay. Correlation problem in open-shell atoms and molecules: A non-perturbative linked cluster formulation. *Molecular Physics*, 30(6):1861–1888, 1975.
- [139] Bogumil Jeziorski and Hendrik J Monkhorst. Coupled-cluster method for multideterminantal reference states. *Physical Review A*, 24(4):1668, 1981.
- [140] Werner Kutzelnigg. Quantum chemistry in fock space. i. the universal wave and energy operators. *The Journal of Chemical Physics*, 77(6):3081–3097, 1982.
- [141] Leszek Z Stolarczyk and Hendrik J Monkhorst. Coupled-cluster method in fock space. i. general formalism. *Physical Review A*, 32(2):725, 1985.
- [142] Debashis Mukherjee. The linked-cluster theorem in the open-shell coupled-cluster theory for incomplete model spaces. *Chemical physics letters*, 125(3):207–212, 1986.
- [143] Philippe Durand. Direct determination of effective hamiltonians by wave-operator methods. i. general formalism. *Physical Review A*, 28(6):3184, 1983.
- [144] Philippe Durand and Jean-Paul Malrieu. Effective hamiltonians and pseudo-operators as tools for rigorous modelling. *Ab Initio Methods in Quantum Chemistry, Part I, Ed. KP Lawley, John Wiley & Sons Ltd*, page 321, 1987.
- [145] Bogumil Jeziorski and Josef Paldus. Valence universal exponential ansatz and

- the cluster structure of multireference configuration interaction wave function. *The Journal of chemical physics*, 90(5):2714–2731, 1989.
- [146] Uzi Kaldor. The fock space coupled cluster method: theory and application. *Theoretica chimica acta*, 80(6):427–439, 1991.
- [147] CML Rittby and RJ Bartlett. Multireference coupled cluster theory in fock space. *Theoretica chimica acta*, 80(6):469–482, 1991.
- [148] James P Finley, Rajat K Chaudhuri, and Karl F Freed. Applications of multireference perturbation theory to potential energy surfaces by optimal partitioning of h: Intruder states avoidance and convergence enhancement. *The Journal of chemical physics*, 103(12):4990–5010, 1995.
- [149] Stanisław D Głazek and Kenneth G Wilson. Renormalization of hamiltonians. *Physical Review D*, 48(12):5863, 1993.
- [150] Leszek Meissner and Marcel Nooijen. Effective and intermediate hamiltonians obtained by similarity transformations. *The Journal of chemical physics*, 102(24):9604–9614, 1995.
- [151] Leszek Meissner. Fock-space coupled-cluster method in the intermediate hamiltonian formulation: Model with singles and doubles. *The Journal of chemical physics*, 108(22):9227–9235, 1998.
- [152] Haruyuki Nakano, Kimihiko Hirao, and Mark S Gordon. Analytic energy gradients for multiconfigurational self-consistent field second-order quasidegenerate perturbation theory (mc-qedpt). *The Journal of chemical physics*, 108(14):5660–5669, 1998.
- [153] Celestino Angeli, Renzo Cimiraglia, and Jean-Paul Malrieu. N-electron valence

- state perturbation theory: a fast implementation of the strongly contracted variant. *Chemical physics letters*, 350(3-4):297–305, 2001.
- [154] Sergey Bravyi, David P DiVincenzo, and Daniel Loss. Schrieffer–wolff transformation for quantum many-body systems. *Annals of physics*, 326(10):2793–2826, 2011.
- [155] Dominic W Berry, Andrew M Childs, Richard Cleve, Robin Kothari, and Rolando D Somma. Exponential improvement in precision for simulating sparse hamiltonians. In *Proceedings of the forty-sixth annual ACM symposium on Theory of computing*, pages 283–292, 2014.
- [156] Dominic W Berry, Graeme Ahokas, Richard Cleve, and Barry C Sanders. Efficient quantum algorithms for simulating sparse hamiltonians. *Communications in Mathematical Physics*, 270(2):359–371, 2007.
- [157] Andrew M Childs and Robin Kothari. Limitations on the simulation of non-sparse hamiltonians. *arXiv preprint arXiv:0908.4398*, 2009.
- [158] Tyler Takeshita, Nicholas C Rubin, Zhang Jiang, Eunseok Lee, Ryan Babbush, and Jarrod R McClean. Increasing the representation accuracy of quantum simulations of chemistry without extra quantum resources. *Physical Review X*, 10(1):011004, 2020.
- [159] Nicholas P Bauman, Eric J Bylaska, Sriram Krishnamoorthy, Guang Hao Low, Nathan Wiebe, Christopher E Granade, Martin Roetteler, Matthias Troyer, and Karol Kowalski. Downfolding of many-body hamiltonians using active-space models: Extension of the sub-system embedding sub-algebras approach to unitary coupled cluster formalisms. *The Journal of chemical physics*, 151(1):014107, 2019.

- [160] Nicholas P Bauman, Guang Hao Low, and Karol Kowalski. Quantum simulations of excited states with active-space downfolded hamiltonians. *The Journal of chemical physics*, 151(23):234114, 2019.
- [161] Nicholas P Bauman, Bo Peng, and Karol Kowalski. Coupled cluster green's function formulations based on the effective hamiltonians. *Molecular Physics*, 118(19-20):e1725669, 2020.
- [162] Burak Sahinoglu and Rolando D Somma. Hamiltonian simulation in the low energy subspace. *arXiv preprint arXiv:2006.02660*, 2020.
- [163] Alexander A Rusakov, Jordan J Phillips, and Dominika Zgid. Local hamiltonians for quantitative green's function embedding methods. *The Journal of chemical physics*, 141(19):194105, 2014.
- [164] Nils Erik Dahlen and Robert van Leeuwen. Self-consistent solution of the dyson equation for atoms and molecules within a conserving approximation. *The Journal of Chemical Physics*, 122(16):164102, 2005.
- [165] Jordan J. Phillips and Dominika Zgid. Communication: The description of strong correlation within self-consistent green's function second-order perturbation theory. *The Journal of Chemical Physics*, 140(24):241101, 2014.
- [166] Alexander A. Rusakov and Dominika Zgid. Self-consistent second-order green's function perturbation theory for periodic systems. *The Journal of Chemical Physics*, 144(5):054106, 2016.
- [167] Sergei Isakov, Alexander A. Rusakov, Dominika Zgid, and Emanuel Gull. Effect of propagator renormalization on the band gap of insulating solids. *Phys. Rev. B*, 100:085112, Aug 2019.

- [168] Lars Hedin. New method for calculating the one-particle green's function with application to the electron-gas problem. *Phys. Rev.*, 139:A796–A823, Aug 1965.
- [169] Gökhan Esirgen and N. E. Bickers. Fluctuation-exchange theory for general lattice hamiltonians. *Phys. Rev. B*, 55:2122–2143, Jan 1997.
- [170] V Drchal, V Janiš, J Kudrnovský, VS Oudovenko, X Dai, Kristjan Haule, and G Kotliar. Dynamical correlations in multiorbital hubbard models: fluctuation exchange approximations. *Journal of Physics: Condensed Matter*, 17(1):61, 2004.
- [171] G. Ortiz, J. E. Gubernatis, E. Knill, and R. Laflamme. Quantum algorithms for fermionic simulations. *Phys. Rev. A*, 64:022319, Jul 2001.
- [172] Bela Bauer, Dave Wecker, Andrew J. Millis, Matthew B. Hastings, and Matthias Troyer. Hybrid quantum-classical approach to correlated materials. *Phys. Rev. X*, 6:031045, Sep 2016.
- [173] Thomas E Baker. Lanczos recursion on a quantum computer for the green's function and ground state. *Physical Review A*, 103(3):032404, 2021.
- [174] Hongxiang Chen, Max Nusspickel, Jules Tilly, and George H Booth. A variational quantum eigensolver for dynamic correlation functions. *arXiv preprint arXiv:2105.01703*, 2021.
- [175] Trevor Keen, Thomas Maier, Steven Johnston, and Pavel Lougovski. Quantum-classical simulation of two-site dynamical mean-field theory on noisy quantum hardware. *Quantum Science and Technology*, 5(3):035001, 2020.
- [176] Taichi Kosugi and Yu-ichiro Matsushita. Construction of green's functions on a quantum computer: applications to molecular systems. *arXiv preprint arXiv:1908.03902*, 2019.

- [177] Pauli Virtanen, Ralf Gommers, Travis E. Oliphant, Matt Haberland, Tyler Reddy, David Cournapeau, Evgeni Burovski, Pearu Peterson, Warren Weckesser, Jonathan Bright, Stéfan J. van der Walt, Matthew Brett, Joshua Wilson, K. Jarrod Millman, Nikolay Mayorov, Andrew R. J. Nelson, Eric Jones, Robert Kern, Eric Larson, C J Carey, İlhan Polat, Yu Feng, Eric W. Moore, Jake VanderPlas, Denis Laxalde, Josef Perktold, Robert Cimrman, Ian Henriksen, E. A. Quintero, Charles R. Harris, Anne M. Archibald, Antônio H. Ribeiro, Fabian Pedregosa, Paul van Mulbregt, and SciPy 1.0 Contributors. SciPy 1.0: Fundamental Algorithms for Scientific Computing in Python. *Nature Methods*, 17:261–272, 2020.
- [178] Dave Wecker, Bela Bauer, Bryan K Clark, Matthew B Hastings, and Matthias Troyer. Gate-count estimates for performing quantum chemistry on small quantum computers. *Physical Review A*, 90(2):022305, 2014.
- [179] Hongbin Liu, Guang Hao Low, Damian S Steiger, Thomas Häner, Markus Reiher, and Matthias Troyer. Prospects of quantum computing for molecular sciences. *arXiv preprint arXiv:2102.10081*, 2021.
- [180] Pascual Jordan and Eugene Wigner. Pauli’s equivalence prohibition. *Z. Physik*, 47:631, 1928.
- [181] Sergey B. Bravyi and Alexei Yu. Kitaev. Fermionic quantum computation. *Annals of Physics*, 298(1):210–226, May 2002.
- [182] Jarrod R. McClean, Kevin J. Sung, Ian D. Kivlichan, Yudong Cao, Chengyu Dai, E. Schuyler Fried, Craig Gidney, Brendan Gimby, Pranav Gokhale, Thomas Häner, Tarini Hardikar, Vojtěch Havlíček, Oscar Higgott, Cupjin Huang, Josh Izaac, Zhang Jiang, Xinle Liu, Sam McArdle, Matthew Neeley, Thomas O’Brien, Bryan O’Gorman, Isil Ozfidan, Maxwell D. Radin, Jhonathan

- Romero, Nicholas Rubin, Nicolas P. D. Sawaya, Kanav Setia, Sukin Sim, Damian S. Steiger, Mark Steudtner, Qiming Sun, Wei Sun, Daochen Wang, Fang Zhang, and Ryan Babbush. Openfermion: The electronic structure package for quantum computers, 2017.
- [183] Jacob T. Seeley, Martin J. Richard, and Peter J. Love. The bravyyi-kitaev transformation for quantum computation of electronic structure. *The Journal of Chemical Physics*, 137(22):224109, dec 2012.
- [184] Ryan Babbush, Nathan Wiebe, Jarrod McClean, James McClain, Hartmut Neven, and Garnet Kin-Lic Chan. Low-depth quantum simulation of materials. *Physical Review X*, 8(1):011044, 2018.
- [185] Mario Motta, Erika Ye, Jarrod R McClean, Zhendong Li, Austin J Minnich, Ryan Babbush, and Garnet Kin-Lic Chan. Low rank representations for quantum simulation of electronic structure. *npj Quantum Information*, 7(1):1–7, 2021.
- [186] Bo Peng and Karol Kowalski. Highly efficient and scalable compound decomposition of two-electron integral tensor and its application in coupled cluster calculations. *Journal of chemical theory and computation*, 13(9):4179–4192, 2017.
- [187] Alexei A. Kananenka, Emanuel Gull, and Dominika Zgid. Systematically improvable multiscale solver for correlated electron systems. *Phys. Rev. B*, 91:121111(R), Mar 2015.
- [188] Dominika Zgid and Emanuel Gull. Finite temperature quantum embedding theories for correlated systems. *New Journal of Physics*, 19(2):023047, feb 2017.
- [189] Alexander A. Rusakov, Sergei Isakov, Lan Nguyen Tran, and Dominika Zgid.



- Self-energy embedding theory (seet) for periodic systems. *Journal of Chemical Theory and Computation*, 15(1):229–240, 2019.
- [190] Sergei Isakov, Chia-Nan Yeh, Emanuel Gull, and Dominika Zgid. Ab initio self-energy embedding for the photoemission spectra of nio and mno. *Phys. Rev. B*, 102:085105, Aug 2020.
- [191] Alberto Peruzzo, Jarrod McClean, Peter Shadbolt, Man-Hong Yung, Xiao-Qi Zhou, Peter J Love, Alán Aspuru-Guzik, and Jeremy L O’Brien. A variational eigenvalue solver on a photonic quantum processor. *Nature communications*, 5(1):1–7, 2014.
- [192] Yudong Cao, Jonathan Romero, Jonathan P Olson, Matthias Degroote, Peter D Johnson, Mária Kieferová, Ian D Kivlichan, Tim Menke, Borja Peropadre, Nicolas PD Sawaya, et al. Quantum chemistry in the age of quantum computing. *Chemical reviews*, 119(19):10856–10915, 2019.
- [193] RJ Bartlett, SA Kucharski, and J Noga. Chem phys lett 155: 133. *Watts JD, Trucks GW and Bartlett RJ (1989) Chem Phys Lett (1989)*, 157:359, 1989.
- [194] John Hubbard. The description of collective motions in terms of many-body perturbation theory. ii. the correlation energy of a free-electron gas. *Proceedings of the Royal Society of London. Series A. Mathematical and Physical Sciences*, 243(1234):336–352, 1958.
- [195] Luogen Xu, Joseph T Lee, and JK Freericks. Test of the unitary coupled-cluster variational quantum eigensolver for a simple strongly correlated condensed-matter system. *Modern Physics Letters B*, 34(19n20):2040049, 2020.
- [196] Gerardo Ortiz, James E Gubernatis, Emanuel Knill, and Raymond Laflamme. Quantum algorithms for fermionic simulations. *Physical Review A*, 64(2):022319, 2001.

- [197] Lars Hedin. New method for calculating the one-particle green's function with application to the electron-gas problem. *Physical Review*, 139(3A):A796, 1965.
- [198] Ferdi Aryasetiawan and Olle Gunnarsson. The gw method. *Reports on Progress in Physics*, 61(3):237, 1998.
- [199] Adrian Stan, Nils Erik Dahlen, and Robert Van Leeuwen. Fully self-consistent gw calculations for atoms and molecules. *EPL (Europhysics Letters)*, 76(2):298, 2006.
- [200] K Kowalski, K Bhaskaran-Nair, and WA Shelton. Coupled-cluster representation of green function employing modified spectral resolutions of similarity transformed hamiltonians. *The Journal of Chemical Physics*, 141(9):094102, 2014.
- [201] Gerald Knizia and Garnet Kin-Lic Chan. Density matrix embedding: A simple alternative to dynamical mean-field theory. *Physical review letters*, 109(18):186404, 2012.
- [202] Gerald Knizia and Garnet Kin-Lic Chan. Density matrix embedding: A strong-coupling quantum embedding theory. *Journal of chemical theory and computation*, 9(3):1428–1432, 2013.
- [203] Hung Q Pham, Matthew R Hermes, and Laura Gagliardi. Periodic electronic structure calculations with the density matrix embedding theory. *Journal of Chemical Theory and Computation*, 16(1):130–140, 2019.
- [204] Francesco Libbi, Jacopo Rizzo, Francesco Tacchino, Nicola Marzari, and Ivano Tavernelli. Effective calculation of the green's function in the time domain on near-term quantum processors. *arXiv preprint arXiv:2203.12372*, 2022.

[205] MD SAJID ANIS, Abby-Mitchell, Héctor Abraham, AduOffei, Rochisha Agarwal, Gabriele Agliardi, Merav Aharoni, Vishnu Ajith, Ismail Yunus Akhalwaya, Gadi Aleksandrowicz, Thomas Alexander, Matthew Amy, Sashwat Anagolum, Anthony-Gandon, Israel F. Araujo, Eli Arbel, Abraham Asfaw, Anish Athalye, Artur Avkhadiev, Carlos Azaustre, PRATHAMESH BHOLE, Abhik Banerjee, Santanu Banerjee, Will Bang, Aman Bansal, Panagiotis Barkoutsos, Ashish Barnawal, George Barron, George S. Barron, Luciano Bello, Yael Ben-Haim, M. Chandler Bennett, Daniel Bevenius, Dhruv Bhatnagar, Prakhar Bhatnagar, Arjun Bhobe, Paolo Bianchini, Lev S. Bishop, Carsten Blank, Sorin Bolos, Soham Bopardikar, Samuel Bosch, Sebastian Brandhofer, Brandon, Sergey Bravyi, Nick Bronn, Bryce-Fuller, David Bucher, Artemiy Burov, Fran Cabrera, Padraic Calpin, Lauren Capelluto, Jorge Carballo, Ginés Carrascal, Adam Carriker, Ivan Carvalho, Adrian Chen, Chun-Fu Chen, Edward Chen, Jielun (Chris) Chen, Richard Chen, Franck Chevallier, Kartik Chinda, Rathish Cholarajan, Jerry M. Chow, Spencer Churchill, CisterMoke, Christian Claus, Christian Clauss, Caleb Clothier, Romilly Cocking, Ryan Cocuzzo, Jordan Connor, Filipe Correa, Zachary Crockett, Abigail J. Cross, Andrew W. Cross, Simon Cross, Juan Cruz-Benito, Chris Culver, Antonio D. Córcoles-Gonzales, Navaneeth D, Sean Dague, Tareq El Dandachi, Animesh N Dangwal, Jonathan Daniel, Marcus Daniels, Matthieu Dartiailh, Abdón Rodríguez Davila, Faisal Debouni, Anton Dekusar, Amol Deshmukh, Mohit Deshpande, Delton Ding, Jun Doi, Eli M. Dow, Patrick Downing, Eric Drechsler, Eugene Dumitrescu, Karel Dumon, Ivan Duran, Kareem EL-Safty, Eric Eastman, Grant Eberle, Amir Ebrahimi, Pieter Eendebak, Daniel Egger, ElePT, Emilio, Alberto Espiricueta, Mark Everitt, Davide Facchetti, Farida, Paco Martín Fernández, Samuele Ferracin, Davide Ferrari, Axel Hernández Ferrera, Romain Fouilland, Albert Frisch, Andreas Fuhrer, Bryce Fuller, MELVIN GEORGE, Julien Gacon, Borja Godoy Gago, Clau-

dio Gambella, Jay M. Gambetta, Adhisha Gammanpila, Luis Garcia, Tanya Garg, Shelly Garion, James R. Garrison, Jim Garrison, Tim Gates, Hristo Georgiev, Leron Gil, Austin Gilliam, Aditya Giridharan, Glen, Juan Gomez-Mosquera, Gonzalo, Salvador de la Puente González, Jesse Gorzinski, Ian Gould, Donny Greenberg, Dmitry Grinko, Wen Guan, Dani Guijo, Guillermo-Mijares-Vilarino, John A. Gunnels, Harshit Gupta, Naman Gupta, Jakob M. Günther, Mikael Haglund, Isabel Haide, Ikko Hamamura, Omar Costa Hamido, Frank Harkins, Kevin Hartman, Areeq Hasan, Vojtech Havlicek, Joe Hellmers, Lukasz Herok, Stefan Hillmich, Colin Hong, Hiroshi Horii, Connor Howington, Shaohan Hu, Wei Hu, Chih-Han Huang, Junye Huang, Rolf Huisman, Haruki Imai, Takashi Imamichi, Kazuaki Ishizaki, Ishwor, Raban Iten, Toshinari Itoko, Alexander Ivrii, Ali Javadi, Ali Javadi-Abhari, Wahaj Javed, Qian Jianhua, Madhav Jivrajani, Kiran Johns, Scott Johnstun, Jonathan-Shoemaker, JosDenmark, JoshDumo, John Judge, Tal Kachmann, Akshay Kale, Naoki Kanazawa, Jessica Kane, Kang-Bae, Annanay Kapila, Anton Karazeev, Paul Kassebaum, Tobias Kehrer, Josh Kelso, Scott Kelso, Hugo van Kemenade, Vismai Khanderao, Spencer King, Yuri Kobayashi, Kovi11Day, Arseny Kovyrshin, Rajiv Krishnakumar, Pradeep Krishnamurthy, Vivek Krishnan, Kevin Krsulich, Prasad Kumkar, Gawel Kus, Ryan LaRose, Enrique Lacal, Raphaël Lambert, Haggai Landa, John Lapeyre, Joe Latone, Scott Lawrence, Christina Lee, Gushu Li, Tan Jun Liang, Jake Lishman, Dennis Liu, Peng Liu, Lolcroc, Abhishek K M, Liam Madden, Yunho Maeng, Saurav Maheshkar, Kahan Majmudar, Aleksei Malyshev, Mohamed El Mandouh, Joshua Manela, Manjula, Jakub Marecek, Manoel Marques, Kunal Marwaha, Dmitri Maslov, Paweł Maszota, Dolph Mathews, Atsushi Matsuo, Farai Mazhandu, Doug McClure, Maureen McLanney, Joseph McElroy, Cameron McGarry, David McKay, Dan McPherson, Srujan Meesala, Dekel Meirum, Corey Mendell, Thomas Metcalfe, Martin Mevis-

sen, Andrew Meyer, Antonio Mezzacapo, Rohit Midha, Daniel Miller, Hannah Miller, Zlatko Minev, Abby Mitchell, Nikolaž Moll, Alejandro Montanez, Gabriel Monteiro, Michael Duane Mooring, Renier Morales, Niall Moran, David Morcuende, Seif Mostafa, Mario Motta, Romain Moyard, Prakash Murali, Daiki Murata, Jan Müggenburg, Tristan NEMOZ, David Nadlinger, Ken Nakanishi, Giacomo Nannicini, Paul Nation, Edwin Navarro, Yehuda Naveh, Scott Wyman Neagle, Patrick Neuweiler, Aziz Ngoueya, Thien Nguyen, Johan Nicander, Nick-Singstock, Pradeep Niroula, Hassi Norlen, NuoWenLei, Lee James O’Riordan, Oluwatobi Ogunbayo, Pauline Ollitrault, Tamiya Onodera, Raul Otaolea, Steven Oud, Dan Padilha, Hanhee Paik, Soham Pal, Yuchen Pang, Ashish Panigrahi, Vincent R. Pascuzzi, Simone Perriello, Eric Peterson, Anna Phan, Kuba Pilch, Francesco Piro, Marco Pistoia, Christophe Piveteau, Julia Plewa, Pierre Pocreau, Alejandro Pozas-Kerstjens, Rafał Pracht, Milos Prokop, Viktor Prutyaynov, Sumit Puri, Daniel Puzzuoli, Pythonix, Jesús Pérez, Quant02, Quintiii, Rafey Iqbal Rahman, Arun Raja, Roshan Rajeev, Isha Rajput, Nipun Ramagiri, Anirudh Rao, Rudy Raymond, Oliver Reardon-Smith, Rafael Martín-Cuevas Redondo, Max Reuter, Julia Rice, Matt Riedemann, Rietesh, Drew Risinger, Pedro Rivero, Marcello La Rocca, Diego M. Rodríguez, RohithKarur, Ben Rosand, Max Rossmannek, Mingi Ryu, Tharrmashastha SAPV, Nahum Rosa Cruz Sa, Arijit Saha, Abdullah Ash-Saki, Sankalp Sanand, Martin Sandberg, Hirmay Sandesara, Ritvik Sapra, Hayk Sargsyan, Aniruddha Sarkar, Ninad Sathaye, Niko Savola, Bruno Schmitt, Chris Schnabel, Zachary Schoenfeld, Travis L. Scholten, Eddie Schoute, Mark Schulterbrandt, Joachim Schwarm, James Seaward, Sergi, Ismael Faro Sertage, Kanav Setia, Freya Shah, Nathan Shammah, Will Shanks, Rohan Sharma, Polly Shaw, Yunong Shi, Jonathan Shoemaker, Adenilton Silva, Andrea Simonetto, Deeksha Singh, Divyanshu Singh, Parmeet Singh, Phattharaporn Singkanipa, Yukio Siraichi, Siri, Jesús

Sistos, Iskandar Sitdikov, Seyon Sivarajah, Slavikmew, Magnus Berg Sletfjering, John A. Smolin, Mathias Soeken, Igor Olegovich Sokolov, Igor Sokolov, Vicente P. Soloviev, SooluThomas, Starfish, Dominik Steenken, Matt Stypulkoski, Adrien Suau, Shaojun Sun, Kevin J. Sung, Makoto Suwama, Oskar Słowik, Rohit Taeja, Hitomi Takahashi, Tanvesh Takawale, Ivano Tavernelli, Charles Taylor, Pete T aylour, Soolu Thomas, Kevin Tian, Mathieu Tillet, Maddy Tod, Miroslav Tomasik, Caroline Tornow, Enrique de la Torre, Juan Luis Sánchez Toural, Kenso Trabing, Matthew Treinish, Dimitar Trenev, TrishaPe, Felix Truger, Georgios Tsilimigkounakis, Davindra Tulsi, Doğukan Tuna, Wes Turner, Yotam Vaknin, Carmen Recio Valcarce, Francois Varchon, Adish Vartak, Almudena Carrera Vazquez, Prajjwal Vijaywargiya, Victor Villar, Bhargav Vishnu, Desiree Vogt-Lee, Christophe Vuillot, James Weaver, Johannes Weidenfeller, Rafal Wieczorek, Jonathan A. Wildstrom, Jessica Wilson, Erick Winston, WinterSoldier, Jack J. Woehr, Stefan Woerner, Ryan Woo, Christopher J. Wood, Ryan Wood, Steve Wood, James Wootton, Matt Wright, Lucy Xing, Jintao YU, Yaiza, Bo Yang, Unchun Yang, Jimmy Yao, Daniyar Yeralin, Ryota Yonekura, David Yonge-Mallo, Ryuhei Yoshida, Richard Young, Jessie Yu, Lebin Yu, Yuma-Nakamura, Christopher Zachow, Laura Zdanski, Helena Zhang, Iulia Zidaru, Bastian Zimmermann, Christa Zoufal, aeddins ibm, alexzhang13, b63, bartek bartlomiej, bcamorrison, brandhsn, chetmurthy, choerst ibm, deeplokhande, dekel.meirom, dime10, dlasecki, ehchen, ewinston, fanizzamarco, fs1132429, gadial, galeinston, georgezhou20, georgios ts, gruu, hhorii, hhyap, hykavitha, itoko, jeppevinkel, jessica angel7, jezerjojo14, jliu45, johannesgreiner, jscott2, kUmezawa, klinvill, krutik2966, ma5x, michelle4654, msuwama, nico lgrs, nrhawkins, ntgiwsvp, ordmoj, sagar pahwa, pritamsinha2304, rithikaadiga, ryancocuzzo, saktar unr, saswati qiskit, septembrr, sethmerkel, sg495, shaashwat, smturro2, sternparky, strickroman, tigerjack,

tsura crisaldo, upsideon, vadebayo49, welien, willhbang, wmurphy collabstar, yang.luh, yuri@FreeBSD, and Mantas Čepulkovskis. Qiskit: An open-source framework for quantum computing, 2021.

- [206] Bei Zeng, Xie Chen, Duan-Lu Zhou, Xiao-Gang Wen, et al. *Quantum information meets quantum matter*. Springer, 2019.